ADDIS ABABA UNIVERSITY
SCHOOL OF GRADUATE STUDIES
FACULTY OF TECHNOLOGY
DEPARTMENT OF MECHANICAL ENGINEERING

Bending-Torsion Decoupling In Eigen Mode Of Subsonic and Supersonic Composite Monocoque Aircraft wing

By
Muluken Masresha

A thesis submitted to the School of Graduate Studies of Addis Ababa University in partial fulfillment of the requirements for the Degree of Masters of Science in Mechanical Engineering

(Applied Mechanics Stream)

Advisor: ***Dr.A.Ramman***

November, 2007

Bending-Torsion Decoupling In Eigen Mode Of Subsonic and Supersonic Composite Monocoque Aircraft wing

By
Muluken Masresha

A thesis submitted to the School of Graduate Studies of Addis Ababa University in partial fulfillment of the requirements for the Degree of Masters of Science in Mechanical Engineering

Faculty of Technology

Approved by a Board of Examiner

Ato Hamsasew Moges
____
Chair man Department Graduate Committee
Signature

Dr.A.Ramman
____
Advisor
Signature

Dr.Alem Bazezew
____
Internal Examiner
Signature

Dr.Sharma
____
External Examiner
Signature

ACKNOWLEDGMENT

This Study would be impossible with out the help of God

I would like, my utmost gratitude and thanks are extended to my advisor, Dr.A.Ramman, for his constant encouragement, unwavering support and valuable advice throughout the research. His vast knowledge and insight in to the area of mechanics of composite material and aeronautics have helped me get through some obstacles along the way.

I wish to thank all instructors from Department of Mechanical Engineering for their give me a lectures during stay in addis ababa university.

I would like to express special thanks to Dr.Alem Bazezew for his useful committee for the final drafts of the research.

I would like to express special thanks to all computer lab administrator of Mechanical Engineering Department during my stay at Addis Ababa University

Last but not least, I would like to thank my wife Tsehaynesh Getaneh and my friends, for their unwavering support and encouragement which provided me the strength to complete this study.

ABSTRACT

The thesis deals with bending-torsion decoupling in eigen modes of monocoque laminated composite aircraft (subsonic and supersonic) wing using commercial software ANSYS.

Theoretical background, mathematical formulation and finite element solution for a laminated composite shell structure are presented in this study. A monocoque aircraft wing is made of laminated composite with fiber angles in each ply aligned in different direction.

Various airfoil thickness and ply angles were considered to study the effect of bending-torsion decoupling. Results obtained are presented and parametric studies are made to show the effect of airfoil thickness variation and ply orientation. The effect of location of shear center relative to the center of gravity is also studied and the results are presented.

TABLE OF CONTENTS

List of Figure

List of Table

Abbrebations

CFC	Carbon fiber composite
FE	Finite element
LCO	Limit cycle oscillation
SHM	Structural health monitoring
CUS	Circumferentially uniform stiffness
CAS	Circumferentially Asymmetric stiffness
DFE	Dynamic finite element
STAGS	Structural analysis of general shell
C	Airfoil chord
C_l	Lift coefficient
t	thickness
x	Distance along the chord
y	Airfoil ordinate normal to the chord
θ	Twist angle parameter
GA	Genetic algorithm
NACA	National Advisory committee for Aeronautic
$\frac{T}{C}$	Thickness to chord ration
E_l	Modulus of elasticity in the fiber direction
E_t	Modulus of elasticity perpendicular to the fiber direction
G_{lt}	Modulus of rigidity
θ_1	Fiber orientation angle
[B]	Strain displacement matrix
[Q]	Elastic stiffness matrix
$[T_3]$	Transformation matrix
A_{ij}	Extensional stiffness
B_{ij}	Coupling stiffness
D_{ij}	Bending stiffness
DMO	Discrete material optimization

CHAPTER ONE

1. Introduction

Airplane wing is often improved for better performance such as increases in flutter speed and reduction in control problem. This research will help to improve the performance of the aircraft.

1.1 Background of The Problem

The wing of an airplane is subjected to a lift force during the operations. The lift force "L" is induced to the angle of attack "β"(which the angle between the direction of the air flow and the chord line of the airfoil).But the flexibility of the wing will make β to be increase by $\beta+\Delta\beta$ as shown in the figure (1.1).

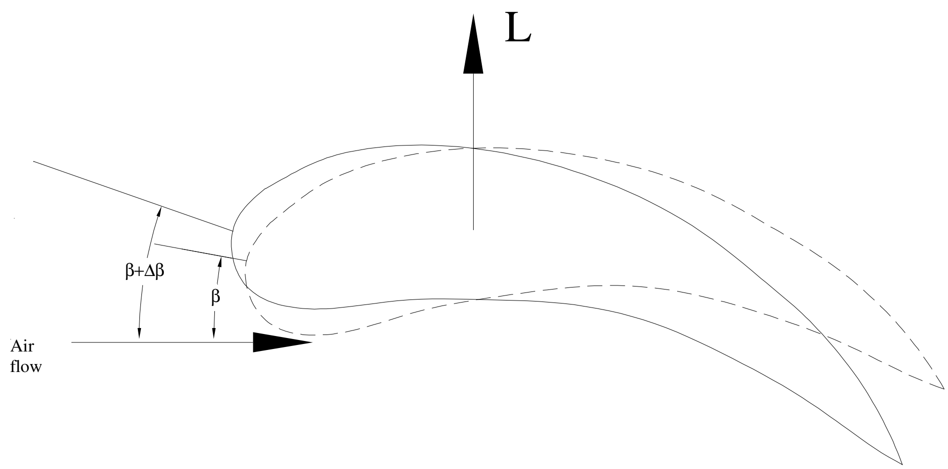

Figure 1.1 Airfoil cross section with angle of attack

Because of this increase in β by $\Delta\beta$ (the flexibility effect) will make the lift to be increased for L to $L+\Delta L$. This increased lift $L+\Delta L$ will produce more $\Delta\beta$ say $\Delta\beta_2$ thus as a cumulative cycle the angle will keep on increase till it reaches the stalling angle (the angle of attack at which the airflow will separate from the airfoil and has produce no lift) hence this types of sudden drop in lift force due to the flexibility of the wing should be avoided.(Incidentally this is known as aroelastic study).

To reduce this aroelastic effect it is usually solved in literature at the level of due to aerodynamic load vibration response.

The proposed solution for this aroelastic effect in this research it is planned to decouple the bending-torsion of the airfoil in the eigen modes. It may be noted that the dynamic response for any dynamic load is a sum of modal responses. Hence if we reduce or decouple the bending-torsion of the wing for the first ten mode, it is likely that the bending-torsion coupling out of the aerodynamic force will be a minimum and the control problem.

This reduction (elimination) of bending-torsion is planned by tailoring (change the thickness) the aerofoil section. That the monocoque (only shell without stiffness) section is changed in the thickness variation and ply angle.

The coupled bending-torsion motion be it from the structural element or the loading element in an aircraft wing is undesirable. Since the angle of attack will unintentionally increase and stall will occur. Hence an investigation of this problem for all composite monocoque structure is useful. Structural tailoring of the wing by the modification of topology or fiber orientation of the ply. The eigen analysis of composite wing will pave the way for structural tailoring to decouple or minimize the effect of bending- torsion coupling. Since the excitation loads are in a low frequency range, modification is planned for first few coupled modes. The wing is made of composite material with fiber angles in each ply aligned in different direction. The wing is clamped at one end and allowed free at the other. Free vibration analysis of an aircraft wing made of composite material will be presented. The result will indicate changes in natural frequencies with fiber orientation. This study will help in increasing the critical divergence/ flutter speed. It may be noted that not only the fiber angle but also the elastic (shear) center and center of gravity location and also the aerodynamic center play an important role in increasing flutter/ divergence speed. However in the first phase of this study, the effect of applied load will not be included.

The data obtained From Wikipedia; the free encyclopedia Aerospace research center will be used in this study for generating the FE model of NACA 8516 airfoil geometry [20] for an aircraft wing using a material of composite structure.

1.2 Objectives of the Study

The general objective of the study is to minimize bending-torsion coupling effect on composite monocoque aircraft wing structure.

The specific objectives of the studies are:-

- To develop a model of a composite monocoque (only shell without stiffness) aircraft wing (subsonic and Supersonic)
- To estimate the eigen value and eigen vectors
- To perform structural tailoring (modification of airfoil thickness along the profile) to decouple the bending-torsion mode using the results of mode shapes of first few modes
- To reduce of bending-torsion coupling in the eigen analysis by varying the ply angles (fiber orientation in each laminate)

1.3 Organization of the Study

The paper is organized in seven chapters. Chapter one deal with the introduction, background of the problem, objective of the study and scope of the study. The second chapter describes supportive literature parts. Chapter three focuses on basic theories of composite material, aircraft wing nomenclatures and airfoil designation. The fourth chapter describes basic mathematical modeling of the problem. The governing equation of motion for a bending-torsion coupling of composite shell element, using classical laminated theory, mechanics of composite material and finite element formulation method is stated. On chapter five a computer modeling using ANSYS is presented. In this chapter, the basic geometric modeling is done using ANSYS for finite element analysis. In chapter six results obtained are discussed. From the results, select the minimum twist angle parameter model and describe the mode shape character for the selected model by the effect of reducing the bending-torsion coupling. The final chapter focus on conclusions and recommendations for future work.

1.4 Scope of the Study

In this thesis, low aspect ratio wings are analyzed and their vibrational characteristics are determined. Finite element formulation of super parametric elements is used to represent shell-like structure of the wing. Composite material element is used to obtain the generalized equation of motion as assemble of numbers of finite elements. Free Vibration characteristics and the bending- torsion decoupling of the wing are found out for selected aerofoil geometries using ANSYS. The effects of laminated composite ply angle for different orientation angles and thickness of leading edge and trailing edge are determined. Finally the obtained results for different orientation angles, different thickness, different natural frequency and mode shape will obtained from the result point of view select the minimum twist angle parameter and describe the characteristic of the mode shape for the reduced bending- torsion coupled wing.

CHAPTER TWO

2. LTERATURE REVIEW

Various researchers have analyzed vibration characteristics of composite wing structure so and so has done analytical analysis composite model as a cantilever beam,an analytical model of cracked composite beams vibrating in coupled bending-torsion is developed. The beam is made of fiber-reinforced composite with fiber angles in each ply aligned in the same direction. [23] The crack is assumed open. The local flexibility concept is implemented to model the open crack and the associated compliance matrix is derived. The crack introduces additional boundary conditions at the crack location and these effects in conjunction with those of material properties are investigated. Free vibration analysis of the cracked composite beam is presented. The results indicate that variation of natural frequencies in the presence of a crack is affected by the crack ratio and location, as well as the fiber orientation. In particular, the variation pattern is different as the magnitude of bending-torsion coupling changes due to different fiber angles. When bending and torsional modes are essentially decoupled at a certain fiber angle if there is no crack, the crack introduces coupling to the initially uncoupled bending and torsion. Based on the crack model, aeroelastic characteristics of an upswept composite wing with an edge crack are investigated. The cracked composite wing is modeled by a cracked composite cantilever and the inertia coupling terms are included in the model. An approximate solution on critical flutter and divergence speeds is obtained by Galerkin's method in which the fundamental mode shapes of the cracked wing model in free vibration are used. It is shown that the critical divergence/flutter speed is affected by the elastic axis location, the inertia axis location, fiber angles, and the crack ratio and location. Moreover, model-based crack detection (size and location) by changes in natural frequencies is addressed.

Jan Stegmann [18] had stated to develop finite element based optimization techniques for laminated composite shell structures. The platform of implementation is the finite element based analysis and design tool MUST (Multidisciplinary Synthesis Tool) and a number of features have been added and updated. This includes an updated implementation of finite elements for shell analysis, tools for investigation of nonlinear effects in multilayered topology optimization and a novel framework called Discrete Material Optimization (DMO) for solving the material layout and orientation problem.

Hiro Miura [17] had deal with Composite wings have become increasingly popular in recent years due to significant potential of weight savings and stiffness tailoring. For aircraft wings made out of composite materials, aeroelastic tailoring presents an opportunity to enhance the aircraft performance by utilizing their unique stiffness and strength properties.

Guo et al., [16] had investigated the paper presents an analytical study on optimization of a laminated composite wing structure for achieving a maximum flutter speed and a minimum weight without strength penalty. The investigation is carried out within the range of incompressible airflow and subsonic speed. In the first stage of the optimization, attention has been paid mainly to the effect on flutter speed of the bending, torsion and, more importantly, the bending-torsional coupling rigidity, which is usually associated with asymmetric laminate lay-up. The study has shown that the torsional rigidity plays a dominant role, while the coupling rigidity has also quite a significant effect on the flutter speed. In the second stage of the optimization, attention has been paid to the weight and laminate strength of the wing structure, which is affected by the variation in laminate lay-up in the first stage. Results from a thin-walled wing box made of laminated composite material show that up to 18 per cent increase in flutter speed and 13 per cent reduction in weight can be achieved without compromising the strength. The investigation has shown that a careful choice of initial lay-up and design variables leads to a desirable bending, torsional and coupling rigidities, with the provision of an efficient approach when achieving a maximum flutter speed with a minimum mass of a composite wing.

Aditi Chattopadhyay [1] provided a good review in the development of a composite wing box section using a higher order-theory is proposed for accurate and efficient estimation of both static and dynamic responses. The theory includes the effect of through-the-thickness transverse shear deformations which is important in laminated composites and is ignored in the classical approach. The box beam analysis is integrated with an aeroelastic analysis to investigate the effect of composite tailoring using a formal design optimization technique. A hybrid optimization procedure is proposed for addressing both continuous and discrete design variables.

Shyama Kumari and P.K. Sinha [31] took with numerical studies of composite T-joints which are made of carbon fiber composite (CFC) materials. CFC materials are used due to their high load carrying capacity and lightweight. The composite T-section is formed at the spar-lower skin joint section in aircraft wings. The behavior of such joints is very complex. In this study, a brief account of the problem is first presented and areas of principal interest which most influence joint behavior are identified. A thick composite shell finite element is specially developed and it is then used for a detailed finite element analysis of composite T-joints. Though several types of forces act on the spar, in the present case, a pull-out force is applied on the top of the web to determine strength and to study the behavior of T-joints. Parametric variations account for two different stacking sequences and variations in filler area and radius of curvature at the web/skin interface.

Alastair F. Johnson and Nathalie Pentecôte [4] had proposed on materials modeling and numerical simulation of foreign Object impact damage in fiber reinforced composite aircraft structures. The work is based on the application of finite element (FE) analysis codes to simulate damage in composite shell structures under impact loads. Composites ply damage models and interply delamination models have been developed and implemented in commercial explicit FE codes. The failure models and code developments are validated in the paper by predicting transverse impact damage in composite aircraft sandwich structures and comparing numerical simulations with high velocity gas gun impact test data.

Boyangliu [7] introduce the design of complex composite structures used in aerospace or automotive vehicles presents a major challenge in terms of computational cost. Discrete choices for ply thicknesses and ply angles leads to a combinatorial optimization problem that is too expensive to solve with presently available computational resources. We developed the following methodology for handling this problem for wing structural design: we used a two-level optimization approach with response-surface approximations to optimize panel failure loads for the upper-level wing optimization. We tailored efficient permutation genetic algorithms to the panel stacking sequence design on the lower level. We also developed approach for improving continuity of ply stacking sequences among adjacent panels.

Erik Lund and Jan Stegmann [10] found that structural optimization of composite laminate shell structures is presented. The method is based on ideas from multi-phase topology optimization where the material stiffness (or density) is computed as a weighted sum of candidate materials. Examples illustrate the potential of the method to solve the problem of proper choice of material, stacking sequence and fiber orientation simultaneously for maximum stiffness or lowest eigen frequency design.

Osama J Aldraihem and Robert C Wetherhold [26] had deal with a shear-deformable beam theory is proposed to model the coupled bending and twisting vibration in laminated beams. Two types of coupling are considered: mass coupling and stiffness coupling. The control of the coupled vibration is accomplished by smart layers incorporated in the host structure. The capability of two different types of piezoelectric layers in detecting and supplying bending and twisting motion is addressed in this article. Traditional lead zirconate titanate (PZT) piezoelectric layers can detect and supply a twisting motion only

Indirectly, while a PZT/epoxy piezoelectric composite (PZT/Ep) has been shown to sense and actuate both bending and twisting motion. A modal cost and controllability analysis is discussed to compare the performance of the actuation configurations. In a series of examples, the PZT/Ep actuator has provided the best bending–twisting actuation for vibration damping.

G. Dietz et.al [13] took with the experiments have been performed in order to explore the Limit-Cycle Oscillation (LCO) behavior of a transport aircraft wing at transonic airspeeds. Therefore an aeroelastically scaled model of the outer part of a typical wing has been designed for investigations in a wind tunnel. The research model has a supercritical airfoil and an aspect ratio of 3.68 with a leading-edge sweepback angle of 32^0. The static and dynamic structural properties as well as the aerodynamic shape of the wing model are reported. Experiments have been conducted in order to determine its static aeroelastic behavior. The LCO behavior can be investigated depending on several inflow parameters. The research model provides an excellent opportunity for investigating the governing physics of LCOs due to its properties and its instrumentation.

G. R. Benini et.al.[15] had reviewed a numerical model for the simulation of fixed wings aeroelastic response is presented. The methodology used in the work is to treat the aerodynamics and the structural dynamics separately and then couple them in the equations of motion. The dynamic characterization of the wing structure is done by the finite element method and the equations of motion are written in modal coordinates. The unsteady aerodynamic loads are predicted using the vortex lattice method. The exchange of information between the aerodynamic and Structural meshes are done by the surface spines interpolation scheme, and the equations of motion are solved iteratively in the time domain, employing a predictor-corrector method. Numerical simulations are performed for a prototype aircraft wing. The aeroelastic response is represented by time histories of the modal coordinates for different airspeeds, and the flutter occurrence is verified when the time histories diverge (i.e. the amplitudes keep growing). Fast Fourier Transforms of these time histories show the coupling of frequencies typical of the flutter phenomenon.

Seong-Wook Hong et.al [29] proposed beams are often subject to bending-torsion coupled vibration due to mass coupling and/or stiffness coupling. This paper proposes a dynamic analysis method using the exact dynamic element for bending-torsion coupled vibration of general plane beam structures with joints. The exact dynamic element matrix for a bending-torsion coupled beam is derived, and the detailed procedure of using the exact dynamic element matrix is also presented. Three examples are provided for validating and illustrating the proposed method. The numerical study proves the proposed method to be useful for dynamic analysis of bending-torsion coupled beam structures with joints.

Peter W.G. De Baets et.al [27] the research looked into the aeroelastic properties and modal response of a composite rectangular wing box. This research attempted to assess the sensitivity of the flutter speed, divergence speed and modal response when varying the composite skin lay-up, fiber orientation, and the root flexibility of the model. All this research was conducted using the finite element code. An attempt was made to cover as extensive a field as possible and identify interesting areas that required further examination. Interesting relations were found between the following properties: *EI*/*GJ* versus fiber orientation and various mode ratios versus root stiffness. These could be linked with the changes in flutter and divergence speed of the composite model.

In certain regions of the root flexibility, the flutter and divergence speeds showed dips and peaks. These coincided with changes in modal behavior and were verified with a visualization tool.

Prashant M. Pawar [28] had investigated with the helicopter rotor system operates in a highly dynamic and unsteady aerodynamic environment leading to severe vibratory loads on the rotor system. Repeated exposure to these severe loading conditions can induce damage in the composite rotor blade which may lead to a catastrophic failure. Therefore, an interest in the structural health monitoring (SHM) of the composite rotor blades has grown markedly in recent years. Two important issues are addressed in this thesis: (1) structural modeling and aeroelastic analysis of the damaged rotor blade and (2) development of a model based rotor health monitoring system. The effect of matrix cracking, the failure mode in composites, is studied in detail for a circular section beam, box-beam and two-cell airfoil section beam. Later, the effect of further progressive damages such as debonding/delamination and fiber breakage are considered for a two-cell airfoil section beam representing a stiff-in plane helicopter rotor blade. It is found that the stiffness decreases rapidly in the initial phase of matrix cracking but becomes almost constant later as matrix crack saturation is reached. Due to matrix cracking, the bending and torsion stiffness losses at the point of matrix crack saturation are about 6-12 percent and about 25-30 percent, respectively. Due to debonding/delamination, the bending and torsion stiffness losses are about 6-8 percent and about 40-45 percent after matrix crack saturation, respectively. The stiffness loss due to fiber breakage is very rapid and leads to the final failure of the blade. An aeroelastic analysis is performed for the damaged composite rotor in forward flight and the numerically simulated results are used to develop an online health monitoring system. For fault detection, the variations in rotating frequencies, tip bending and torsion response, blade root loads and strains along the blade due to damage are investigated. It is found that peak-to-peak values of blade response and loads provide a good global damage indicator and result in considerable data reduction. Also, the shear strain is a useful indicator to predict local damage. The structural health monitoring system is developed using the physics based models to detect and locate damage from simulated noisy rotor system data.

Gamal M. Ashawesh et.al.[12] This paper discussed the effect of fiber orientations, composite skin lay-up, bending-torsion material coupling, and the root flexibility or stiffness of a composite rectangular wing box model for different fibre orientations on the dynamic and aeroelastic analysis (flutter and divergence speeds) for the Circumferentially Uniform Stiffness (CUS) and Circumferentially Asymmetric Stiffness (CAS) configurations.

Andreas P F Bernhard and Inderjit Chopra [5] had deal with an Active rotor blade tips offer an alternative approach to the challenge of main rotor active vibration control. The tips are pitched with respect to the main blade via a piezo-driven bending-torsion coupled actuator beam that runs down the length of the blade. A Vlasov based, specialized one-dimensional finite beam element is developed to model the rotating actuator beam and is validated with the free-vibration and static forced response of 4:1 and 2:1 aspect ratio, bending-torsion coupled, active and passive plates. A one-eighth scale, reduced tip-speed rotor model (tip mach 0.26), incorporating the bending-torsion actuator beam, has been previously hover tested (open loop). In these tests, blade tip deflections of the order of 2^0 (half peak-to-peak) were achieved at 2, 3, 4, 5/rev with corresponding dynamic vertical blade root shear variations of the order of 10–20% of the nominal blade lift at 8^0 collective ($CT/\sigma = 0.07$). The test results are used to validate a coupled actuator and elastic rotor blade model. The correlation of the predicted active blade-tip pitch deflections and the experimental data is within 20%. The predicted values for the active vertical root shears are within the same margin for 4^0 and 6^0 collective.

Zhanming Qin [36] introduced based on a refined analytical anisotropic thin-walled beam model, aeroelastic instability, dynamic aeroelastic response, active/passive aeroelastic control of advanced aircraft wings modeled as thin-walled beams are systematically addressed. The refined thin-walled beam model is based on an existing framework of the thin-walled beam model and a couple of non-classical effects that are usually also important are incorporated and the model herein developed is validated against the available experimental, Finite Element Analysis (FEA), Dynamic Finite Element (DFE), and other analytical predictions. The concept of indicial functions is used to develop unsteady aerodynamic model, which broadly encompasses the cases of incompressible, compressible subsonic, compressible supersonic and hypersonic flows. State-space conversion of the indicial function based unsteady aerodynamic model is also developed. Based on the piezoelectric material technology, a worst case control strategy based on the mini - max theory towards the control of aeroelastic systems is further developed. Shunt damping within the aeroelastic tailoring environment is also investigated.

Ferdinando Auricchio And Elio Sacco [11], this paper had proposed a new 4-node finite-element for the analysis of laminated composite plates. The element is based on a first-order shear deformation theory and is obtained through a mixed-enhanced approach. In fact, the adopted variational formulation includes as variables the transverse shear as well as enhanced incompatible modes introduced to improve the in-plane deformation. The problem is then discretized using bubble functions for the rotational degrees of freedom and functions linking the transverse displacement to the rotations. The proposed element is locking free, it does not have zero energy modes and provides accurate in-plane/out-of-plane deformations. Furthermore, a procedure for the computation of the through-the-thickness shear stresses is discussed, together with an iterative algorithm for the evaluation of the shear correction factors. Several applications are investigated to assess the features and the performances of the proposed element.

J.B. Kosmatka [19] further more Current helicopter rotor blade designs incorporate fiber composite materials as a means of controlling weight, deformation, and vibration (i.e., structural tailoring).Although fiber composites are orthotropic in material property classification, they can exhibit general anisotropic material behavior to applied loads (extension-bend-twist Coupling) when the fiber orientations do not coincide with the structural coordinate system. Exact analytical solutions of this problem based upon three-dimensional elasticity are intractable. Three dimensional finite-element modeling may be applied; however, this approach is too costly for the discretization necessary for accurate stress and deformation determination.

Jonathan E. Rich [21] had studied on an optimization strategy for the design of composite shells is investigated. This study differs from previous work in that an advanced analysis package is utilized to provide buckling information on potential designs. The Structural Analysis of General Shells (STAGS) finite element code is used to provide linear buckling calculations for a minimum buckling load constraint. A response surface, spanning the design space, is generated from a set of design points and corresponding buckling load data. This response surface is incorporated into a genetic algorithm for optimization of composite cylinders. Laminate designs are limited to those that are balanced and symmetric. Three load cases and four different variable formulations are examined. In the first approach, designs are limited to those who are normalized in-plane and out-of-plane stiffness parameters would be feasible with laminates consisting of two independent fiber orientation angles. The second approach increases the design space to include those that are bordered by those in the first approach. The third and fourth approaches utilize stacking sequence designs for optimization, with continuous and discrete fiber orientation angle variation, respectively. For each load case and different variable formulation, additional runs are made to account for inaccuracies inherent in the response surface model. This study concluded that this strategy was effective at reducing the computational cost of optimizing the composite cylinders.

Won-Hong Lee · Sung-Cheon Han [34] had deal with the natural frequencies of isotropic and composite laminates are presented. The forced vibration analysis of laminated composite plates and shells subjected to arbitrary loading is investigated. In order to overcome membrane and shear locking phenomena, the assumed natural strain method is used. To develop a laminated shell element for free and forced vibration analysis, the equivalent constitutive equation that makes the computation of composite structures efficient was applied. The Mindlin-Reissner theory which allows the shear deformation and rotary inertia effect to be considered is adopted for development of nine-node assumed strain shell element. The present shell element offers significant advantages since it consistently uses the natural co-ordinate system. Results of the present theory show good agreement with the 3-D elasticity and analytical solutions. In addition the effect of damping is investigated on the forced vibration analysis of laminated composite plates and shells.

Wu Qian et.al [35] had stated that active vibration control of composite laminated shells has been studied via embedded magnetostrictive layers. Targets the coupled strains or stresses; hence it is very important to develop a layer wise theory for laminates to determine the coupled strains and stresses accurately. The present layer wise theory satisfies the continuity conditions of transverse shear stresses and in-plane displacements at the interfaces of neighboring layers. This higher order layer wise theory has an advantage over the equivalent single layer theory and provides an intuitively correct computational model, which follows Newton's third law in perfect bonding conditions for laminated materials. The displacements of the layer wise theory combine classical thin shell theory and the displacements caused by the transverse shear stresses which satisfy the condition of zero transverse shear stresses at the free surface. Laminated composite shells with surface layers of magnetostrictive. The direct and converse effects of these properties of smart materials are exploited here. Negative velocity feedback and constant gain controllers are used to achieve effective vibration suppression. The numerical results show that vibration suppression of the shell with magnetostrictive layers can be achieved by negative velocity feedback constant gain controllers.

S.K. Basu et.al. [32] had studied a standard four node rectangular elements with seven degrees of freedom at each node is used for the analysis of laminated plate, having a constant thickness of each layer. The displacement model is chosen in accordance with the higher order shear deformation theory. The detailed formulation and evaluation of a rectangular laminated plate element stiffness matrix is presented. a four node finite element is developed with non conforming shape functions for transverse displacement and conforming shape functions for in-plane displacements and shear rotations. The stiffness matrix is derived using the principle of minimum potential energy. In addition, free vibration analysis of the plate is carried out and three eigen values are found. The results are compared with those of isotropic plate and found in good agreement. The above element confirms its applicability to wide variety of laminated plates.

GoranJanevski [14] stated that, two-frequency vibrations of laminated angle-ply rectangular plate which is freely supported on its own edges are analyzed. The classical Kirhhoff theory is used and the vibration equations of Karman type are analyzed using the Airy function. Asymptotic solution in the first approximation is given. Numerical example includes analysis of the two-frequency plate vibrations under non-stationary conditions and under the activity of time-dependent external impulse. Amplitude-frequency and phase-frequency characteristics of plate under non-stationary conditions for different laminate characteristics are presented graphically.

Stegmann [22] had referred finite elements for shell analysis has since the introduction of shell elements been a major goal. The goal seems to be almost reached with the introduction of the assumed natural Strain methods, which include the mixed Interpolation of tonsorial Components approach applied in the present work. A natural next step is to generalize these robust elements to allow the analysis of structures ranging from conventional metal structures, over composite laminates to sandwich structures. Furthermore, the use of these enhanced elements in other fields such as design optimization seems an obvious development. Such work has already begun and the present work is to a great extend related to the work robust shell finite elements into the field of topology optimization. These robust shell elements are essential for future design and optimization of advanced structures such as wind turbine blades.

K. N. khatri [24] had deal with a vibration and damping analysis based on individual layer deformation is presented for axisymmetric vibrations of laminated composite material conical shells the analysis includes consideration of bending\ extension and transverse shear deformations in each of the laminate layers and also includes its rotary\ meridional and circumferential translatory and transverse inertias the Galerkin method has been applied for finding the approximate solutions for the simply supported conical shells The correspondence principle of linear viscoelasticity has been used to evaluate the damping effectiveness of the shell the variations of the resonance frequencies and of the associated system loss factors with fiber orientation angles and cone apex angles for axisymmetric vibrations of cross ply and angle ply fiber reinforced plastic conical shells are reported.

B. Malott and R.C. Averill [6] had deal with a genetic algorithm approach is used for optimization of a cantilever sandwich plate (an idealization of an airfoil) with a vertical force applied to one free corner. The number of face sheet plies and the ply orientations are designed so as to minimize the weight of the structure while maximizing the twist in the direction opposite that caused by the loading, subject to stiffness, strength, and ply clustering penalties. A new type of GA topology called island injection, developed in a previous study for design of composite beams, is extended to the present case of sandwich panel design. Island injection GA showed slightly better performance over ring and single-node topologies with identical parameters and population sizes. In all cases, the GA successfully identified designs with the desired structural response.

Ahmed K. Noor and Michael D. Mathers [3] had studied several finite-element models are applied to the linear static, stability, and vibration analysis of laminated composite plates and shells. The study is based on linear shallow-shell theory, with the effects of shear deformation, anisotropic material behavior, and bending-extensional coupling included. Discussion is focused on the effects of shear deformation and anisotropic material behavior on the accuracy and convergence of different finite-element models. Numerical studies are presented which show the effects of (a) increasing the order of the approximating polynomials, (b) adding internal degrees of freedom, and (c) using derivatives of generalized displacements as nodal parameters. Both stiffness (displacement) and mixed finite-element models are considered.

Brian E Tatting [8] had investigated with the possible performance improvements of thin circular cylindrical shells through the use of the variable stiffness concept is presented. The variable stiffness concept implies that the stiffness parameters change spatially throughout the structure. This situation is achieved mainly through the use of curvilinear fibers within a fiber-reinforced composite laminate, though the possibility of thickness variations and discrete stiffening elements is also allowed. These three mechanisms are incorporated into the constitutive laws for thin shells through the use of Classical Lamination Theory. The existence of stiffness variation within the structure warrants a formulation of the static equilibrium equations from the most basic principles. The governing equations include sufficient detail to correctly model several types of nonlinearity, including the formation of a nonlinear shell boundary layer as well as the Brazier effect due to nonlinear bending of long cylinders. Stress analysis and initial buckling estimates are formulated for a general variable stiffness cylinder. Results and comparisons for several simplifications of these highly complex governing equations are presented so that the ensuing numerical solutions are considered reliable and efficient enough for in-depth optimization studies. Four distinct cases of loading and stiffness variation are chosen to investigate possible areas of improvement that the variable stiffness concept may offer over traditional constant stiffness and/or stiffened structures.

Seung Joon Lee [30] had deal with theoretical formulations, analytical solutions, and finite element solutions for laminated composite plate and shell structures with smart material laminas are presented in the study. A unified third-order shear deformation theory is formulated and used to study vibration/deflection suppression characteristics of plate and shell structures. The von karman type geometric nonlinearity is included in the formulation. Third-order shear deformation theory based on Donnell and Sanders nonlinear shell theories is chosen for the shell formulation.

The smart material used in this study to achieve damping of transverse deflection is the terfenol-D magnetostrictive material. A negative velocity feedback control is used to control the structural system with the constant control gain.The Navier solutions of laminated composite plates and shells of rectangular plane form are obtained for the simply supported boundary conditions using the linear theories. Displacement finite element models that account for the geometric nonlinearity and dynamic response are developed. The conforming element which has eight degrees of freedom per node is used to develop the finite element model. Newmark's time integration scheme is used to reduce the ordinary differential equations in time to algebraic equations. Newton-Raphson iteration scheme is used to solve the resulting nonlinear finite element equations. A number of parametric studies are carried out to understand the damping characteristics of laminated composites with embedded smart material layers.

Metin Aydogdu [25] had studied vibration analysis of angle-ply laminated beams subjected to different sets of boundary conditions is investigated. The analysis is based on a three-degrees-of-freedom shear deformable beam theory. The governing equations are obtained by means of Hamilton's principle. Six different combinations of free, clamped, and simply supported edge boundary conditions are considered. The free vibration frequencies are obtained by applying the Ritz method where the three displacement components are expressed in a series of simple algebraic polynomials.

Having seen the studies of others, it can be noticed there is not much of systematic study is made on the topological optimization of material composite monocoque wing of subsonic and supersonic to reduce the bending torsion coupling due to structural element. Thus the scope of the research conducted in this thesis may be summarized as:-

a) To vary the thickness and angle of orientation of subsonic and supersonic aircraft wing to have minimal bending torsion coupling due to structural element.
b) To prove these modifications are equally applicable to the composite wings with airoelastic loads aswell.

CHAPTER THREE

3. THEORETICAL BACK GROUND

3.1 Thin Airfoil Theory- Terminology and Definitions

The straight line that joins the leading and trailing ends of the mean camber line is called the chord line. The length of the chord line is called chord, and given the symbol 'C'.To the mean camber line, a thickness distribution is added in a direction normal to the camber line to produce the final airfoil shape.

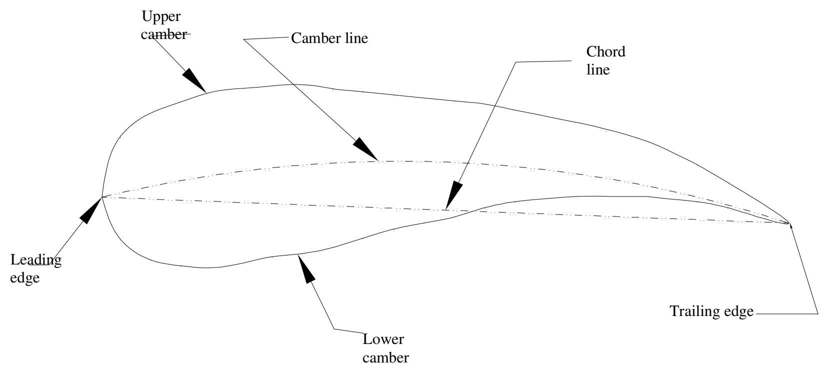

Figure 3.1 Airfoil terminology

Equal amounts of thickness are added above the camber line, and below the camber line. An airfoil with no camber (i.e. a flat straight line for camber) is a symmetric airfoil. The angle that a free stream makes with the chord line is called the angle of attack.

3.1.1 Lift and Drag

The x and y- forces act along the x- and y- axes, respectively. Lift is defined as the component of pressure force that is normal to the free stream direction, and drag is defined as the component of pressure force along the free stream direction. If the airfoil was initially located so that the chord line is along the x- axis, then the angle between the free stream direction and the x- axis is the angle of attack.

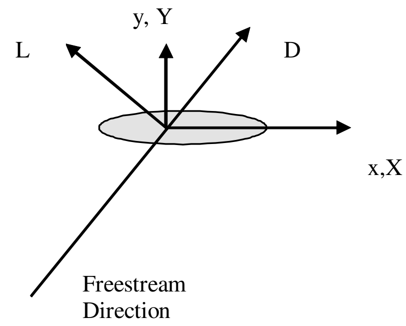

Figure 3.2 Lift and drag relation with air flow stream

3.1.2 Pitching Moment

pitch moment is defined as the pitching moment about any point on the chord line. While the pitching moment can be defined about any point in space, it is customary to compute the pitching moment M and the pitching moment coefficient C_m about the quarter chord, i.e. a location 25%C downstream of the leading edge.

3.1.3 Center of Pressure

The center of pressure is defined as the point about which the pitching moment is zero. As the flow conditions change (example, angle of attack changes), the center of pressure will change.

3.1.4 Aerodynamic Center

The aerodynamic pressure is defined as the point where the pitching moment (or the pitching moment coefficient) is independent of angle of attack.

3.1.5Airfoil Geometry Naming Conventions

The following is an expert from the web site [2] to respect the copyright, and to acknowledge the considerable effort the author of the web site has made in preparing the material. Airfoil geometry can be characterized by the coordinates of the upper and lower surface. It is often summarized by a few parameters such as: maximum thickness, maximum camber, position of maximum thickness, position of maximum camber, and nose radius. One can generate a reasonable airfoil

Section given these parameters.

3.1.5.1 NACA 4-Digit Series

Consider the airfoil NACA 4412. The first digit gives maximum camber in percentage of chord, the second digit gives in tenth of a chord where the maximum camber occurs, and the last two digits give the maximum thickness in percentage chord.

Table 3.1 NACA 4 digit series

4	4	12
Maximum camber in percentage chord	Position of maximum camber	Maximum thickness in percentage chord

3.2 Laminated type composite structure

A typical composite structure consists of a system of layer bonded together. The layers can be made of different isotropic or anisotropic materials, and have different structure, thickness, and mechanical properties. The laminate characteristics [33] are usually calculated using the number of layer, stacking sequence, geometric and mechanical properties. A finite number of layers can be combined to form so many laminates, the laminates characterized with 21 coefficients and demonstrating coupling effect. The behavior of laminates as a system of layer with given properties. The only restriction that is imposed on the laminate as an element of composite structure concerns its total thickness which is assumed to be much smaller than the other dimensions of the structure.

3.2.1 Stiffness Coefficient of Laminated Layer

A laminate consisting of a number of layers with [35]different thickness h_i and stiffness $A^i_{mn}(i = 1,2,3,...k)$. Assuming that material stiffness coefficient do not change with in the thickness of the layer and using piece-wise integration, it is possible to write the parameter I_{mn} as:

$$I^i{}_{mn} = \frac{1}{r+1}\sum_{i=1}^{k} A^i_{mn}\left(t_i^{i+1} - t_{i-1}^{i+1}\right) \tag{3.1}$$

Where $r = 0,1,2$ and $t_o = 0, t_k = h$ for thin layer

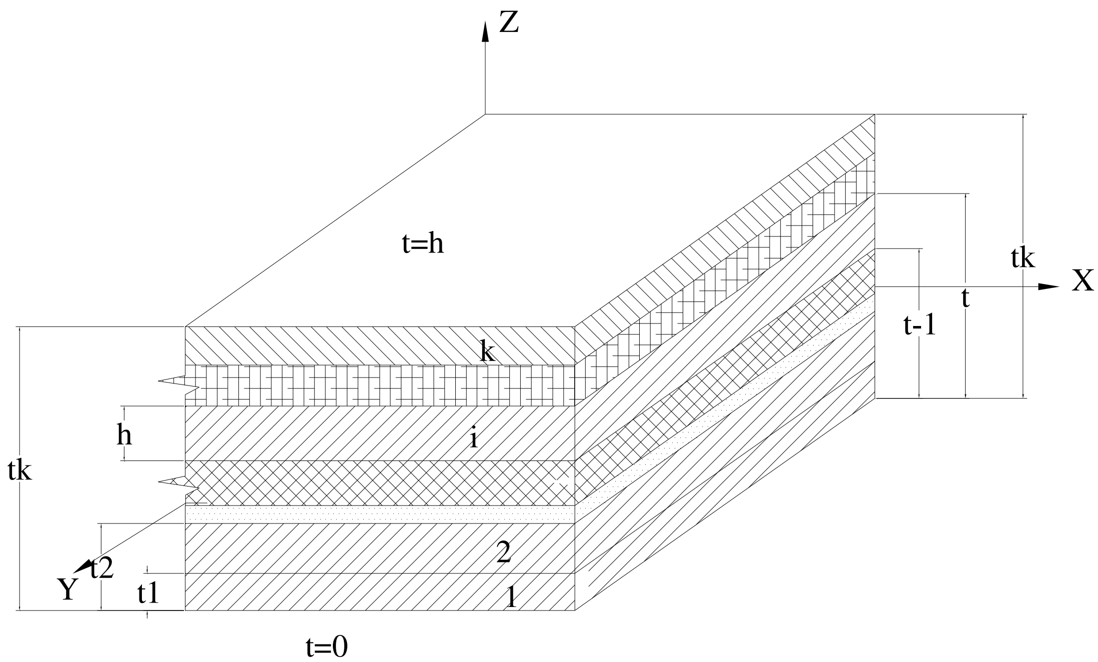

Figure 3.3 Structure of the laminate

The member, coupling and bending stiffness coefficient of the laminate are given respectively

$$B_{mn} = \int A_{mn}\, dz \tag{3.2}$$

$$D_{mn} = \int A_{mn} z^2 dz \tag{3.3}$$

$$C_{mn} = \int A_{mn} z dz \tag{3.4}$$

Where B_{mn} is member stiffness

D_{mn} is coupling stiffness

C_{mn} is bending stiffness

In plane strains of the layer, ε_x , ε_y , *and* γ_{xy} can be found

$$\begin{aligned}
\varepsilon_x &= \frac{\partial u_x}{\partial x} = \varepsilon_x^o + zk_x, \\
\varepsilon_y &= \frac{\partial u_y}{\partial y} = \varepsilon_y^o + zk_y, \\
\gamma_{xy} &= \frac{\partial u_x}{\partial y} + \frac{\partial u_y}{\partial x} = \gamma_{xy}^o + zk_{xy}
\end{aligned} \tag{3.5}$$

Where

$$\varepsilon_x^o = \frac{\partial u}{\partial x}, \quad \varepsilon_y^o = \frac{\partial v}{\partial y}, \quad \gamma_{yx}^o = \frac{\partial u}{\partial y} + \frac{\partial v}{\partial x},$$
$$k_x = \frac{\partial \theta_x}{\partial x}, \; k_y = \frac{\partial \theta_y}{\partial y}, k_{xy} = \frac{\partial \theta_x}{\partial y} + \frac{\partial \theta_y}{\partial x} \tag{3.6}$$

This generalized strains corresponding to the following basic deformation of the layer shown in the figure (3.4)

- In plane tension or compression $(\varepsilon_x^o, \varepsilon_y^o)$
- In plane shear (γ_{xy}^o)
- Bending in xz-and yz plane (k_x, k_y) and
- Twisting (k_{xy})

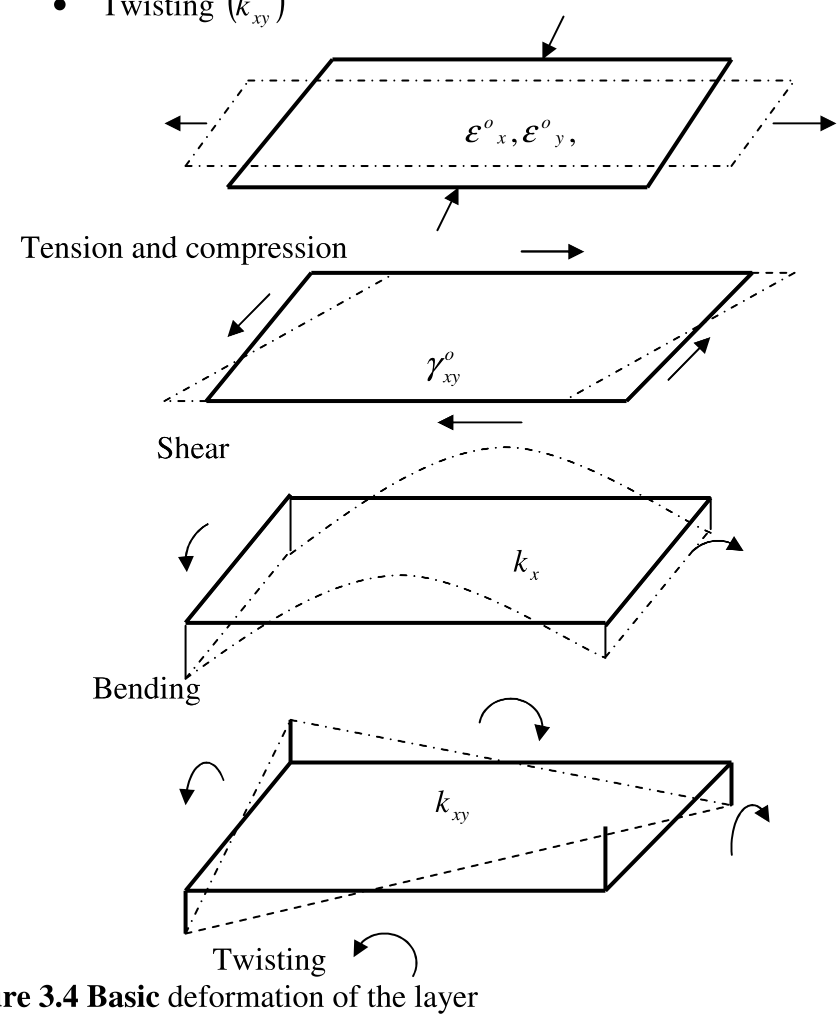

Figure 3.4 Basic deformation of the layer

3.2.2 Laminate composed of Cross -ply layer

The laminate have the structure $[0^o/90^o]_p$ where p=1,2,3,…k specified the number of elementary cross-ply couple of 0^o and 90^o plies

3.2.3 Laminate composed of angle-ply layer

Consider a laminate with the structure $[+\phi/-\phi]_p$ where p is the number of layers each consisting of $+\phi$ and $-\phi$ unidirectional ply

3.2.4 Symmetrical laminates

Symmetrical laminates are composed of layers that are symmetrically arranged with respect to the laminate middle plane

3.2.5 Antisymmetric laminates

In antisymmetric laminates, symmetrical located layer have mutually reversed orientation. For example, while laminates $[0^o/90^o/90^o/0^o]$ and $[+\phi/-\phi/-\phi/+\phi]$ are symmetrical, laminates $[0^o/90^o/0^o/90^o]$ or $[0^o/0^o/90^o/90^o]$ and $[+\phi/-\phi/+\phi/-\phi]$ are antisymmetric.

CHAPTER FOUR

4. MATHEMATICAL FORMULATION

4.1 Finite Element Formulation of Composite Shell Structure

This chapter discuss on the mathematical formulation based on finite element method. This also elaborates the effect of the stacking sequence on the stiffness of layered composite material and equations of motions are stated.

These types of wing, behave more like a plate or a shell. In this chapter the equation of motion is developed for a single cell monocoque wing by using elemental composite shell finite element formulation. Out of the various shell-representing techniques the one selected for the purpose of this thesis is the shell-99 element representation that uses large curvilinear elements for three dimensional analyses [31].

4.1.1 Strain Displacement Relation

The strains at any depth z of a shell laminate Figure (4.1) are denoted as:

$$\begin{Bmatrix} \varepsilon_{xx} \\ \varepsilon_{yy} \\ \varepsilon_{zz} \\ \gamma_{yz} \\ \gamma_{xz} \\ \gamma_{xy} \end{Bmatrix} = \begin{Bmatrix} \varepsilon^0{}_{xx} \\ \varepsilon^0{}_{yy} \\ \varepsilon^0{}_{zz} \\ \gamma^0{}_{yz} \\ \gamma^0{}_{xz} \\ \gamma^0{}_{xy} \end{Bmatrix} + z \begin{Bmatrix} k_{xx} \\ k_{yy} \\ k_{zz} \\ k_{yz} \\ k_{xz} \\ k_{xy} \end{Bmatrix} \tag{4.1}$$

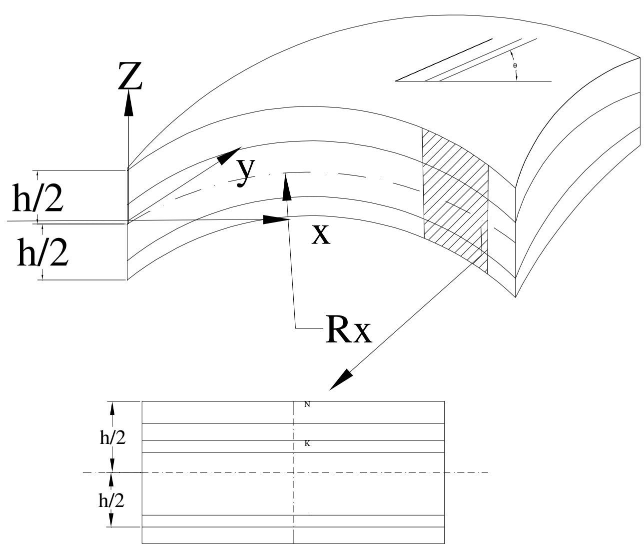

Figure 4.1composite shell and laminated configuration

The mid-plane and curvature figure (4.1) strains are express in terms of the mid-plane displacement as follows

$$\begin{Bmatrix} \varepsilon^0{}_{xx} \\ \varepsilon^0{}_{yy} \\ \varepsilon^0{}_{zz} \\ \gamma^0{}_{yz} \\ \gamma^0{}_{xz} \\ \gamma^0{}_{xy} \end{Bmatrix} = \begin{Bmatrix} \dfrac{\partial u_0}{\partial x} + \dfrac{w_0}{R_x} \\ \dfrac{\partial v_0}{\partial y} + \dfrac{w_0}{R_x} \\ \theta_{zz} \\ \theta_y + \dfrac{\partial w_0}{\partial y} \\ \theta_x + \dfrac{\partial w_0}{\partial x} \\ \dfrac{\partial u_0}{\partial y} + \dfrac{\partial v_0}{\partial x} + \dfrac{w_0}{R_{xy}} \end{Bmatrix} \tag{4.2}$$

$$\begin{Bmatrix} k_{xx} \\ k_{yy} \\ k_{zz} \\ k_{yz} \\ k_{xz} \\ k_{xy} \end{Bmatrix} = \begin{Bmatrix} \dfrac{\partial \theta_0}{\partial x} + \dfrac{\theta_x}{R_x} \\ \dfrac{\partial \theta_y}{\partial y} + \dfrac{\theta_y}{R_y} \\ 0 \\ \dfrac{\partial \theta_z}{\partial y} \\ \dfrac{\partial \theta_z}{\partial x} \\ \dfrac{\partial \theta_x}{\partial y} + \dfrac{\partial \theta_y}{\partial x} + \dfrac{\theta_z}{R_{xy}} \end{Bmatrix} \tag{4.3}$$

Combine equations (4.2) and (4.3), one obtains

$$\begin{Bmatrix} \varepsilon^0{}_{xx} \\ \varepsilon^0{}_{yy} \\ \varepsilon^0{}_{zz} \\ \gamma^0{}_{yz} \\ \gamma^0{}_{xz} \\ \gamma^0{}_{xy} \\ k_{xx} \\ k_{yy} \\ k_{yz} \\ k_{xz} \\ k_{xy} \end{Bmatrix} = \begin{bmatrix} \frac{\partial}{\partial x} & 0 & \frac{1}{R_x} & 0 & 0 & 0 \\ 0 & \frac{\partial}{\partial y} & \frac{1}{R_y} & 0 & 0 & 0 \\ 0 & 0 & 0 & 0 & 0 & 1 \\ 0 & 0 & \frac{\partial}{\partial y} & 0 & 1 & 0 \\ 0 & 0 & \frac{\partial}{\partial x} & 1 & 0 & 0 \\ \frac{\partial}{\partial y} & \frac{\partial}{\partial x} & \frac{1}{R_{xy}} & 0 & 0 & 0 \\ 0 & 0 & 0 & \frac{\partial}{\partial x} & 0 & \frac{1}{R_x} \\ 0 & 0 & 0 & 0 & \frac{\partial}{\partial y} & \frac{1}{R_y} \\ 0 & 0 & 0 & 0 & 0 & \frac{\partial}{\partial y} \\ 0 & 0 & 0 & 0 & 0 & \frac{\partial}{\partial x} \\ 0 & 0 & 0 & \frac{\partial}{\partial y} & \frac{\partial}{\partial x} & \frac{1}{R_{xy}} \end{bmatrix} 0 \begin{Bmatrix} u^0 \\ v^0 \\ w^0 \\ \theta_x \\ \theta_y \\ \theta_z \end{Bmatrix} \tag{4.4}$$

Equation (4.4) can be expressed in compact form as given below

$$\{\varepsilon\} = [B]\{d_e\} \tag{4.5}$$

Where $[B]$ is the strain displacement matrix defined in equation (4.4)

4. 1.2 Elasticity Matrix

A three-dimensional elasticity property is considered as required by the element in this model. Here E_1, E_2 are young's modules in 1 and 2 direction respectively. υ_{ij}=poission ratio for transverse strain in the j-direction when stressed in the i-dirction, i.e, $\upsilon_{ij} = -\varepsilon_i / \varepsilon_j$ for $\sigma_i = \sigma$ and all other stress are Zero. $G_{12} =$ Shear modul us Figure (4.2). From a material symmetry we can write $\upsilon_{21}/E_2 = \upsilon_{12}/E_1$ and so on. Considering a unidirectional lamina shown in Figure (4.2) with lamina axis system and reference axis system, the generalized Hook's law for an orthotropic material can be expressed as

$$
\begin{Bmatrix} \varepsilon_{11} \\ \varepsilon_{22} \\ \varepsilon_{33} \\ \gamma_{23} \\ \gamma_{13} \\ \gamma_{12} \end{Bmatrix} = \begin{bmatrix} \frac{1}{E_{11}} & \frac{-\upsilon_{21}}{E_{22}} & \frac{-\upsilon_{31}}{E_{33}} & 0 & 0 & 0 \\ \frac{-\upsilon_{12}}{E_{11}} & \frac{1}{E_{22}} & \frac{-\upsilon_{32}}{E_{33}} & 0 & 0 & 0 \\ \frac{-\upsilon_{13}}{E_{11}} & \frac{-\upsilon_{23}}{E_{22}} & \frac{1}{E_{33}} & 0 & 0 & 0 \\ 0 & 0 & 0 & \frac{1}{G_{23}} & 0 & 0 \\ 0 & 0 & 0 & 0 & \frac{1}{G_{13}} & 0 \\ 0 & 0 & 0 & 0 & 0 & \frac{1}{G_{12}} \end{bmatrix} \begin{Bmatrix} \sigma_{11} \\ \sigma_{22} \\ \sigma_{33} \\ \tau_{23} \\ \tau_{13} \\ \tau_{12} \end{Bmatrix} \tag{4.6}
$$

For a laminate, the on-axis stress–strain relation for a unidirectional composite in a three dimensional elastic domain can be written as

$$
\{\sigma\} = [Q]\{\varepsilon\} \tag{4.7}
$$

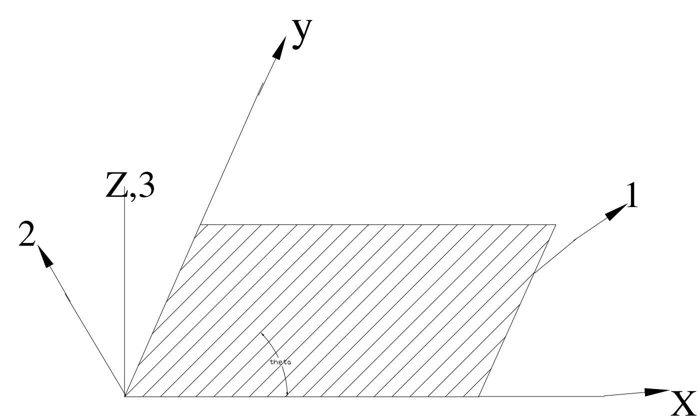

Fig 4.2 An off-axis lamina

When expanded assumes the form given as

$$
\begin{Bmatrix} \sigma_{11} \\ \sigma_{22} \\ \sigma_{33} \\ \tau_{23} \\ \tau_{13} \\ \tau_{12} \end{Bmatrix} = \begin{bmatrix} Q_{11} & Q_{12} & Q_{13} & 0 & 0 & 0 \\ Q_{21} & Q_{22} & Q_{23} & 0 & 0 & 0 \\ Q_{31} & Q_{32} & Q_{33} & 0 & 0 & 0 \\ 0 & 0 & 0 & Q_{44} & 0 & 0 \\ 0 & 0 & 0 & 0 & Q_{55} & 0 \\ 0 & 0 & 0 & 0 & 0 & Q_{66} \end{bmatrix} \begin{Bmatrix} \varepsilon_{11} \\ \varepsilon_{22} \\ \varepsilon_{33} \\ \gamma_{23} \\ \gamma_{13} \\ \gamma_{12} \end{Bmatrix} \tag{4.8}
$$

Assuming a state of plane stress in the material plane gives

$$\begin{Bmatrix} \sigma_{11} \\ \sigma_{22} \\ \tau_{12} \end{Bmatrix} = \begin{bmatrix} Q_{11} & Q_{12} & 0 \\ Q_{12} & Q_{22} & 0 \\ 0 & 0 & Q_{66} \end{bmatrix}_K \begin{bmatrix} \varepsilon_{11} \\ \varepsilon_{22} \\ \gamma_{12} \end{bmatrix} \tag{4.9}$$

Where

$$\begin{aligned} Q_{11} &= \frac{E_1}{1-\upsilon_{12}\upsilon_{21}} \\ Q_{22} &= \frac{E_2}{1-\upsilon_{12}\upsilon_{21}} \\ Q_{12} &= \frac{\upsilon_{12}E_2}{1-\upsilon_{12}\upsilon_{21}} = \frac{\upsilon_{21}E_1}{1-\upsilon_{12}\upsilon_{21}} \\ Q_{66} &= G_{12} \\ Q_{16} &= 0 \\ Q_{26} &= 0 \end{aligned} \tag{4.10}$$

For the kth lamina, the off-axis elastic rigidity matrix with respect to x–y–z coordinate system Figure (4.2) can be expressed as

$$[\overline{Q}] = [T]^T [Q][T] \tag{4.11}$$

Where the transformation matrix $[T]$ is given by

$$[T] = \begin{bmatrix} m^2 & n^2 & 0 & 0 & 0 & mn \\ n^2 & m^2 & 0 & 0 & 0 & -mn \\ 0 & 0 & 1 & 0 & 0 & 0 \\ 0 & 0 & 0 & m & -n & 0 \\ 0 & 0 & 0 & n & m & 0 \\ -2mn & 2mn & 0 & 0 & 0 & (m^2-n^2) \end{bmatrix} \tag{4.12}$$

Where $m = \cos\theta$ and $n = \sin\theta$,

And the off-axis stiffness matrix $[\overline{Q}]$ for a lamina is defined as

$$[\overline{Q}] = \begin{bmatrix} \overline{Q_{11}} & \overline{Q_{12}} & \overline{Q_{16}} \\ \overline{Q_{12}} & \overline{Q_{22}} & \overline{Q_{16}} \\ \overline{Q_{16}} & \overline{Q_{16}} & \overline{Q_{66}} \end{bmatrix} \tag{4.13}$$

4.1.3 Stress–Strain Relation

The stress–strain relations with respect to the reference axis system can be expressed as

$$\begin{Bmatrix} \sigma_{xx} \\ \sigma_{yy} \\ \tau_{xy} \end{Bmatrix} = \left[\overline{Q}\right] \begin{Bmatrix} \varepsilon_{xx} \\ \varepsilon_{yy} \\ \gamma_{xy} \end{Bmatrix} = \left[\overline{Q}\right] \left[\begin{Bmatrix} \varepsilon^0{}_{xx} \\ \varepsilon^0{}_{yy} \\ \gamma^0{}_{xy} \end{Bmatrix} + z \begin{Bmatrix} K_{xx} \\ K_{yy} \\ K_{xy} \end{Bmatrix} \right] \tag{4.14}$$

The stress resultants Figure (4.3) are given by

$$\begin{Bmatrix} N_{xx} \\ N_{yy} \\ N_{zz} \\ S_{yz} \\ S_{xz} \\ N_{xy} \end{Bmatrix} = \int_{-h/2}^{h/2} \begin{Bmatrix} \sigma_{xx} \\ \sigma_{yy} \\ \sigma_{zz} \\ \tau_{yz} \\ \tau_{xz} \\ \tau_{xy} \end{Bmatrix} dz \tag{4.15}$$

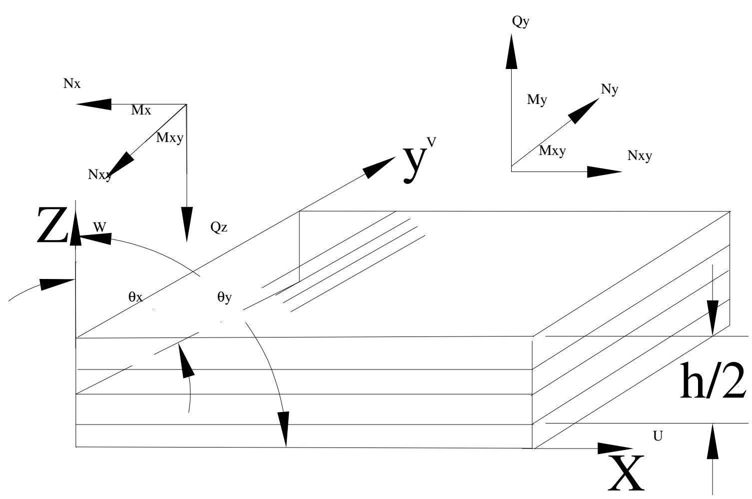

Figure 4.3 The laminated composite plate with positive displacements, rotations and stress resultants.

And the moment resultants are expressed as,

$$\begin{Bmatrix} M_{xx} \\ M_{yy} \\ R_{yz} \\ R_{xz} \\ M_{xy} \end{Bmatrix} = \int_{-h/2}^{h/2} \begin{Bmatrix} \sigma_{xx} \\ \sigma_{yy} \\ \tau_{yz} \\ \tau_{xz} \\ \tau_{xy} \end{Bmatrix} z\,dz \tag{4.16}$$

From Equations (4.15) and (4.16) the stress and moment resultants can be written as

$$\begin{Bmatrix} N_{xx} \\ N_{yy} \\ N_{zz} \\ S_{yz} \\ S_{xz} \\ N_{xy} \\ M_{xx} \\ M_{yy} \\ R_{yz} \\ R_{xz} \\ M_{xy} \end{Bmatrix} = [D] \begin{Bmatrix} \varepsilon^0{}_{xx} \\ \varepsilon^0{}_{yy} \\ \varepsilon^0{}_{zz} \\ \gamma^0{}_{yz} \\ \gamma^0{}_{xz} \\ \gamma^0{}_{xy} \\ k_{xx} \\ k_{yy} \\ k_{yz} \\ k_{xz} \\ k_{xy} \end{Bmatrix} \tag{4.17}$$

Where $$[D] = \begin{Bmatrix} A_{11} & & & & & & & & & & \\ A_{21} & A_{22} & & & & & & & & & \\ A_{31} & A_{32} & A_{33} & & & & & Sym & & & \\ 0 & 0 & 0 & A_{44} & & & & & & & \\ 0 & 0 & 0 & A_{54} & A_{55} & & & & & & \\ A_{61} & A_{62} & A_{63} & 0 & 0 & A_{66} & & & & & \\ B_{11} & B_{12} & B_{13} & 0 & 0 & B_{16} & D_{11} & & & & \\ B_{21} & B_{22} & B_{23} & 0 & 0 & B_{26} & D_{21} & D_{22} & & & \\ 0 & 0 & 0 & B_{44} & B_{45} & 0 & 0 & 0 & D_{44} & & \\ 0 & 0 & 0 & B_{54} & B_{55} & 0 & 0 & 0 & D_{54} & D_{55} & \\ B_{61} & B_{62} & B_{63} & 0 & 0 & B_{66} & D_{61} & D_{62} & 0 & 0 & D_{66} \end{Bmatrix} \tag{4.18}$$

With $$A_{ij}, B_{ij}, D_{ij} = \int_{\frac{-h}{2}}^{\frac{h}{2}} \overline{Q_{ij}} (1, Z, Z^2) dz \tag{4.19}$$

Where, using indicial notation

$$A_{ij} = \sum_{K=1}^{N} \left[\overline{Q_{ij}}\right]_K (Z_K - Z_{K-1}) \qquad \text{Extensional stiffness} \tag{4.20}$$

$$B_{ij} = \frac{1}{2} \sum_{K=1}^{N} \left[\overline{Q_{ij}}\right]_K (Z^2{}_K - Z^2{}_{K-1}) \qquad \text{Coupling Stuffiness} \tag{4.21}$$

$$D_{ij} = \frac{1}{3} \sum_{K=1}^{N} \left[\overline{Q_{ij}}\right]_K (Z_K^3 - Z^3{}_{K-1}) \qquad \text{Bending Stiffness} \tag{4.22}$$

Where $Z_{K-1} = \frac{-h}{2}$ and $Z_K = \frac{h}{2}$

4.1.4 Element Matrices

The element stiffness and element load matrices are given by

$$[K]_e = \iint [B]^T [D][B] dxdy \tag{4.23}$$

$$\{F_e\} = \iint [N]^T \{q_e\} dxdy \tag{4.24}$$

Where $[B]$ and $[D]$ are defined in Equations (4.4) and (4.18), respectively.

4.1.5 Transformation Matrix

The relations between local and global displacements Figure (4.4 are derived as

$$\begin{Bmatrix} u' \\ v' \\ w' \\ \theta'_x \\ \theta'_y \\ \theta'_z \end{Bmatrix} = \begin{bmatrix} \cos(x,x') & \cos(y,x') & \cos(z,x') & 0 & 0 & 0 \\ \cos(x,y') & \cos(y,y') & \cos(z,y') & 0 & 0 & 0 \\ \cos(x,z') & \cos(y,z') & \cos(z,z') & 0 & 0 & 0 \\ 0 & 0 & 0 & -\cos(y,y') & -\cos(x,y') & -\cos(z,y') \\ 0 & 0 & 0 & -\cos(y,x') & \cos(x,x') & -\cos(z,x') \\ 0 & 0 & 0 & \cos(y,z') & -\cos(x,z') & \cos(z,z') \end{bmatrix} \begin{Bmatrix} u \\ v \\ w \\ \theta_x \\ \theta_y \\ \theta_z \end{Bmatrix} \tag{4.25}$$

Finally, the element and mass matrices are transformed to global coordinates using

$$[K]_e = [T]^T [K']_e [T] \tag{4.26}$$

$$\{F\}_e = [T]^T \{F\}_e \tag{4.27}$$

After all the matrices are calculated at element level, assembly is done for the complete structure in banded matrix form and one obtains

$$[K]\{d\} = \{F\} \tag{4.28}$$

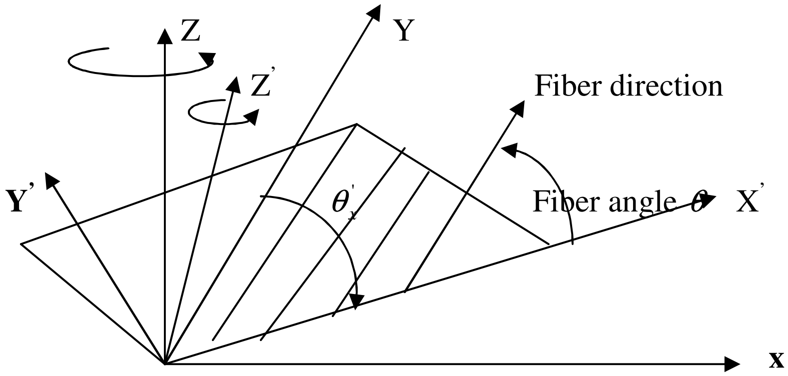

Figure 4.4 Local and Global axis system. The least angle contained between positive x and x' axis denoted as (x, x').

Where $[K]$ is global stiffness matrix, and $\{d\}$ and $\{F\}$are global displacement and force vectors, respectively.

4.2 Dynamic Equations of Motion for Laminated Composite Plate or Shell

In this thesis the equation of motion modeling of a composite plate or shell using finite element method under the assumptions of first order shear deformation theory. The dynamic Characteristic of the structure are studied [37].

4.2.1 First order shear deformation theory

The first order shear deformation theory (FSDT), in the finite element model formulation the equation of motion is stated. The displacement equations under the assumption of FSDT can be written as [37]:

$$\begin{aligned} u(x,y,z,t) &= u_0(x,y,z,t) + z\theta_x(x,y,z,t) \\ v(x,y,z,t) &= v_0(x,y,z,t) + z\theta_y(x,y,z,t) \\ w(x,y,z,t) &= w_0(x,y,z,t) + z\theta_z(x,y,z,t) \end{aligned} \tag{4.29}$$

Where u_0, v_0 & w_0 are the reference surface displacement along x, y &z respectively and θ_x, θ_y and θ_z are the rotational angle of the normal in the xy ,yz and xz planes respectively.

The strain vectors at any point (x,y,z) can be given:

$$\begin{Bmatrix} \varepsilon_x \\ \varepsilon_y \\ \varepsilon_z \\ \gamma_{yz} \\ \gamma_{zx} \\ \gamma_{xy} \end{Bmatrix} = \begin{bmatrix} m^2 & n^2 & 0 & 0 & 0 & mn \\ n^2 & m^2 & 0 & 0 & 0 & -mn \\ 0 & 0 & 1 & 0 & 0 & 0 \\ 0 & 0 & 0 & m & -n & 0 \\ 0 & 0 & 0 & n & m & 0 \\ -2mn & 2mn & 0 & 0 & 0 & (m^2 - n^2) \end{bmatrix} \begin{Bmatrix} \dfrac{\partial u_o}{\partial x} \\ \dfrac{\partial v_o}{\partial y} \\ \dfrac{\partial w_o}{\partial z} \\ \dfrac{\partial w_o}{\partial z} + \theta_y \\ \dfrac{\partial u_o}{\partial x} + \theta_x \\ \dfrac{\partial v_o}{\partial y} + \theta_z \end{Bmatrix} \tag{4.30}$$

In indicial notation

$$\{\varepsilon\} = [T]\{u\} \tag{4.31}$$

Where $m = \cos\theta$ and $n = \sin\theta$ and θ the orintation of fiber

Further considering an Isoperimetric quadratic element, the displacement at any node can be written in terms of shape function.

$$\{u\} = [N_d]\{u_i\} \tag{4.32}$$

Where N_d is shape function.

4.2.2 Internal Work Done

Internal work done by the material layer is given by

$$W_{\text{int}} = \int_v \{\varepsilon\}^T \{\sigma\} dv \tag{4.33}$$

Substitute the stress in terms of the strains using the constitutive relation from equation (4.7)

$$W_{\text{int}} = \int_v \{\varepsilon\}^T \{Q\}\{\varepsilon\} dv \tag{4.34}$$

The expansion of equation (4.34) results in

$$W_{\text{int}} = \{u\}^T \int_v [B]^T [T]^T [Q][T][B] dv \{u\} \tag{4.35}$$

From the relation of equation (4.5) and (4.11) where

$$\{\varepsilon\}^T = [B]^T \{u\}^T$$
$$\{\varepsilon\} = [B]\{u\}$$
$$\{Q\} = [T]^T [Q][T]$$

Further simplification gives:

$$W_{\text{int}} = \{u\}[K]_e\{u\} \tag{4.36}$$

Where $[K_e] = \int_v \{B\}^T [T]^T [Q][T]\{B\} dv$

For a unit thin laminated thickness the above equation will be written as

$$[K_e] = \iint [B]^T [T]^T [Q]^T [T][B] dxdy \tag{4.37}$$

4.2.3 External Work Done

The expression for external work done can be written as:

$$W_{ex} = \int_v \{d\}^T \rho \{d\} dv \tag{4.38}$$

Where $\{d\} = [N][u]$, further substitution and simplification results in to

$$W_{ex} = \{u\}^T \int_v [N]^T \rho [N] dv \left\{ \ddot{U} \right\} \tag{4.39}$$

Where

$$[M] = \int_v [N]^T \rho [N] dv$$

ρ = density of the material

Assuming a proportional or Rayleight damping $[C] = \alpha[M] + \beta[K]$, α and β are constants it can be write in global form

$$[M]\left\{ \ddot{X} \right\} + [C]\left\{ \dot{X} \right\} + [K]\{X\} = \{F\} \tag{4.40}$$

Where M= mass matrix

C= damping coefficient

F= external force

X= nodal displacement

4.2.4 Modal Analysis

$[\phi]$ is the normalized eigen vector matrix,[37] pre multiply both side of equation (4.40) by $[\phi]^T$

$$[\phi]^T [M][\phi]\left\{ \ddot{X} \right\} + [\phi]^T [C][\phi]\left\{ \dot{X} \right\} + [\phi]^T [K][\phi]\{X\} = [\phi]^T \{F\}[\phi] \tag{4.41}$$

Now say

$$
\begin{aligned}
[M_n] &= [\phi]^T [M][\phi] \\
[C_n] &= [\phi]^T [C][\phi] \\
[K_n] &= [\phi]^T [K][\phi] \\
[F_n] &= [\phi]^T [F][\phi]
\end{aligned}
\tag{4.42}
$$

Now from equation (4.41) and (4.42)

$$
[M_n]\left\{\ddot{X}\right\} + [C_n]\left\{\dot{X}\right\} + [K_n]\{X\} = \{F_n\} \tag{4.43}
$$

Where

$$
X = \begin{Bmatrix} u_0 \\ v_0 \\ w_0 \\ \theta_x \\ \theta_y \\ \theta_z \end{Bmatrix} \tag{4.44}
$$

For a free vibration analysis the equation of motion in equation (4.43), the external force will be neglected and the homogenous equation of motion in given by

$$
[M_n]\left\{\ddot{X}\right\} + [C_n]\left\{\dot{X}\right\} + [K_n]\{X\} = 0 \tag{4.45}
$$

4.3 Consequences of Stacking Sequence

The A, B and D Matrix for different lay-up Consider a symmetric about its Mid-plane laminate composed of 0^0 and 90^0 plies the relation of the force and moment gives: -

$$
\begin{aligned}
\begin{Bmatrix} N_x \\ N_y \\ N_{xy} \end{Bmatrix} &= \begin{bmatrix} A_{11} & A_{12} & 0 \\ A_{12} & A_{22} & 0 \\ 0 & 0 & A_{66} \end{bmatrix} \begin{Bmatrix} \varepsilon_x \\ \varepsilon_y \\ \gamma_{xy} \end{Bmatrix} \\
\begin{Bmatrix} M_x \\ M_y \\ M_{xy} \end{Bmatrix} &= \begin{bmatrix} D_{11} & D_{12} & 0 \\ D_{12} & D_{22} & 0 \\ 0 & 0 & D_{66} \end{bmatrix} \begin{Bmatrix} K_x \\ K_y \\ K_{xy} \end{Bmatrix}
\end{aligned}
\tag{4.46}
$$

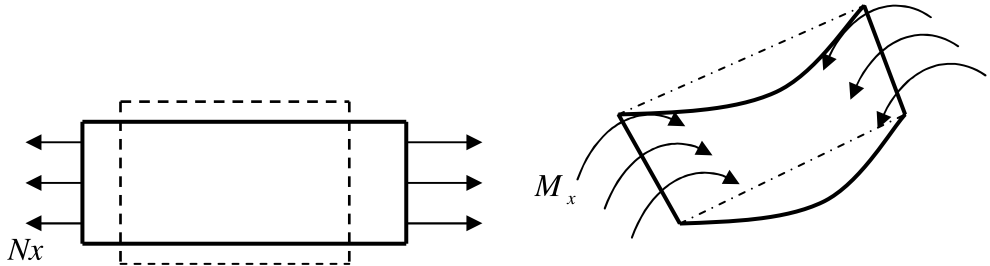

Figure 4.5 Deformation of layer (bending and stretching)

Laminated composed of plies with $+\theta_1,+\theta_2,+\theta_3,+$ but no $-\theta_1,-\theta_2,-\theta_3,-$ and symmetric about its mid-plane but unbalanced ($45^0,22.5^0,22.5^0,45^0$) the relation of the force and moment gives:

$$\begin{Bmatrix} N_x \\ N_y \\ N_{xy} \end{Bmatrix} = \begin{bmatrix} A_{11} & A_{12} & A_{16} \\ A_{12} & A_{22} & A_{26} \\ A_{16} & A_{26} & A_{66} \end{bmatrix} \begin{Bmatrix} \varepsilon_x \\ \varepsilon_y \\ \varepsilon_{xy} \end{Bmatrix}$$
$$\begin{Bmatrix} M_x \\ M_y \\ M_{xy} \end{Bmatrix} = \begin{bmatrix} D_{11} & D_{12} & D_{16} \\ D_{12} & D_{22} & D_{26} \\ D_{16} & D_{26} & D_{66} \end{bmatrix} \begin{Bmatrix} K_x \\ K_y \\ K_{xy} \end{Bmatrix} \tag{4.47}$$

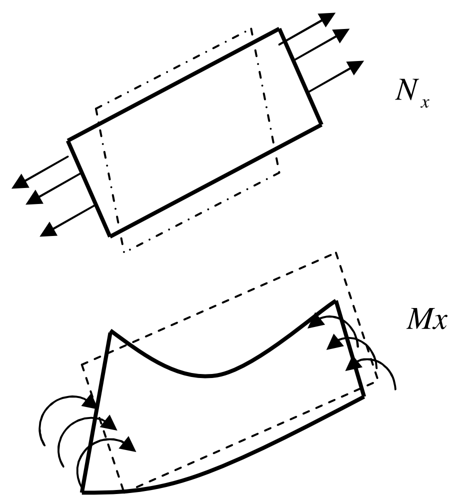

Figure 4.6 Deformation of layer (stretching, shearing, bending and twisting)

The layer is Laminate with symmetric about Mid-plane for every $+\theta$ there is $-\theta$ (Balanced) D_{16} and D_{26} become small for >16 plies $\left[0^0,90^0,45^0,-45^0,-45^0,45^0,90^0,0^0\right]$ the relation of the force and moment gives

$$\begin{Bmatrix} N_x \\ N_y \\ N_{xy} \end{Bmatrix} = \begin{bmatrix} A_{11} & A_{12} & 0 \\ A_{12} & A_{22} & 0 \\ 0 & 0 & A_{66} \end{bmatrix} \begin{Bmatrix} \varepsilon_x \\ \varepsilon_y \\ \varepsilon_{xy} \end{Bmatrix}$$

$$\begin{Bmatrix} M_x \\ M_y \\ M_{xy} \end{Bmatrix} = \begin{bmatrix} D_{11} & D_{12} & D_{16} \\ D_{12} & D_{22} & D_{26} \\ D_{16} & D_{26} & D_{66} \end{bmatrix} \begin{Bmatrix} K_x \\ K_y \\ K_{xy} \end{Bmatrix} \tag{4.48}$$

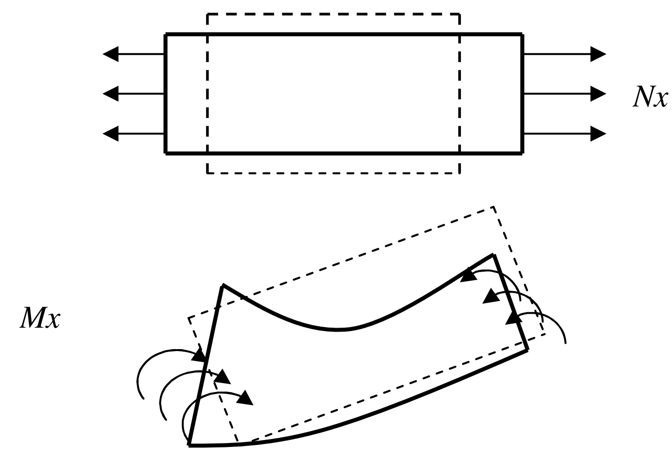

Figure 4.7 Deformation of layer (stretching, bending and twisting)

Anti-symmetric about its Mid-plane laminate composed of 0^0 and 90^0 plies the relation of the force and moment gives: - $\left(90^0, 0^0, 90^0, 0^0\right)$

$$\begin{Bmatrix} N_x \\ N_y \\ N_{xy} \end{Bmatrix} = \begin{bmatrix} A_{11} & A_{12} & 0 \\ A_{12} & A_{22} & 0 \\ 0 & 0 & A_{66} \end{bmatrix} \begin{Bmatrix} \varepsilon_x \\ \varepsilon_y \\ \gamma_{xy} \end{Bmatrix} + \begin{bmatrix} B_{11} & 0 & 0 \\ 0 & B_{22} & 0 \\ 0 & 0 & 0 \end{bmatrix} \begin{Bmatrix} K_x \\ K_y \\ K_{xy} \end{Bmatrix}$$

$$\begin{Bmatrix} M_x \\ M_y \\ M_{xy} \end{Bmatrix} = \begin{bmatrix} B_{11} & 0 & 0 \\ 0 & B_{22} & 0 \\ 0 & 0 & 0 \end{bmatrix} \begin{Bmatrix} \varepsilon_x \\ \varepsilon_y \\ \gamma_{xy} \end{Bmatrix} + \begin{bmatrix} D_{11} & D_{12} & 0 \\ D_{12} & D_{22} & 0 \\ 0 & 0 & D_{66} \end{bmatrix} \begin{Bmatrix} K_x \\ K_y \\ K_{xy} \end{Bmatrix} \tag{4.49}$$

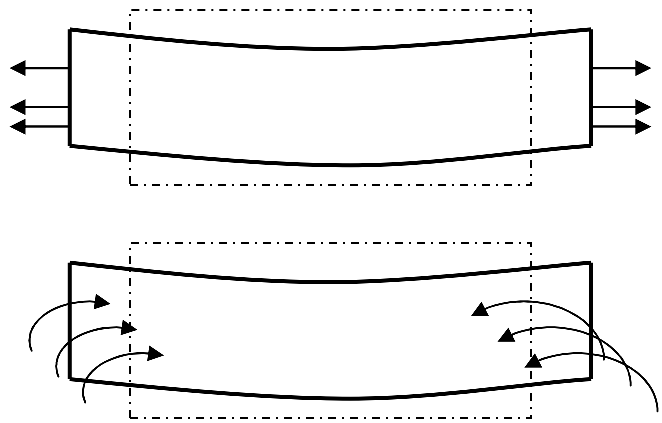

Figure 4.8 Deformation of layer (stretching and bending)

The layer is laminate with Anti-symmetric about the mid-plane with composed of $+\theta$'s and -θ's plies, balanced $\left[45^0,-45^0,45^0,-45^0\right]$

$$\begin{Bmatrix} N_x \\ N_y \\ N_{xy} \end{Bmatrix} = \begin{bmatrix} A_{11} & A_{12} & 0 \\ A_{12} & A_{22} & 0 \\ 0 & 0 & A_{66} \end{bmatrix} \begin{Bmatrix} \varepsilon_x \\ \varepsilon_y \\ \gamma_{xy} \end{Bmatrix} + \begin{bmatrix} 0 & 0 & B_{16} \\ 0 & 0 & B_{26} \\ B_{16} & B_{26} & 0 \end{bmatrix} \begin{Bmatrix} K_x \\ K_y \\ K_{xy} \end{Bmatrix}$$

$$\begin{Bmatrix} M_x \\ M_y \\ M_{xy} \end{Bmatrix} = \begin{bmatrix} 0 & 0 & B_{16} \\ 0 & 0 & B_{26} \\ B_{16} & B_{26} & 0 \end{bmatrix} \begin{Bmatrix} \varepsilon_x \\ \varepsilon_y \\ \gamma_{xy} \end{Bmatrix} + \begin{bmatrix} D_{11} & D_{12} & 0 \\ D_{12} & D_{22} & 0 \\ 0 & 0 & D_{66} \end{bmatrix} \begin{Bmatrix} K_x \\ K_y \\ K_{xy} \end{Bmatrix} \tag{4.50}$$

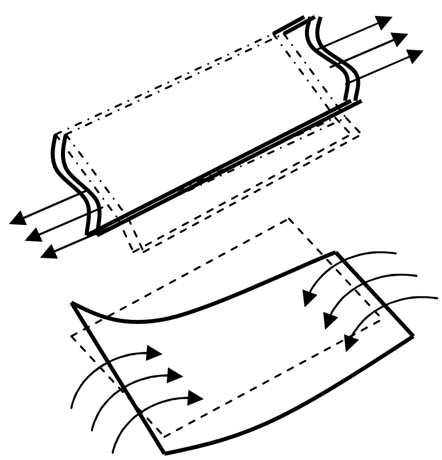

Figure 4.9 Deformation of layer (stretching, twisting, bending and shearing)

The layer is general laminate with not symmetry and no balanced about the mid –plane with composed of $\left[0^0,45^0,90^0,22.5^0,0^0,45^0\right]$ the force and moment equation gives:-

$$\begin{Bmatrix} N_x \\ N_y \\ N_{xy} \end{Bmatrix} = \begin{bmatrix} A_{11} & A_{12} & A_{16} \\ A_{12} & A_{22} & A_{22} \\ A_{16} & A_{26} & A_{66} \end{bmatrix} \begin{Bmatrix} \varepsilon_x \\ \varepsilon_y \\ \gamma_{xy} \end{Bmatrix} + \begin{bmatrix} B_{11} & B_{12} & B_{16} \\ B_{12} & B_{22} & B_{26} \\ B_{16} & B_{26} & B_{66} \end{bmatrix} \begin{Bmatrix} K_x \\ K_y \\ K_{xy} \end{Bmatrix}$$
$$\begin{Bmatrix} M_x \\ M_y \\ M_{xy} \end{Bmatrix} = \begin{bmatrix} B_{11} & B_{12} & B_{16} \\ B_{12} & B_{22} & B_{22} \\ B_{16} & B_{26} & B_{66} \end{bmatrix} \begin{Bmatrix} \varepsilon_x \\ \varepsilon_y \\ \gamma_{xy} \end{Bmatrix} + \begin{bmatrix} D_{11} & D_{12} & D_{16} \\ D_{12} & D_{22} & D_{26} \\ D_{16} & D_{26} & D_{66} \end{bmatrix} \begin{Bmatrix} K_x \\ K_y \\ K_{xy} \end{Bmatrix} \quad (4.51)$$

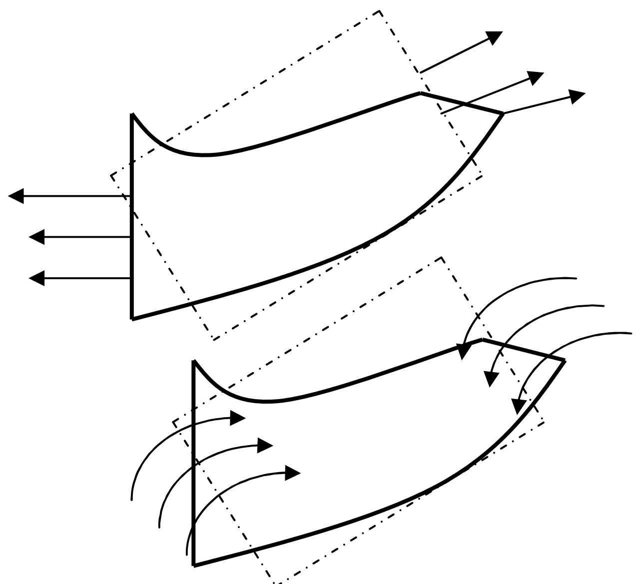

Figure 4.10 Deformation of layer (stretching, shearing, bending and twisting)

CHAPTER FIVE

5. SUBSONIC AND SUPERSONIC AIRCRAFT WING MODEL DESCRIPTION AND CASE STUDIES FOR BENDING-TORSION DECOUPLING

5.1 Physical Model of subsonic Aircraft wing

The physical structure modeled in this work is a monocoque aircraft wing of airfoil cross section NACA8516 series [20] with fiber laminated composite structure, shown in Figure (5.1). Its dimensions are that of a research subsonic aircraft wing. The chord length at the free end is 1.4m and at the fixed end is 2.8m while the length of [9] the wing is 6.096m. The thickness of the monocoque wing for some spatial distance is treated as to reduce the twist angle parameter.

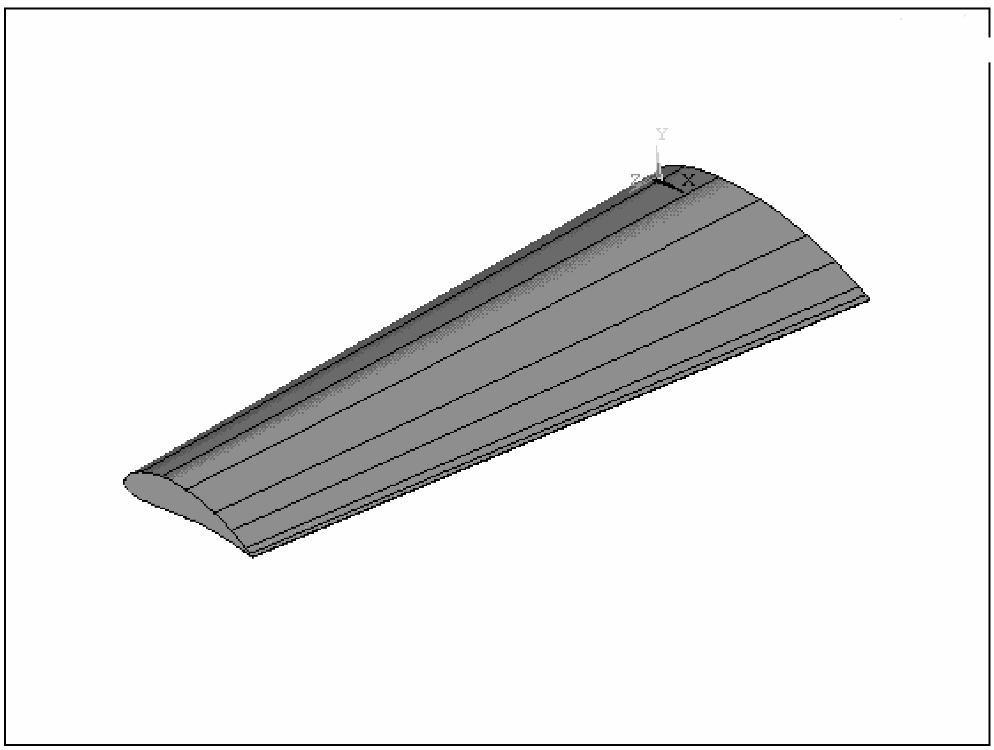

Figure 5.1 Physical model of subsonic aircraft wing

The dimension of this model is a tapered aircraft wing. It is made of a current; carbon- epoxy laminated composite structure without any ribs and longirons

5.1.1 Case Studies for Reducing the Twist Angle Parameter of Subsonic Aircraft Wing To Achieve Bending –Torsion Decoupling

The model is include the following parameter as shown in the table from table (5.1) to table (5.7), that used for reducing the bending-twist coupling effect, and figure (5.2) shows the location of thickness variation along the contour of the airfoil section.

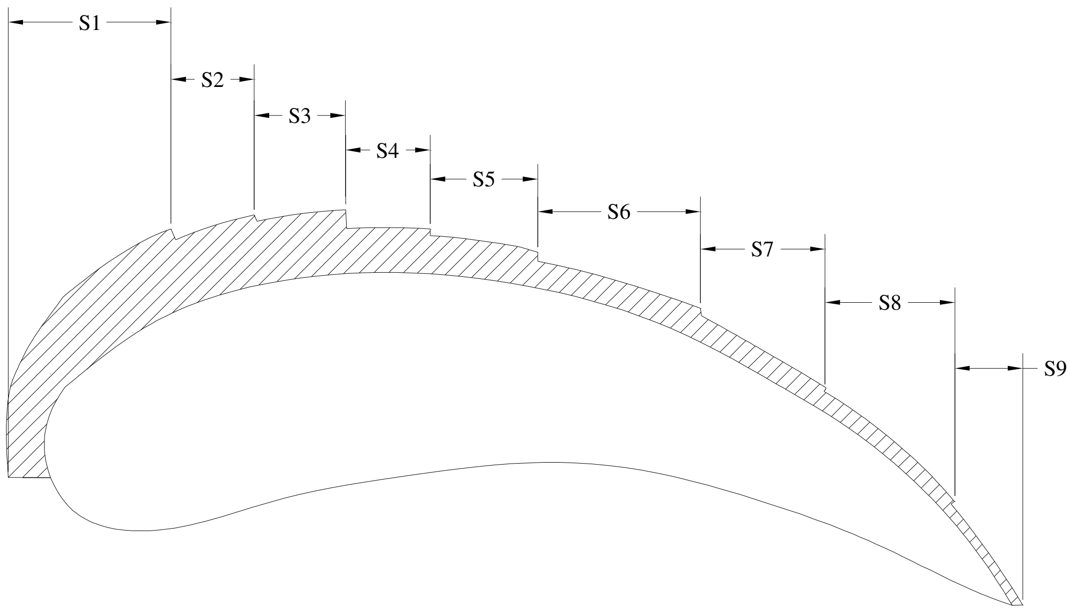

Figure 5.2 Airfoil cross section with variation of thickness

Table 5.1 Variation of stack angle for the thickness varition-1 in the subsonic aircraft wing

Models	Laminated Thickness(thickness variation is symmetrical with respect to the chord)	Angle of orientation
Case-1	S_1=6mm, S_2=5.5mm, S_3=5mm, S_4=4.5mm, S_5=4mm, S_6=3.5mm, S_7=3mm, S_8=2.5mm, S_9=2 mm	Cross-ply (antisymmetric) all along the contour of the airfoil
Case -2	S_1=6mm, S_2=5.5mm, S_3=5mm, S_4=4.5mm, S_5=4mm, S_6=3.5mm, S_7=3mm, S_8=2.5mm, S_9=2 mm	Upper camber cross-ply (antisymmetric)and lower angle ply(antisymmetric) of the airfoil
Case -3	S_1=6mm, S_2=5.5mm, S_3=5mm, S_4=4.5mm, S_5=4mm, S_6=3.5mm, S_7=3mm, S_8=2.5mm, S_9=2 mm	Angle-ply (antisymmetric) all along the contour of the airfoil
Case -4	S_1=6mm, S_2=5.5mm, S_3=5mm, S_4=4.5mm, S_5=4mm, S_6=3.5mm, S_7=3mm, S_8=2.5mm, S_9=2 mm	Angle-ply symmetrical all along the contour of the airfoil
Case -5	S_1=6mm, S_2=5.5mm, S_3=5mm, S_4=4.5mm, S_5=4mm, S_6=3.5mm, S_7=3mm, S_8=2.5mm, S_9=2 mm	Upper camber angle-ply (antisymmetric)and lower cross ply(antisymmetric) of the airfoil

Table 5.2 Variation of stack angle for the thickness vaition-2 in the subsonic aircraft wing

Models	Laminated Thickness(thickness variation is symmetrical with respect to the chord)	Angle of orientation
Case -6	S_1=5mm, $S_{2=}$4.5mm, $S_{3=}$4mm, $S_{4=}$4.5mm, $S_{5=}$3.5mm, $S_{6=}$3mm, $S_{7=}$2.5mm, $S_{8=}$2mm, $S_{9=}$1.5 mm	Cross-ply (antisymmetric) all along the contour of the airfoil
Case -7	S_1=5mm, $S_{2=}$4.5mm, $S_{3=}$4mm, $S_{4=}$4.5mm, $S_{5=}$3.5mm, $S_{6=}$3mm, $S_{7=}$2.5mm, $S_{8=}$2mm, $S_{9=}$1.5 mm	Upper camber cross-ply (antisymmetric)and lower angle ply(antisymmetric) of the airfoil
Case -8	S_1=5mm, $S_{2=}$4.5mm, $S_{3=}$4mm, $S_{4=}$4.5mm, $S_{5=}$3.5mm, $S_{6=}$3mm, $S_{7=}$2.5mm, $S_{8=}$2mm, $S_{9=}$1.5 mm	Angle-ply (antisymmetric) all along the contour of the airfoil
Case -9	S_1=5mm, $S_{2=}$4.5mm, $S_{3=}$4mm, $S_{4=}$4.5mm, $S_{5=}$3.5mm, $S_{6=}$3mm, $S_{7=}$2.5mm, $S_{8=}$2mm, $S_{9=}$1.5 mm	Angle-ply symmetrical all along the contour of the airfoil
Case -10	S_1=5mm, $S_{2=}$4.5mm, $S_{3=}$4mm, $S_{4=}$4.5mm, $S_{5=}$3.5mm, $S_{6=}$3mm, $S_{7=}$2.5mm, $S_{8=}$2mm, $S_{9=}$1.5 mm	Upper camber angle-ply (antisymmetric)and lower cross ply(antisymmetric) of the airfoil

Table 5.3 Variation of stack angle for the thickness vaition-3 in the subsonic aircraft wing

Models	Laminated Thickness(thickness variation is symmetrical with respect to the chord)	Angle of orientation
Case -11	S_1=4mm, $S_{2=}$3.75mm, $S_{3=}$3.5mm, $S_{4=}$3.25mm, $S_{5=}$3mm, $S_{6=}$2.75mm, $S_{7=}$2.5mm, $S_{8=}$2.25mm, $S_{9=}$2 mm	Cross-ply (antisymmetric) all along the contour of the airfoil
Case -12	S_1=4mm, $S_{2=}$3.75mm, $S_{3=}$3.5mm, $S_{4=}$3.25mm, $S_{5=}$3mm, $S_{6=}$2.75mm, $S_{7=}$2.5mm, $S_{8=}$2.25mm, $S_{9=}$2 mm	Upper camber cross-ply (antisymmetric)and lower angle ply(antisymmetric) of the airfoil
Case -13	S_1=4mm, $S_{2=}$3.75mm, $S_{3=}$3.5mm, $S_{4=}$3.25mm, $S_{5=}$3mm, $S_{6=}$2.75mm, $S_{7=}$2.5mm, $S_{8=}$2.25mm, $S_{9=}$2 mm	Angle-ply (antisymmetric) all along the contour of the airfoil
Case -14	S_1=4mm, $S_{2=}$3.75mm, $S_{3=}$3.5mm, $S_{4=}$3.25mm, $S_{5=}$3mm, $S_{6=}$2.75mm, $S_{7=}$2.5mm, $S_{8=}$2.25mm, $S_{9=}$2 mm	Angle-ply symmetrical all along the contour of the airfoil
Case -15	S_1=4mm, $S_{2=}$3.75mm, $S_{3=}$3.5mm, $S_{4=}$3.25mm, $S_{5=}$3mm, $S_{6=}$2.75mm, $S_{7=}$2.5mm, $S_{8=}$2.25mm, $S_{9=}$2 mm	Upper camber angle-ply (antisymmetric)and lower cross ply(antisymmetric) of the airfoil

Table 5.4 Variation of stack angle for the thickness vaition-4 in the subsonic aircraft wing

Models	Laminated Thickness(thickness variation is symmetrical with respect to the chord)	Angle of orientation
Case -16	S_1=5mm, $S_{2=}$5mm, $S_{3=}$5mm, $S_{4=}$5mm, $S_{5=}$5mm, $S_{6=}$5mm, $S_{7=}$5mm, $S_{8=}$5mm, $S_{9=}$5 mm	Cross-ply (antisymmetric) all along the contour of the airfoil
Case -17	S_1=5mm, $S_{2=}$5mm, $S_{3=}$5mm, $S_{4=}$5mm, $S_{5=}$5mm, $S_{6=}$5mm, $S_{7=}$5mm, $S_{8=}$5mm, $S_{9=}$5 mm	Upper camber cross-ply (antisymmetric)and lower angle ply(antisymmetric) of the airfoil
Case -18	S_1=5mm, $S_{2=}$5mm, $S_{3=}$5mm, $S_{4=}$5mm, $S_{5=}$5mm, $S_{6=}$5mm, $S_{7=}$5mm, $S_{8=}$5mm, $S_{9=}$5 mm	Angle-ply (antisymmetric) all along the contour of the airfoil
Case -19	S_1=5mm, $S_{2=}$5mm, $S_{3=}$5mm, $S_{4=}$5mm, $S_{5=}$5mm, $S_{6=}$5mm, $S_{7=}$5mm, $S_{8=}$5mm, $S_{9=}$5 mm	Angle-ply symmetrical all along the contour of the airfoil
Case -20	S_1=5mm, $S_{2=}$5mm, $S_{3=}$5mm, $S_{4=}$5mm, $S_{5=}$5mm, $S_{6=}$5mm, $S_{7=}$5mm, $S_{8=}$5mm, $S_{9=}$5 mm	Upper camber angle-ply (antisymmetric)and lower cross ply(antisymmetric) of the airfoil

Table 5.5 Variation of stack angle for the thickness vaition-5 in the subsonic aircraft wing

Models	Laminated Thickness(thickness variation is symmetrical with respect to the chord)	Angle of orientation
Case -21	S_1=4mm, S_2=4mm, S_3=4mm, S_4=4mm, S_5=4mm, S_6=4mm, S_7=4mm, S_8=4mm, S_9=4 mm	Cross-ply (antisymmetric) all along the contour of the airfoil
Case -22	S_1=4mm, S_2=4mm, S_3=4mm, S_4=4mm, S_5=4mm, S_6=4mm, S_7=4mm, S_8=4mm, S_9=4 mm	Upper camber cross-ply (antisymmetric)and lower angle ply(antisymmetric) of the airfoil
Case -23	S_1=4mm, S_2=4mm, S_3=4mm, S_4=4mm, S_5=4mm, S_6=4mm, S_7=4mm, S_8=4mm, S_9=4 mm	Angle-ply (antisymmetric) all along the contour of the airfoil
Case -24	S_1=4mm, S_2=4mm, S_3=4mm, S_4=4mm, S_5=4mm, S_6=4mm, S_7=4mm, S_8=4mm, S_9=4 mm	Angle-ply symmetrical all along the contour of the airfoil
Case -25	S_1=4mm, S_2=4mm, S_3=4mm, S_4=4mm, S_5=4mm, S_6=4mm, S_7=4mm, S_8=4mm, S_9=4 mm	Upper camber angle-ply (antisymmetric)and lower cross ply(antisymmetric) of the airfoil

Table 5.6 Variation of stack angle for the thickness vaition-6 in the subsonic aircraft wing

Models	Laminated Thickness(thickness variation is symmetrical with respect to the chord)	Angle of orientation
Case -26	S_1=3mm, S_2=3mm, S_3=3mm, S_4=3mm, S_5=3mm, S_6=3mm, S_7=3mm, S_8=3mm, S_9=3 mm	Cross-ply (antisymmetric) all along the contour of the airfoil
Case -27	S_1=3mm, S_2=3mm, S_3=3mm, S_4=3mm, S_5=3mm, S_6=3mm, S_7=3mm, S_8=3mm, S_9=3 mm	Upper camber cross-ply (antisymmetric)and lower angle ply(antisymmetric) of the airfoil
Case -28	S_1=3mm, S_2=3mm, S_3=3mm, S_4=3mm, S_5=3mm, S_6=3mm, S_7=3mm, S_8=3mm, S_9=3 mm	Angle-ply (antisymmetric) all along the contour of the airfoil
Case -29	S_1=3mm, S_2=3mm, S_3=3mm, S_4=3mm, S_5=3mm, S_6=3mm, S_7=3mm, S_8=3mm, S_9=3 mm	Angle-ply symmetrical all along the contour of the airfoil
Case -30	S_1=3mm, S_2=3mm, S_3=3mm, S_4=3mm, S_5=3mm, S_6=3mm, S_7=3mm, S_8=3mm, S_9=3 mm	Upper camber angle-ply (antisymmetric)and lower cross ply(antisymmetric) of the airfoil

Table 5.7 Variation of stack angle for the thickness vaition-7 in the supersonic aircraft wing

Models	Laminated Thickness(thickness variation is symmetrical with respect to the chord)	Angle of orientation
Case -31	S_1=6mm, $S_{2=}$5mm, $S_{3=}$5mm, $S_{4=}$6mm	Cross-ply (antisymmetric) all along the contour of the airfoil
Case -32	S_1=6mm, $S_{2=}$5mm, $S_{3=}$5mm, $S_{4=}$6mm	Upper camber cross-ply (antisymmetric)and lower angle ply(antisymmetric) of the airfoil
Case -33	S_1=6mm, $S_{2=}$5mm, $S_{3=}$5mm, $S_{4=}$6mm	Angle-ply (antisymmetric) all along the contour of the airfoil
Case -34	S_1=6mm, $S_{2=}$5mm, $S_{3=}$5mm, $S_{4=}$6mm	Angle-ply symmetrical all along the contour of the airfoil
Case -35	S_1=6mm, $S_{2=}$5mm, $S_{3=}$5mm, $S_{4=}$6mm	Upper camber angle-ply (antisymmetric)and lower cross ply(antisymmetric) of the airfoil

5.1.2 ANSYS Solutions

By using commercial software ANSYS, NACA8516 airfoil geometry was generated, to get the first ten modes shapes. The procedures involved in the ANSYS usage is listed below.

5.1.2.1 Define Structural Analysis

Structural analysis is used to determine deformation, stain, stress, modal analysis harmonic analysis and other structural analysis. To define structure follows the menu sequence:-

Main menu ►Preference ►Structural

5.1.2.2 Types of Element

Shell-99 is an element on defined the model, it is an 8-node 3D shell with six dgree of freedom at each node. It is layer composite structural material; each element is made of the same orthotropic material. To define element follow the menu sequence:-

Main menu ►Preprocess ►element type► Add/edit/delete

5.1.2.3 Real Constant

Real constants are used for geometric properties that can not be completely defined by elements geometry. Shell-99 element will defined material properties (MAT), layer orientation (THETA) and layer thickness (TK). On the dialog box shown in Appendix B.1 Define the real constant follow the menu sequence:-

Main menu ►Preprocess ►Real constant ► Add/edit/delete

5.1.2.4 Layer section

Figure B.2 shows that the layer section, that defined shell-99 structure on real constant i.e material properties, layer orientation and thickness of shell. Define layer sections follow the menu sequence:-

Main menu ►Preprocess ►Section ►shell ►lay-up ►Add/edit

5.1.2.5 Material properties

Typical fiber-reinforced composite contain orthotropic materials, material of composite were defined on the following menu sequence:-

Main menu►Preprocess►Material properties ►Material Models►Structural►linear► elastic ►Orthotropic and density

5.1.2.6 Displacement constraints

The model is treated as cantilever, fixed at one end and free at the other end. The displacement constraints can be applied through the following menu sequences.

Main menu►Solution►Defined load►Apply►Structural►Displacement ►By line

5.1.2.7 Meshing

Since the shape function for shell-99 is an 8 node element, mesh the model based on the defined geometry properties on real constant as shown in figure B.1, finally select quadratic shape from mesh tools menu. To mesh the model follows the menu sequence:-

Main menu►Preprocess►Meshing►Mesh atribute►By pick area►Mesh tools

5.1.2.8 Solution

The procedure for modal analysis, defined the analysis type and analysis option, and begin the finite element solution for the natural frequencies define the analysis type as modal using the following menu sequence.

Main menu►Solutions►New analysis►Modal. In the analysis option menu choose one of the extraction methods of the mode (i.e. Block Lanzors) methods.

5.1.2.9 Solve

Using the following menu sequence solve the solution for the modal analysis

Main menu►Solutions►solve►current LS

5.1.2.10 Review the Result

Results from a modal analysis (i.e. the modal expansion pass) are written to the structural results; the results consist of natural frequencies expand mode shape, relative stress. using the following menu sequence extract the results and mode shape.

Main menu►General postprocessor►Read result►by pick►natural frequency. And extract mode shape using; Main menu►General postprocessor►plot result►deformed shape►contour display

5.1.3 Finite Element Model of subsonic aircraft wing

Analyses are performed in this study by using a finite element model of the aircraft wing. The model was developed in ANSYS; it has 7282 element, 21923 nodes and 10 layers. Each thickness of the layer in different spatial locations are treated as to reduce twist angle parameter. A typical finite element mesh is shown in Figure (5.3) , an enlarged view figure (5.4) and the layer stacking sequence are shown in figure (5.5). The global z coordinate is directed along the axis of the wing, while the global x coordinate is directed along the chord and the global y direction is perpendicular to both.

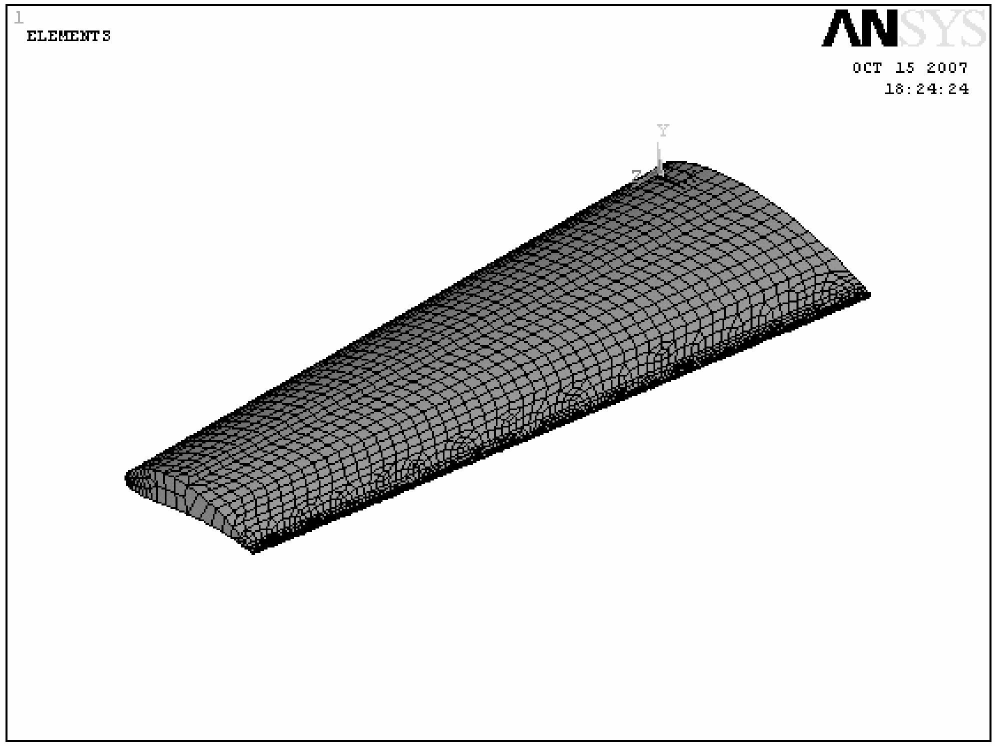

Figure 5.3 finite element models for subsonic wing.

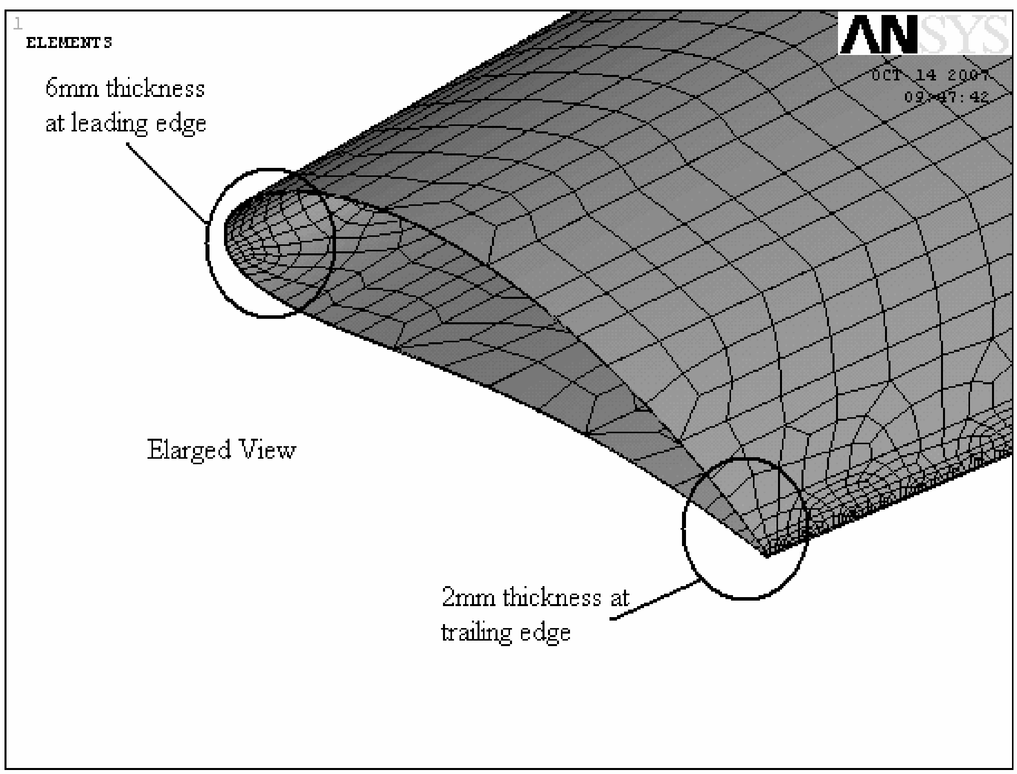

Figure 5.4 Enlarged cross sectional view, with the variation of thickness (subsonic wing)

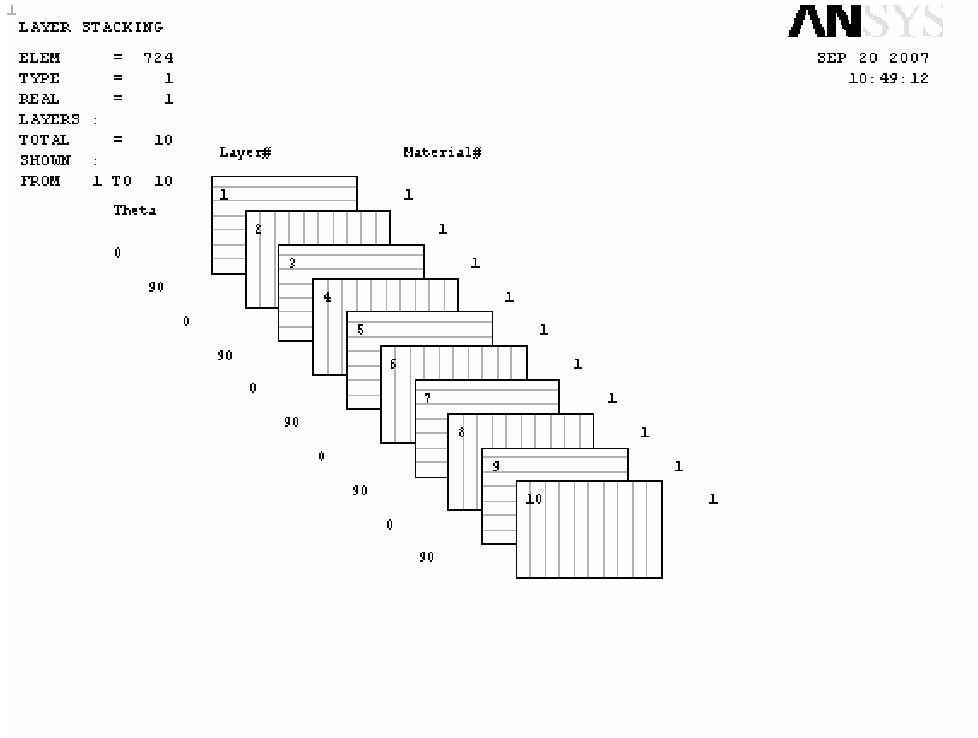

Figure 5.5 Layer stacking sequence of laminated Composite structure (subsonic wing)

5.1.4 Material Properties

The material properties used throughout this study are shown in Table (5.8). These properties are for a carbon/epoxy material is :

Table (5.8) Material Properties (Carbon- epoxy)

Property	Value
E_l	140GN/m^2
E_t	35GN/m^2
G_{lt}	42GN/m^2
υ_{lt}	0.4
ρ	1540Kg/m^3

5.1.5 Boundary Condition

The wing is treated as cantilevered shell. That is fixed at one end (i.e all DOF) and free at the other end, as shown in the figure(5.6)

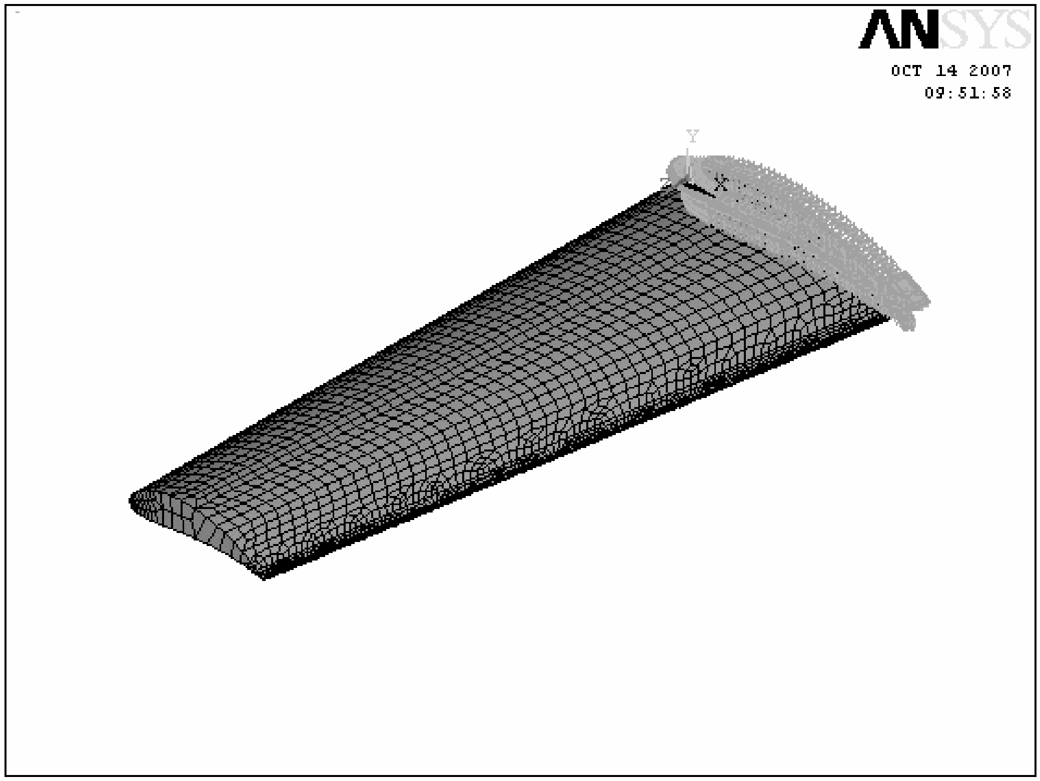

Figure 5.6 F.E Model with the boundary condition(subsonic wing)

5.2 Physical Model of supersonic Aircraft wing

The physical structure modeled in this research is a supersonic aircraft wing, of monocoque structure. It is a laminated composite structure as shown in Figure (5.7). Its dimensions are chord length at the free end 1.4m and 2.8m at the fixed end with a length of 5m. The thickness of this monocoque wing in spatial locations are treated as to reduce the twist angle parameter.

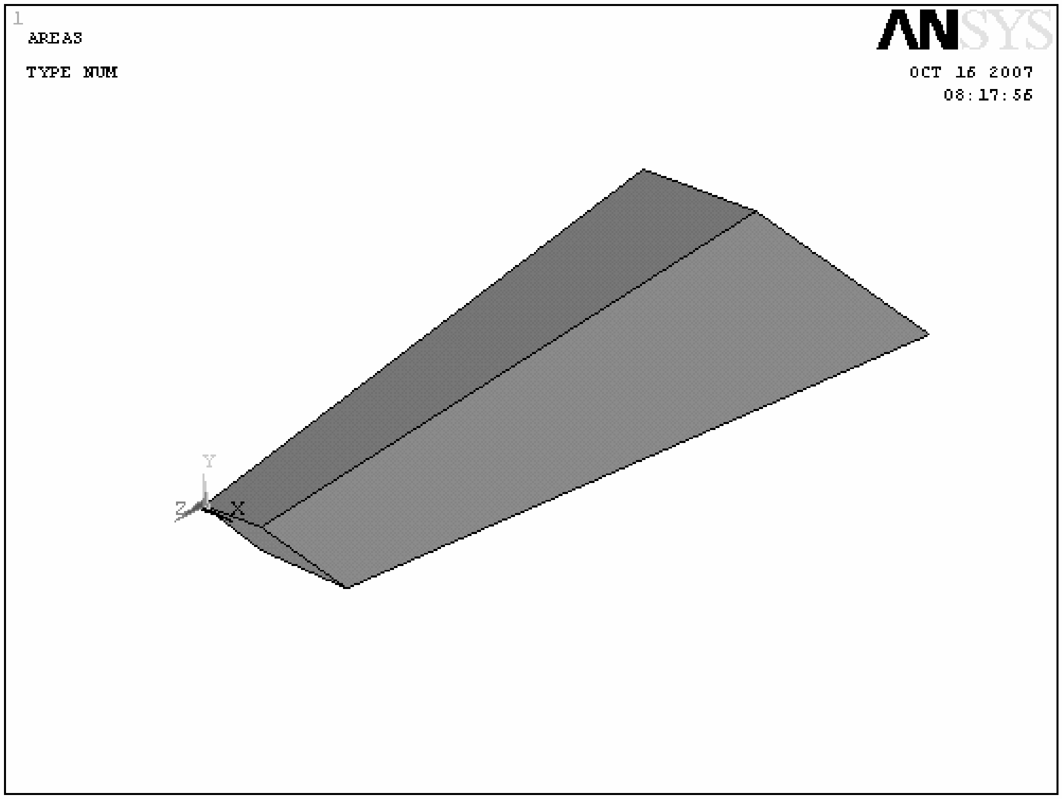

Figure 5.7 Physical Model of the supersonic wing

5.2.1 Case Studies for Reducing the Twist Angle Parameter of Supersonic Aircraft Wing To Achieve Bending –Torsion Decoupling

The model is set similar to subsonic aircraft wing shown from Table (5.1) to Table (5.7), which is used to reduce the bending-torsion coupling effect in the case of supersonic aircraft model.

5.2.2 ANSYS Solutions

By using commercial software ANSYS, a FE model was generated for the supersonic wing to get the first ten modes shapes.

5.2.3 Finite Element Model of supersonic aircraft wing

The finite element model of the supersonic aircraft wing is as shown in figure (5.7). The model was developed in ANSYS, It has 647 element, 1998 nodes and 10 layers. Each thickness of the layer treated as to reducing the twist angle parameter. The finite element mesh is shown in Figure (5.8) and an enlarged view in figure (5.9) with the layer stacking sequence in figure (5.10). The global z coordinate is directed along the axis of the wing, while the global x coordinate is directed along the chord and the global y direction is perpendicular to both.

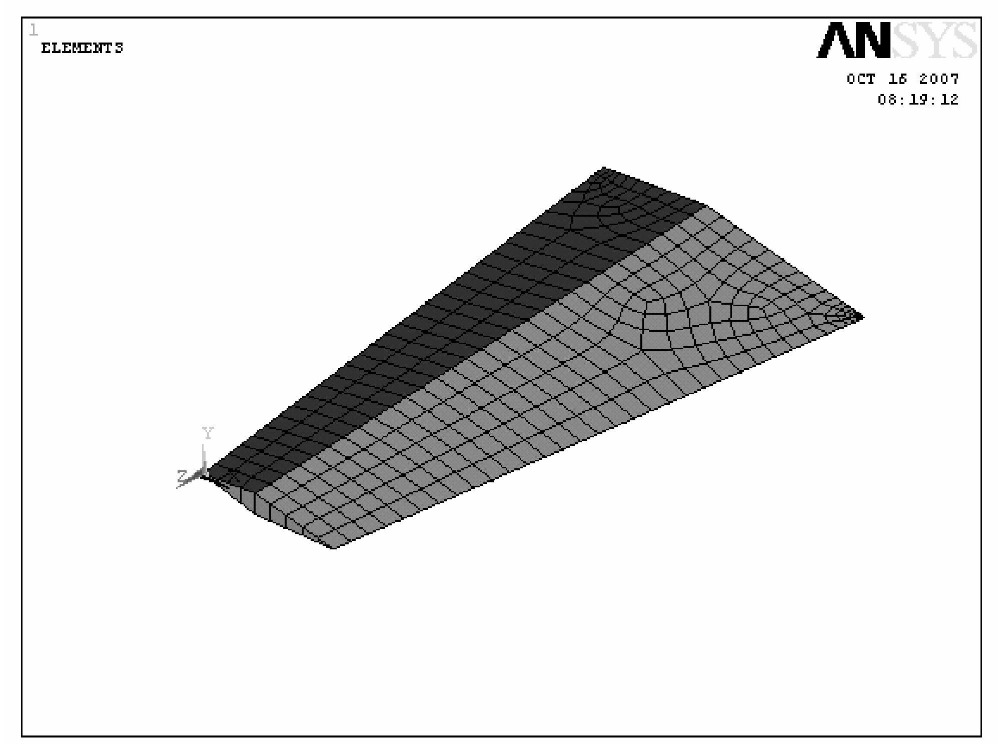

Figure 5.8 Finite element model of the Supersonic wing

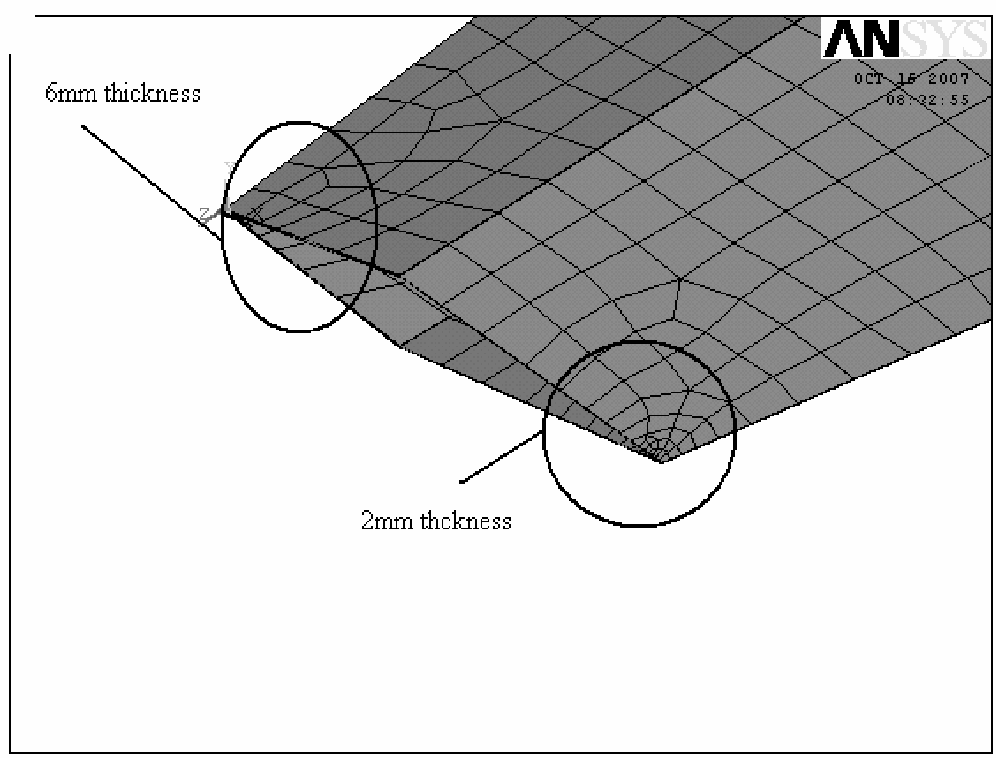

Figure 5.9 Enlarged cross sectional view, with the variation of thickness (supersonic wing)

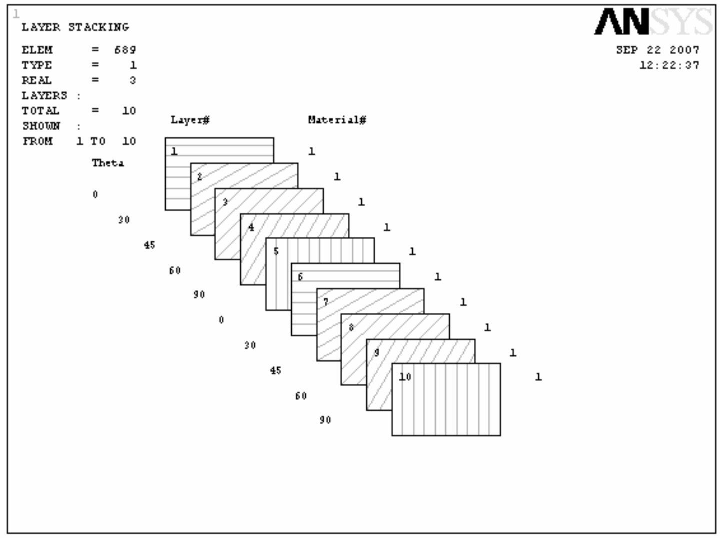

Figure 5.10 Layer stacking sequence of laminated Composite structure (supersonic wing)

5.2.4 Material Properties

The material properties used throughout the model of supersonic is similar to that of subsonic aircraft wing shown in Table (5.8). That is the properties of carbon-epoxy material; it is a laminated type composite structure.

5.2.5 Boundary Condition

Since the wing is treated as cantilever structure. That is fixed at one end (i.e all DOF)and free at the other end, as shown in the figure(5.11)

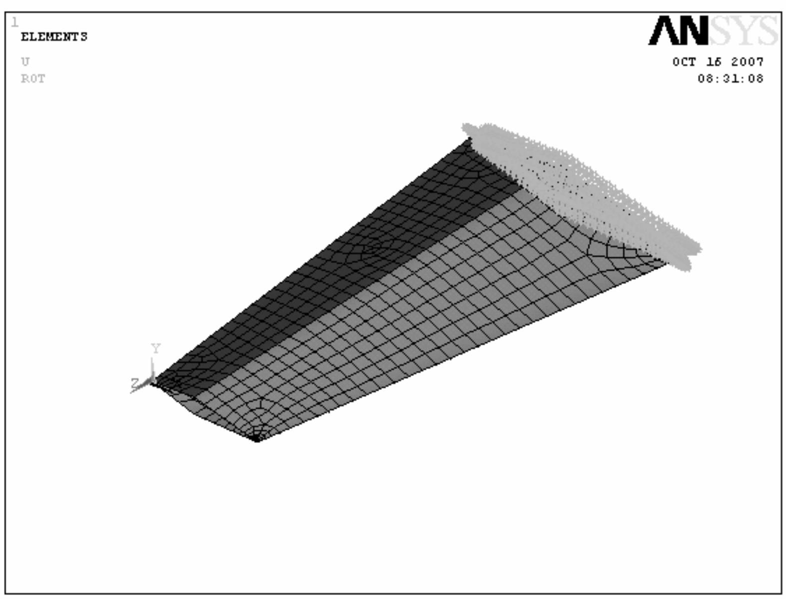

Figure 5.11 F.E Model with the boundary condition (supersonic wing)

5.3 Reduction of Bending-Torsion Coupling Flow Chart

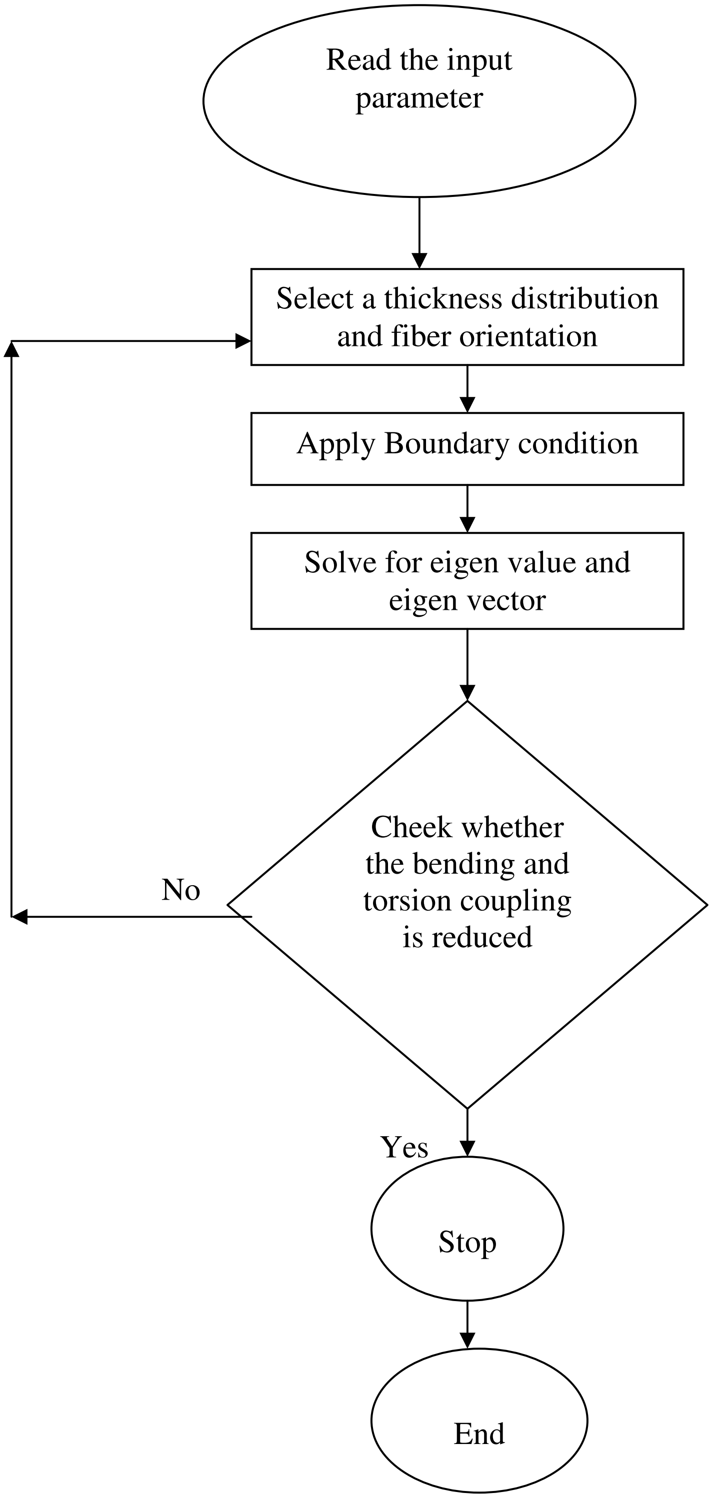

Figure 5.12 Flow chart for reduced bending-torsion coupling effect

CHAPTER Six

RESULTS AND DISCUSSION

6.1. Results

The outputs of simulation, which are related to the objectives of the thesis are interpreted and discussed under this chapter, by varying the influenced parameter.

The effect of fiber angle orientation through the contour of the model (subsonic and supersonic) aircraft wing and the effect of thickness variation along the chord until the bending-torsion decouple occur. Figure (6.1.) and figure (6.2) summarized different case study made on this research. Figure (6.1) shows twist angle parameter (which is proportional to the bending-torsion coupling magnitude) for all modes and all cases. Figure (6.3 - 6.8) represent the effect of ply orientation for a specific special thickness distribution of the subsonic Aircraft wing.

Figure (6.2) show the variation of twist angle parameter for different parameter cases for the first ten modes of supersonic aircraft wing similar to that of fig (6.1) which is depict the subsonic case. In figure (6.9 -6.15) the effect of stack orientation on supersonic aircraft wing for a particular thickness distribution is shown. In appendix (A) shows the coordinates of NACA 8516 airfoil geometry given in table (A-1). In appendix (D) and appendix (E) all the results presented in this thesis by vary different permanent for all cases of wing structure.

In appendix (F) and appendix (G) shows mode shape contour results of the bending- torsion coupling is minimal model characteristic, when compared to other models.

6.2. Discussion

It is worth noting the angle "θ" obtain by this study is on mode shape, hence it is only relative value and thus it is called here as twist angle parameter. However the mode shape those are relative along contributes the response. Hence attempting the decoupling bending-torsion in the mode shape is equally valid for the aroeclastic dynamic response.

From figure (6.1) (subsonic air craft wing) case-5 the optimal distribution of thickness of the airfoil to get minimum bending-torsion coupling in the first ninth modes. That is when the thickness variation as given in table (5.1) case -5 the optimal distribution of special thickness of aircraft wing is obtained.

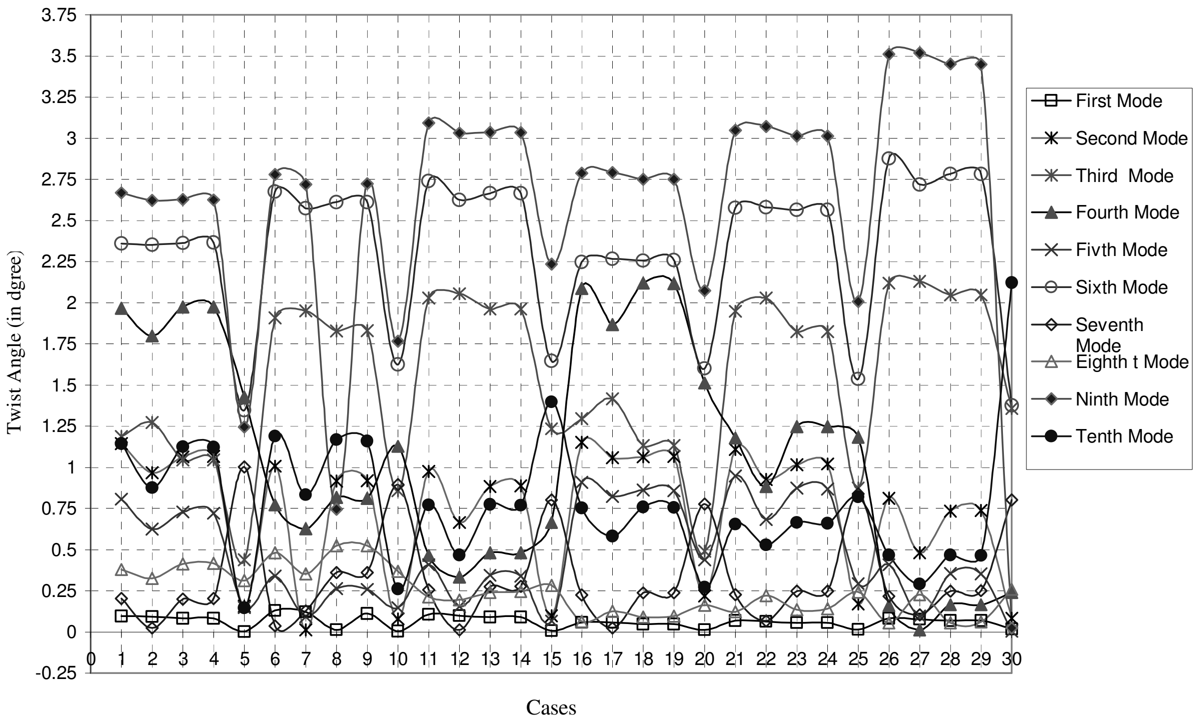

Figure 6.1 Twist angle parameter in all cases for the first ten modes (subsonic aircraft wing)

It may be noted in case-5 the shear center and center of gravity (C.g) comes the near of in the comparison to all other cases. It is worth noting most of the airoelsastic loads will exact the wing in the first ten modes. That is this optimal distribution is not only good from structural decoupling point of view but also equally varied when aerodynamic loads are also applied near the divergence/flutter speed. This can also been seen as the excitation of the structure by spectral load will make the modes to participate whose frequencies are less than or equal to the maximum frequencies in the input spectrum.

Secondly for the worst thickness distribution (center of gravity moving away from shear center) the twist angle parameter is increases. There is qualitative approximate similarly all modes for different cases. It may be seen for case-26 in all the mode the twist angle parameter is high this is due to the fact case-26 is equal thickness distribution of the airfoil crossection incidentally this is the distribution commonly use as of now in the aircraft industries thus if the change the thickness distribution such that the shear center and center of gravity as near as possible the airoelasic instability the speed can be vastly be increased.

The similarity of behavior of twist angle parameter for different modes in different case can also be seen in figure (6.1). Hence this study also shows the worst thickness distribution in comparison to uniform distribution thickness which may be avoid in the fabrication composite aircraft wing.

In the case of supersonic aircraft wing shown in the figure (6.2) that much of similarity case for different mode as seen in figure (6.1) is absent this may be due to two factors

1) The shape (topology) is different
2) The thickness variation consider in different case not identical to the subsonic aircraft wing.

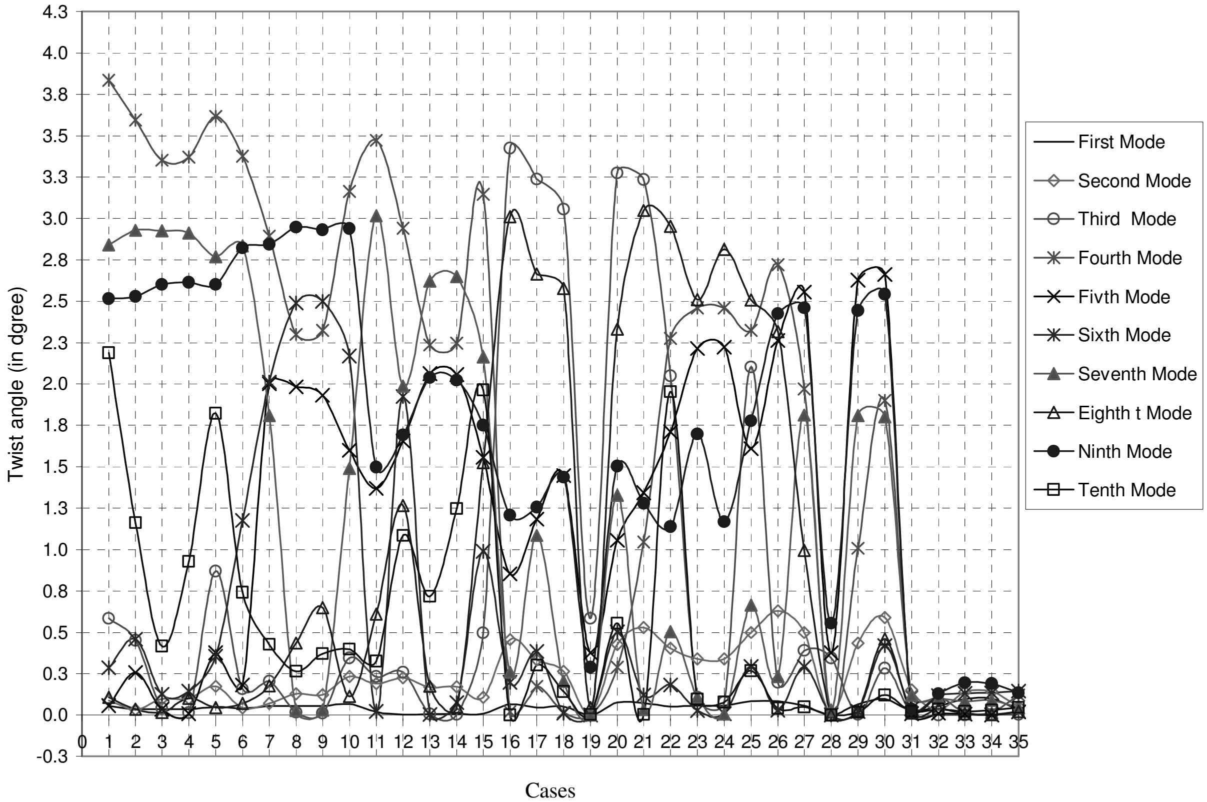

Fig (6.2) Twist angle parameter in all cases for the first ten modes (supersonic aircraft wing)

It may be possible, if a refined thickness variation is introduce in the wedge airfoil, we may get curve similar to figure (6.1). It can be seen from figure (6.2) case – 19 and case -28 are more optimal than other cases, a closer check investigation was done case-31 it was conclude that this two case make the C.g and shear center come closer and thus the decoupling is minimum. It is always possible the tailor the thickness such that C.g and shear center coincide and pave way for total decoupling of bending-torsion.

6.2.1 Effect of Lamination Schemes

The effect of lamination schemes on the twist angle parameter characteristic is also studied in this research. While Figures (6.3-6.8) shows the effect of lamination for subsonic aircraft wing and figure (6.9-6.15) shows the effect of lamination for supersonic aircraft wing. From these figures it can be the lesser role by played the stack angle in comparison to the thickness distribution.

It is worth noting the ply angle modifications done in this research

a. All along cross ply (0/90/0/90)
b. Upper camber cross ply (0/90/0/90) and lower camber angle ply (0/30/45/60)
c. Angle ply antisymmetirc (0/30/45/60/ 0/30/45/60)
d. Angle ply symmetrical (0/30/45/60 / 60/45/30/0)
e. Upper camber angle ply (antisymmetrical) (0/30/45/60 / 0/30/45/0) and lower camber cross ply (antisymmetrical) (0/90/0/90/0/90)

Laminations are considered for subsonic aircraft wing, the effect laminated on the twist angle parameter, for different thickness variations, is shown in figurers below. Upper camber angle ply antisymmetric and lower camber cross ply antisymmetrcaly laminated has relatively minimum twist angle parameter for most of the thickness variations while in the case of supersonic aircraft wing the effect of laminated on twist angle parameter for different thickness variation shown in the figures, angle ply symmetrical laminated has minimum twist angle parameter but the other lamination schemes are maximum twisted angle parameter.

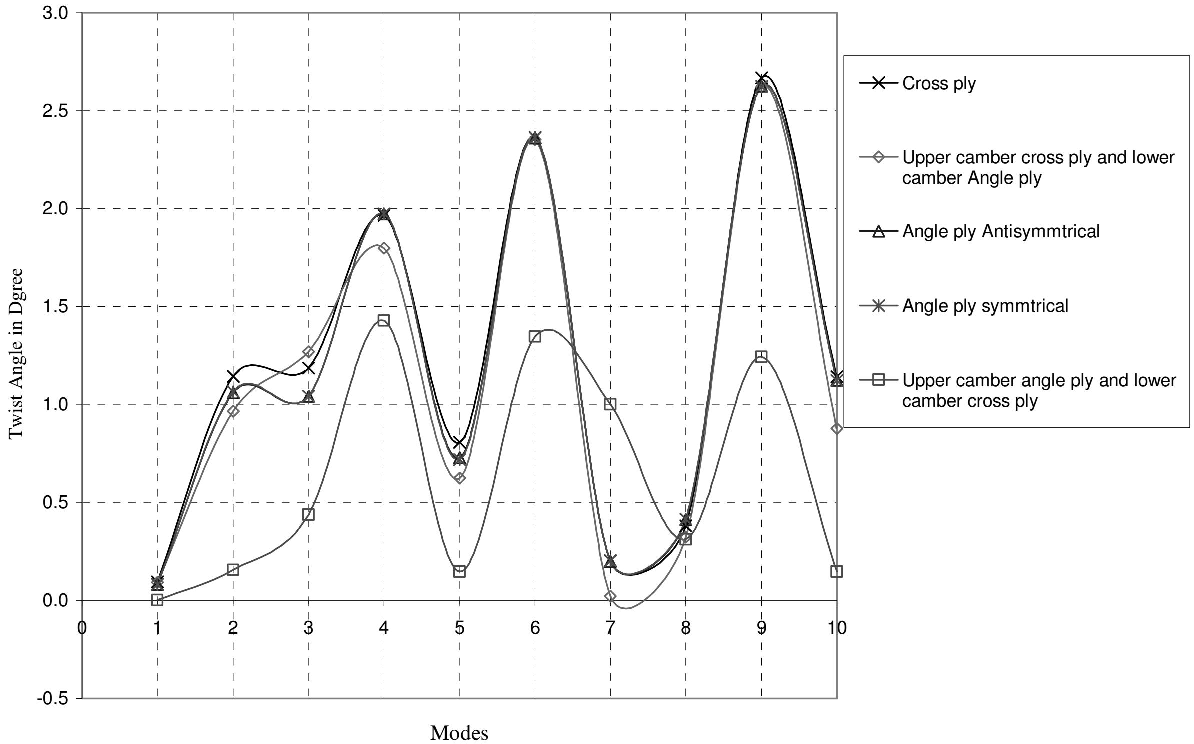

Figure 6.3 Variation of twist angle parameter with the variation of stack angle (for a thickness variation-1 subsonic aircraft wing)

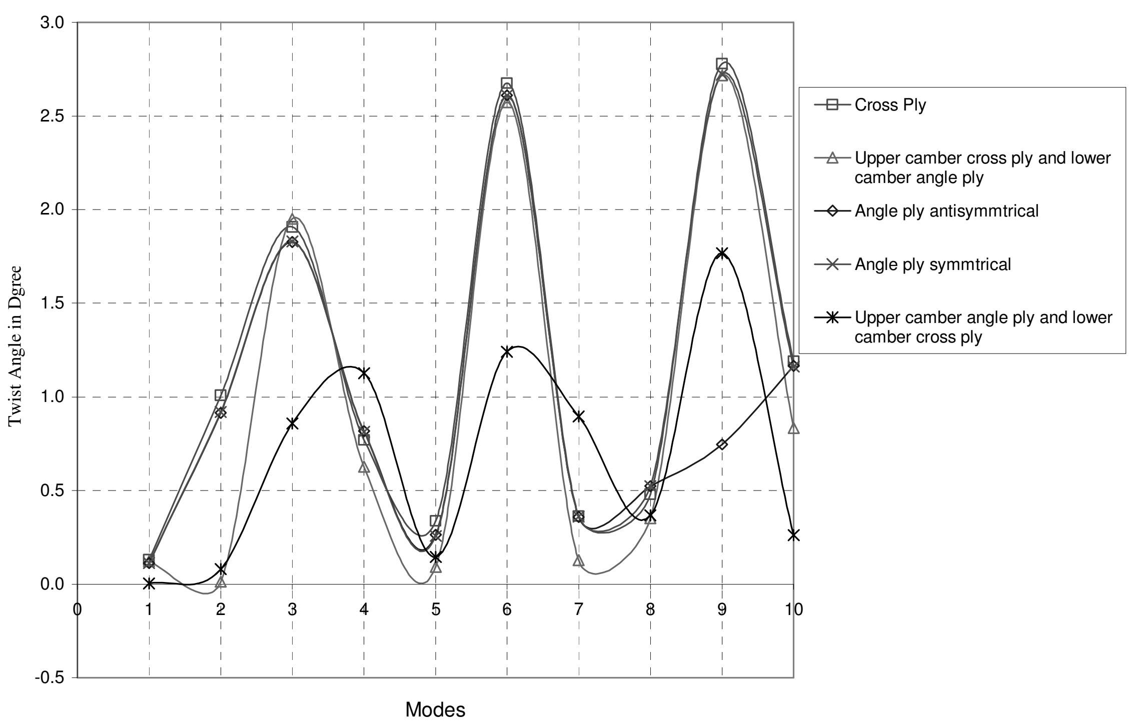

Figure 6.4 Variation of twist angle parameter with the variation of stack angle

(for a thickness variation-2 subsonic aircraft wing)

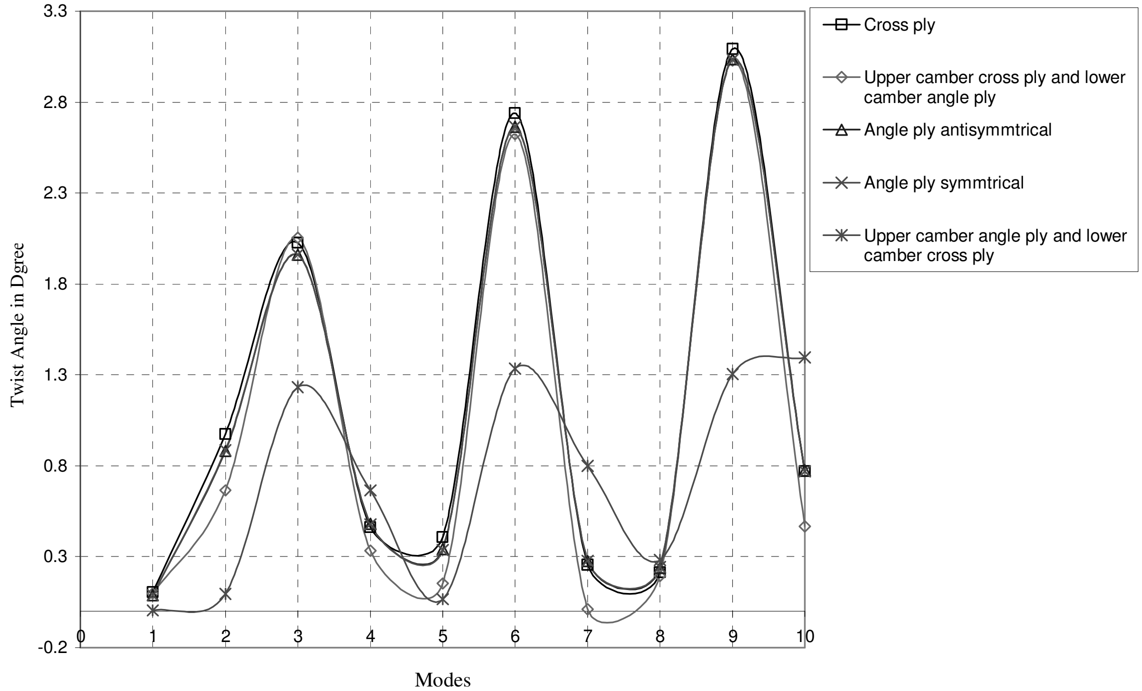

Figure 6.5 Variation of twist angle parameter with the variation of stack angle

(for a thickness variation-3 subsonic aircraft wing)

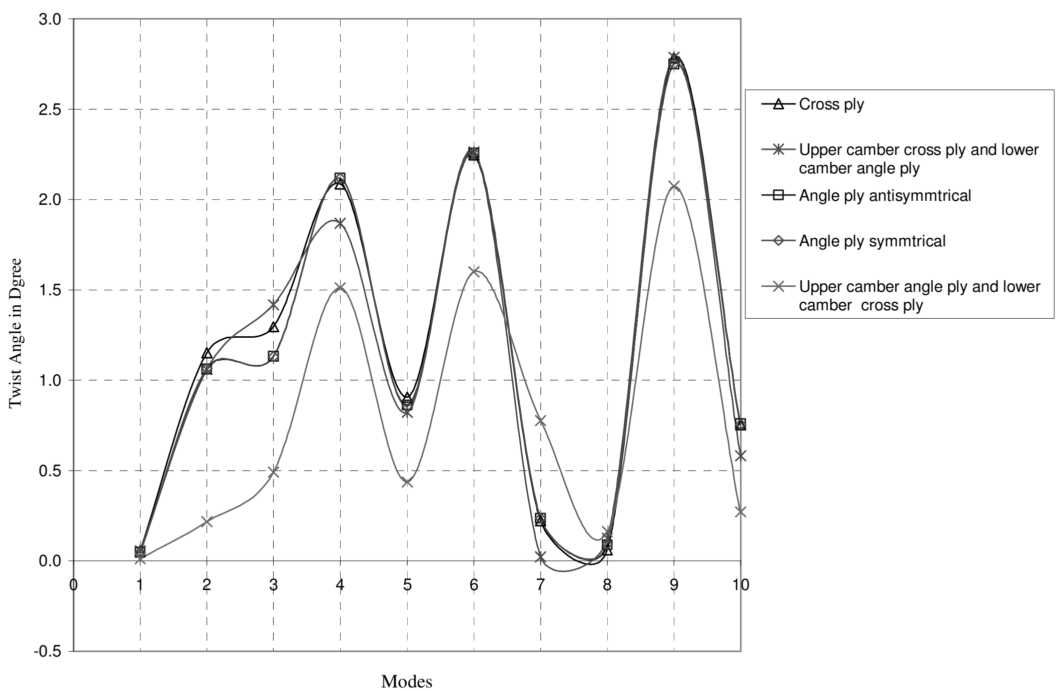

Figure 6.6 Variation of twist angle parameter with the variation of stack angle

(for a thickness variation-4 subsonic aircraft wing)

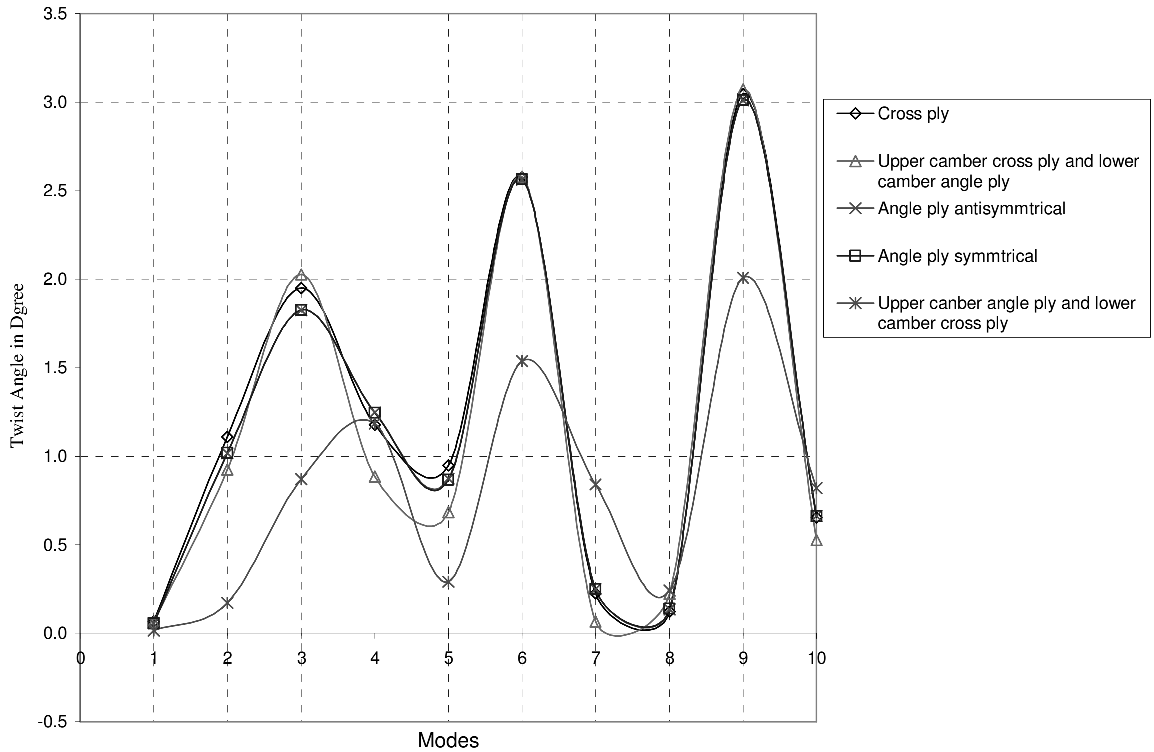

Figure 6.7 Variation of twist angle parameter with the variation of stack angle

(for a thickness variation-5 subsonic aircraft wing)

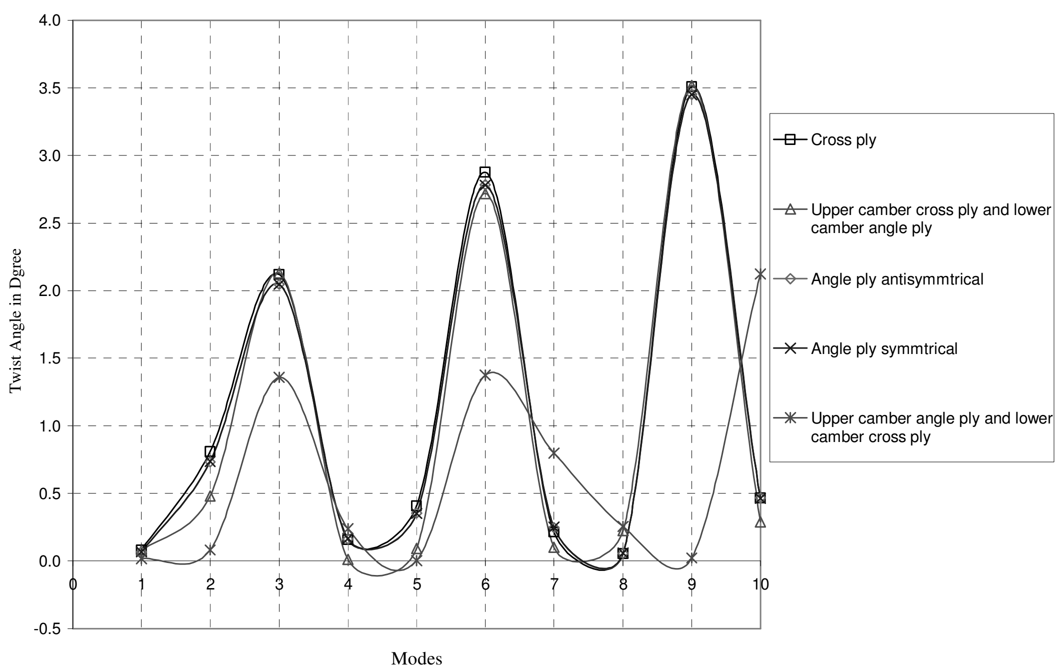

Figure 6.8 Variation of twist angle parameter with the variation of stack angle

(for a thickness variation-6 subsonic aircraft wing)

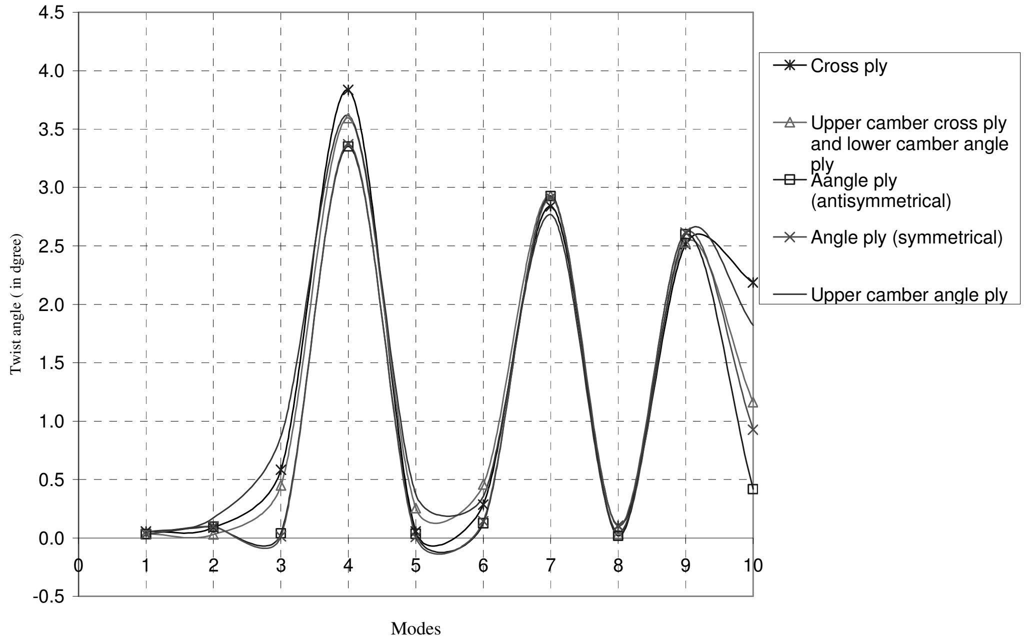

Figure 6.9 Variation of twist angle parameter with the variation of stack angle

(for a thickness variation-1 supersonic aircraft wing)

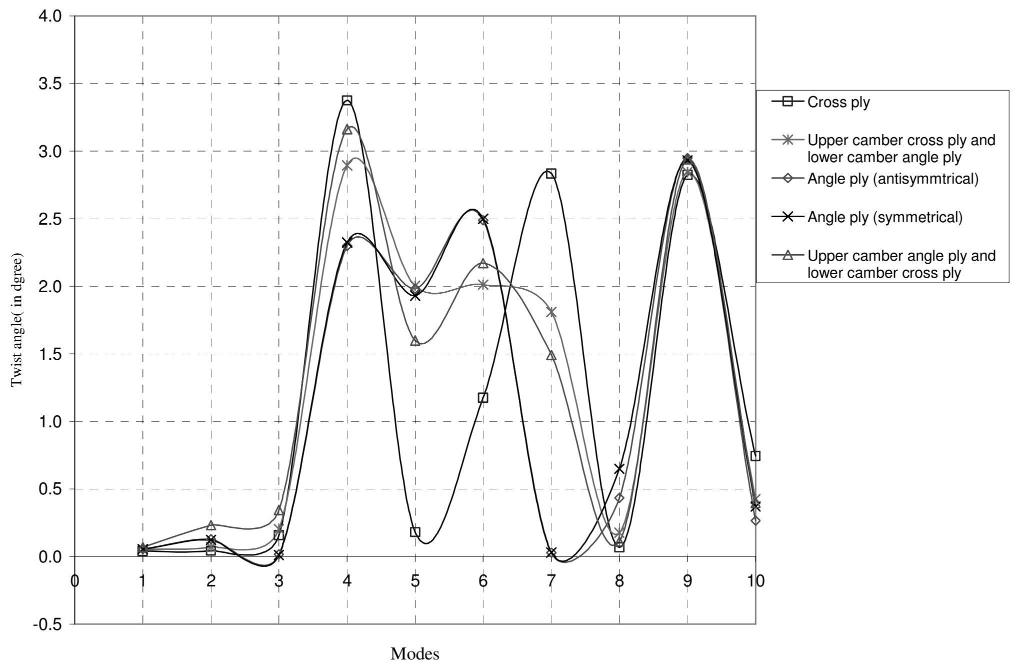

Figure 6.10 Variation of twist angle parameter with the variation of stack angle

(for a thickness variation-2 supersonic aircraft wing)

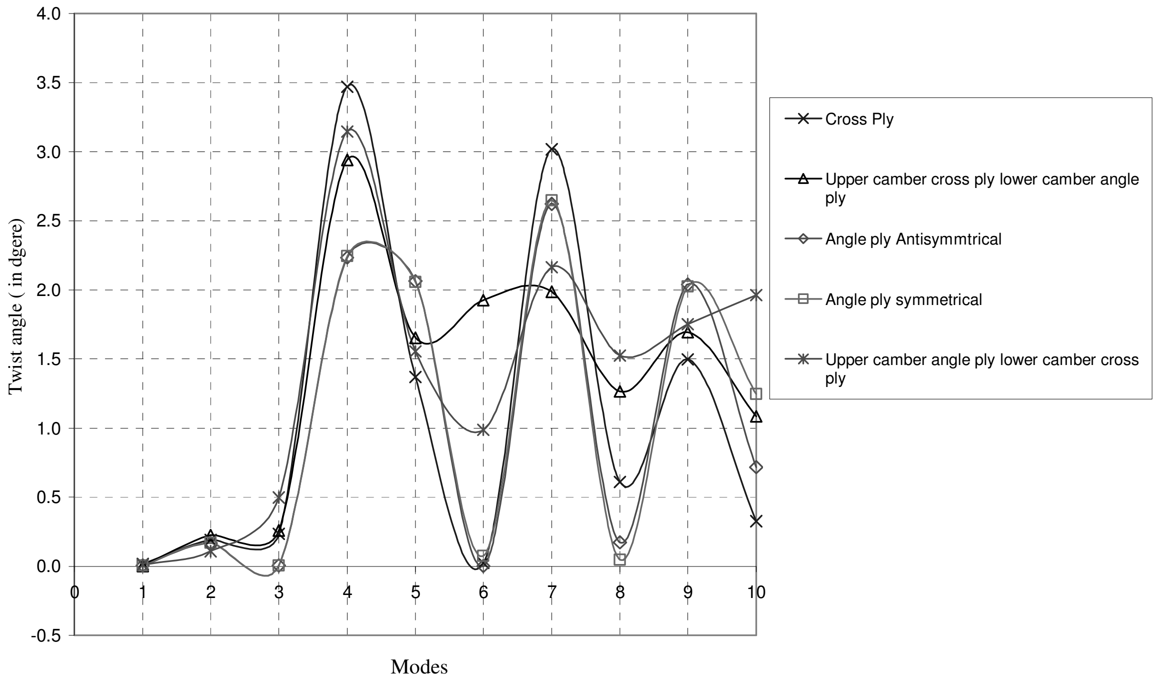

Figure 6.11 Variation of twist angle parameter with the variation of stack angle (for a thickness variation-3 supersonic aircraft wing)

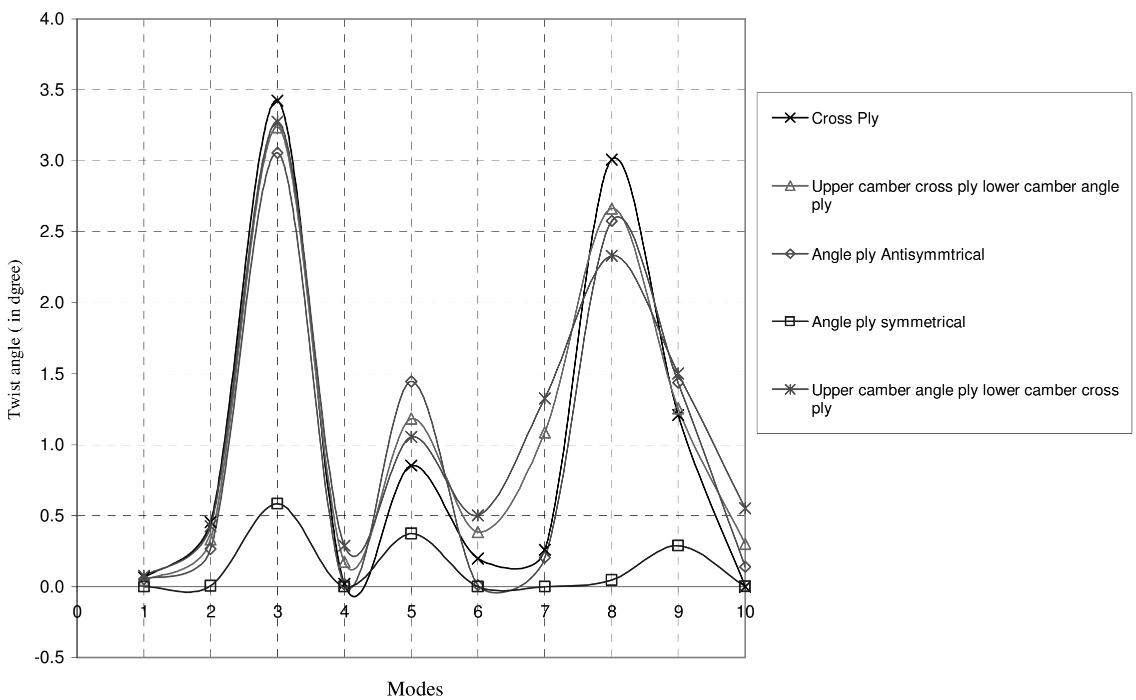

Figure 6.12 Variation of twist angle parameter with the variation of stack angle (for a thickness variation-4 supersonic aircraft wing)

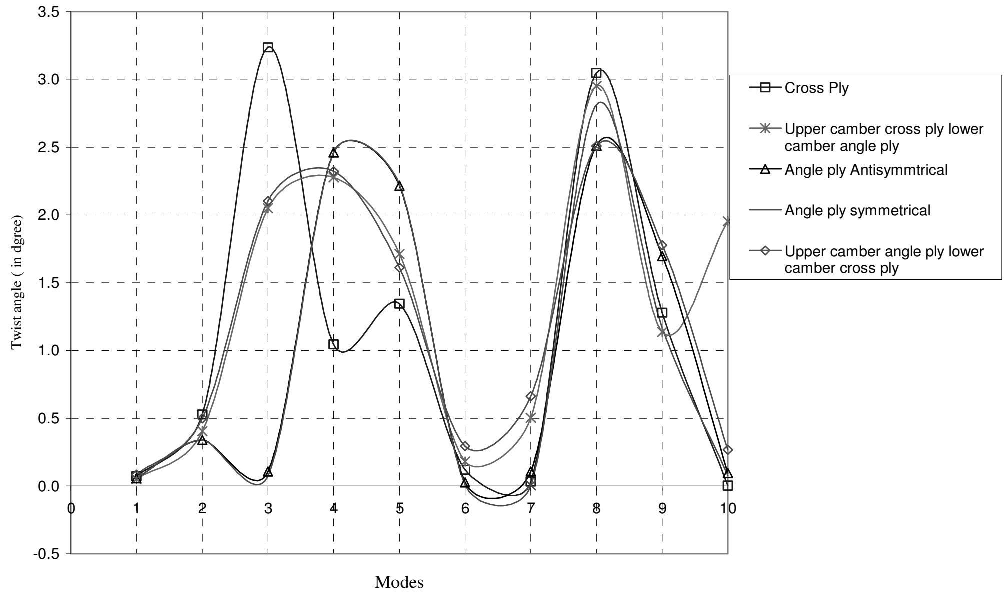

Figure 6.13 Variation of twist angle parameter with the variation of stack angle (for a thickness variation-5 supersonic aircraft wing)

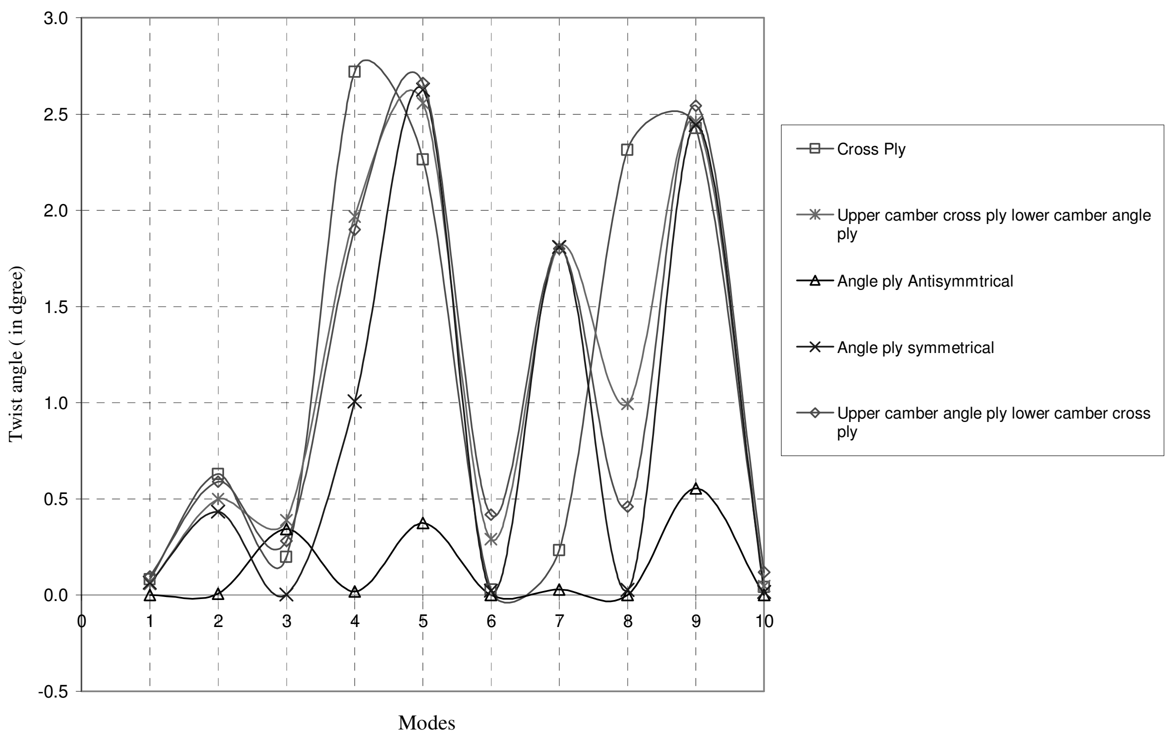

Figure 6.14 Variation of twist angle parameter with the variation of stack angle (for a thickness variation-6 supersonic aircraft wing)

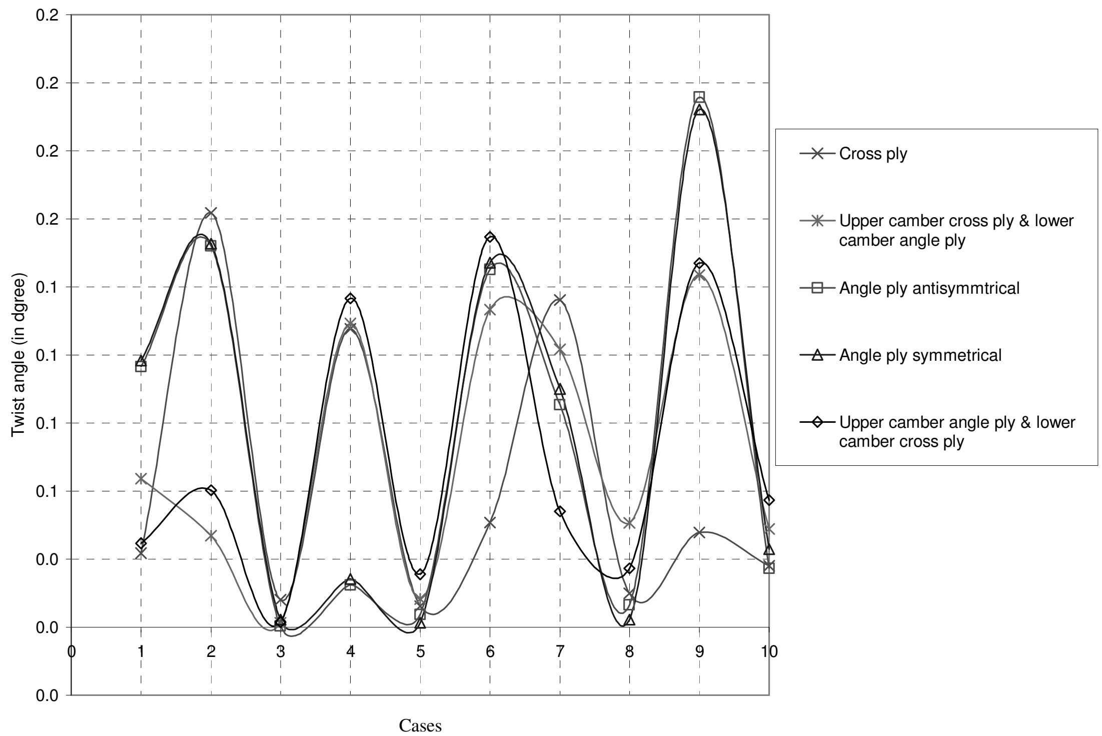

Figure 6.15 Variation of twist angle parameter with the variation of stack angle (for a thickness variation-7 supersonic aircraft wing)

Figure (F.1-F.10) shows the contour plot of mode shape of case-5 model subsonic aircraft wing and figure (G.1-G10) shows the contour plot of mode shape characteristic on supersonic aircraft wing. While Table (6.1) and Table (6.2) shows the general description of the mode shapes (i.e bending, torsion, extension and breathing) character of the minimal bending-torsion effect.

Table 6.1 Minimal Bending-torsion coupling result mode shape descriptions (Case-5 subsonic aircraft wing)

Mode number	Information about the mode shape
1	Fully bending in the x-o-y--plane
2	Bending in x-o-y--plane with little twist
3	Twisted with little bending in the x-o-z-plane
4	Bending in x-o-y-plane and in the x-o-z-plane
5	Bending in x-o-y-plane with little extension
6	Bending in x-o-y-plane, extension and with a very small twist
7	Bending in the x-o-z-plane and extension
8	Fully bending in the x-o-y--plane
9	Bending in the x-o-y-plane, extension and with a little twist
10	Bending in the x-o-y, extension and little twist

Table 6.2 Minimal Bending-torsion coupling result mode shape descriptions (Case-31supersonic aircraft wing)

Mode Number	Information about the mode shape
1	Bending in x-o-y plane with twist
2	Bending in x-o-y plane
3	Bending in x-o-y plane with little twist
4	Bending in x-o-y plane , twist and extension
5	Bending in x-o-y-plane
6	Bending in x-o-y plane and extension
7	Bending in x-o-y plane with little extension
8	Bending in x-o-y plane and extension
9	Bending in x-o-y plane with little extension
10	Bending in x-o-y plane and extension

CHAPTER-SEVEN

CONCLUSION AND RECOMMENDATION FOR FUTURE WORK

7.1 Conclusion

Theoretical Back ground, mathematical formulation and finite element analysis results for laminated composite shell (monocoque) aircraft wing structures are presented in this study.

A parametric study was carried out to understand the characteristics of bending-torsion decoupling of laminated composite aircraft wing. The effects of thickness variation along the chord, layer orientation are presented. The observations are summarized as below

Using finite element analysis different iterations with thickness variation along the chord and ply angle orientation (cross-ply, upper camber cross-ply, lower camber angle ply, upper camber angle ply, angle ply antisymmetrical and angle ply symmetrical) are carried out for one end fixed model.

As the thickness increased at the leading (in compression to the uniform original thickness) and at trailing edge the twist angle is reduced. The angle ply antisymetrical orientation (as indicated in case (e) of section 6.2.1) is more useful in reducing the twist angle parameter than the other laminate scheme.

This is what is attempted in this research. A solution is found for the example airplane wing considerable in the subsonic and supersonic case. this shows that the shear center (the point on the chord at which, when a bending load is applied, there will not be a twist at that cross section as shown in the figure appendix C) and c.g of the aircraft wing tip sections are near each other.

Aroelastics instability depends on to a great extent on the torsional rigidity of the wing. When the shear center is away from the c.g the critical flutter speed is decrease. To prevent this effect and to increase the divergence/flutter speed the c.g and shear center should be as near as possible so that the bending-torsion coupling is reduced.

7.2 Recommendations for Future Work

Based on this direction of approach the following studies can be carried out for future work

1. Monocoque wing may have some concentrated loads such as sub systems of the aircraft and thus things can be accounted. this will produce a realistic distribution of thickness of the wing to avoid bending-torsion coupling.
2. The variation of thickness trail in this research is based on engineering judgment replaced by the standard optimization techniques, such as genetics algorithm (GA), anhealiing algorithm etc.
3. The weight and cost penalty of this optimization with respect to the gain obtained in flutter speed has to be studied.
4. The realistic aeroelastic loads should be introduced to get the dynamic response and to determine the aeroelastic safe speed which will not produce self induced vibration.
5. The effect of temperature can also be incorporate have airo-thermo-elastic study is also a useful extension.

REFERENCES

[1] Aditi Chattopadhyay , 2005 “Development of a Composite Tailoring Procedure for Airplane Wing” NASA research center

[2] Aeronautical software and design consulting, “Airfoil Geometry Naming Conventions” http://www.desktopaero.com/

[3] Ahmed K. Noor and Michael D. Mathers “Shear-Flexible Finite-Element Models Of Laminated Composite Plates and Shells” National Aeronautics and Space Administration Washington, D. C. December 1975

[4] Alastair F. Johnson and Nathalie Pentecote, 2005 “Modeling Impact Damage In Double-Walled Composite Structures”VIII International Conference on

[5] Andreas P F Bernhard and Inderjit Chopra, 200 “Analysis of a Bending-Torsion Coupling Actuator For A Smart Rotor With Active Blade Tip”, journal of Smart Material Structure 10(2001)35-52

[6] B. Malott and R.C. Averill, 2002 “Use Of Genetic Algorithms For Optimal Design of Laminated Composite Sandwich Panels With Bending-Twisting Coupling” report on American Institute of Aeronautics and Astronautics

[7] Boyang Liu, 2001,” Two-Level Optimization of Composite Wing Structure Based on Panel Genetic Optimization” etd.fcla.edu/UF/ank7116/Dissertation_Boyang_Liu.pdf

[8] Brian E Tatting, 1998 “Analysis and Design of Variable Stiffness Composite Cylinders” thesis of Virginia Polytechnic Institute and State University Blacksburg, Virginia 24061

[9] EF Bruhn, Jacobs, SR , 1973 “Analysis and Design of Flight Vehicle structure”, Published in London,ppA19.27

[10] Erik Lund, Jan Stegmann, 2004 “Structural Optimization Of Composite Shell Structures Using A Discrete Constitutive Parameterization” thesis in institute of mechanical engineering, aalborg university, pontoppidanstraede 101, dk-9220 aalborg east, Denmark

[11] Ferdinando Auricchio And Elio Sacco,1999 “ A Mixed –Enhanced Finite Element For The Analysis Of Laminated Composite Plate” International Journal For Numerical Methods In Engineering 44,1481-1504(1999)

[12] Gamal M.Ashawesh, Ali M. Elmabrok, Tarek A. Abdunabi, Alakrami A.

Nakas, 2003 “Effect Of Root Flexibility On The Aeroelastic Analysis Of A Composite Wing Box”, AIAA journal 2003-0034

[13] G. Dietz , G. Schewe_ , F. Kiebling_ and M. Sinapius, 2003**”** Limit-Cycle-Oscillation Experiments at a Transport Aircraft Wing Model” international forum of on aroelasticty and Structural Dynamic IFASD – Amsterdam

[14] GoranJanevski, 2004“Two-Frequency Nonlinear Vibrations of Antisymmetric Laminated Angle-Ply Plate” Mechanics, Automatic Control and Robotics Vol.4, No 1, 2004, pp. 345 – 358

[15] G. R. Benini, E. M. Belo and F. D. Marques, 2004 “Numerical Model for the Simulation of Fixed Wings Aeroelastic Response” Journal of the Brazil Society of Mechanical Science and Engineering, April-June 2004, Vol. XXVI, No. 2 / 129

[16] Guo, S.J. Bannerjee, J.R. Cheung and C.W, 2002“The Effect of Laminate Lay-Up on the Flutter Speed of Composite Wings” thesis on City University, London, UK

[17] Hiro Miura, 2001 “Development of a Composite Tailoring Technique for Airplane Wing” NASA research center

[18] Jan Stegmmann, 2005 “Analysis and Optimization Of Laminated Composite Shell Structure” www.ime.auc.dk/people/employees/is/docs/stegmann_PhDThesis.pdf

[19] J.B. Kosmatka, 1992 “The Use of Cross-Section Warping Functions In Composite Rotor Blade Analysis” NASA Technical Report, NAG- 1- l 151

[20] Jenst rapp and Robert zores, “NACA 8516 Airfoil Crossection” http://www.pagendarm.de/trapp/programming/java/profiles/NACA4.html

[21] Jonathan E. Rich, 1997 “Design Optimization Procedure for Monocoque composite Cylinder Structures Using Response Surface Techniques” M.SC thesis in Virginia polytechnic institute and state university

[22] J.Stegmann,J.C.RauheL. Rosgaard andE lurd, 2001”Shell Element For Geometrically Non-Linear Analysis Of Composite Laminates And Sandwich Structures” www.ime.auc.dk/~js/docs/AbstractNSCM14.pdf

[23] Kaihong Wang, 2004 “Vibration Analysis OF Cracked Composite Bending-Torsion Beams For Damage Diagnosis” www.scholar.lib.vt.edu/theses/available/etd-12032004-110007/unrestricted/wangk2004.pdf

[24] K. N. khatri and N. T. asnani, 1995 “Vibration and Damping Analysis of Fiber

Reinforced Composite Material Conical Shells”
eprint.iitd.ac.in/dspace/bitstream/2074/232/1/khatrivib96

[25] Metin Aydogdu, 2006” Free Vibration Analysis of Angle-ply Laminated Beams with General Boundary Conditions “Journal of Reinforced Plastics and Composites 2006; 25; 1571

[26] Osama J Aldraihem and Robert C Wetherhold, 1997 **“**Mechanics and Control Of Coupled Bending and Twisting Vibration of Laminated Beams” journal of Smart Material structure 6 (1997) 123–133

[27] Peter W.G. De Baets, Rupinder S. Battoo, and Dimitri N. Mavris, 2000 “Aeroelastic Analysis of a Composite Wing box With Varying Root Flexibility” AIAA journal 2000-1623

[28] Prashant M. Pawar,2006 “Structural Health Monitoring of Composite Helicopter Rotor Blades” etd.ncsi.iisc.ernet.in/bitstream/2005/273/1/G20330.pdf

[29] Seong-Wook Hong, Byung-Sik Kang and Joong-Youn Park, 2003 “Dynamic Analysis of Bending-Torsion Coupled Beam Structures Using Exact Dynamic Elements” International Journal of the Korean Society of Precision Engineering, Vol. 4, No. 1

[30] Seung Joon Lee, 2004 “Nonlinear Analysis of Smart Composite Plate and Shell Structures”txspace.tamu.edu/bitstream/1969.1/2218/1/etd-tamu-2004.pdf

[31] Shyama kumari and P.K sinha, 2002 “Finite Element Analysis of Composite Wing T-Joints” Journal of Reinforced Plastics and Composites 2002; 21; 1561

[32] S.K. Basu,V.B. Tungikar and S.R. Kajale**,** 1994 “Free Vibration Analysis of laminated Composite Plate by FEA using Nonconforming Elements” journal of composite structure VIII-20567

[33] Valery V.vasiliev, 2001 “Mechanics and Analysis of composite materials” 1st edition Published by Elsevier Ltd, Amsterdam London, pp 225-250

[34] Won-Hong Lee · Sung-Cheon Han, 2005 “Free and forced vibration analysis of laminated composite plates and shells using a 9-node assumed strain shell element” Journal of Composite structure, VII-208

[35] Wu Qian, G R Liu, Lu Chun and K Y Lam, 2003 “Active Vibration Control of Composite Laminated Cylindrical Shells Via Surface-Bonded Magnetostrictive Layers” smart materials and structures 12 (2003) 889–897

[36] Zhanming Qin,2001 “ Vibration and Aeroelasticity of Advanced Aircraft Wing

Modeled As Thin-Wall Beam Dynamics, Stability and Control “PhD thesis in Virginia polytechnic institute and state university

[37] Antant patil, S.C.Jain and Rajeev Kumar,2005 “Optimal Active Vibration Control of A smart plate”, international conference on smart material structure and system,ISSS-2005/SA-09,pp SA68-SA70

Appendix A

NACA 8516 Airfoil Geometry Coordinate

Table A.1 Coordinates of NACA 8516 airfoil cross section (upper and lower camber)

Key points	*X -Coordinate*	*Y -Coordinate*	*Key points*	*X -Coordinate*	*Y -Coordinate*
1	2.43868052652147	0.0042007531002164	33	0.63761609784200	0.3473660604357710
2	2.43414011720661	0.0065929482681677	34	0.56749087773808	0.3347334028184410
3	2.42506936316016	0.0113453724626452	35	0.50024822616489	0.3200696254074550
4	2.41148857590944	0.0183946303892881	36	0.43621305984692	0.3035557194352140
5	2.39342866995686	0.0276469466015695	37	0.37568878272535	0.2853973798751820
6	2.37093166531770	0.0389797106198966	38	0.31895462916819	0.2658211545646190
7	2.34405131032935	0.0522434534579515	39	0.26626356702748	0.2450698304176320
8	2.31285378660658	0.0672641953863203	40	0.21784080314000	0.2233974563479420
9	2.27741845154408	0.0838461138457060	41	0.17388288785640	0.2010638757497070
10	2.23783859148743	0.1017744270637630	42	0.13455742261475	0.1783290046751500
11	2.19422213583056	0.1208184683993460	43	0.10000333596413	0.1554470373541120
12	2.14669231511681	0.1407347970157860	44	0.07033161446044	0.1326607607007030
13	2.09538823518901	0.1612703993767500	45	0.04562643146466	0.1101959051489830
14	2.04046535739691	0.1821657499670980	46	0.02594652049738	0.0882560404241083
15	1.98209588580749	0.2031578810960050	47	0.01132670948148	0.0670178663916885
16	1.92046904984618	0.2239833164662120	48	0.00177946168712	0.0466271759942173

Key points	X -Coordinate	Y -Coordinate	Key points	X -Coordinate	Y -Coordinate
17	1.85579130597648	0.2443808866739270	49	-0.00270369507129	0.0271955652032047
18	1.78828643841707	0.2640943448990570	50	0.01352362536898	-0.0237408696245402
19	1.71819558217247	0.2828750370889900	51	0.02823636394194	-0.0370812372006476
20	1.64577714634741	0.3004843904972070	52	0.04738822491185	-0.0484553345739840
21	1.57130661859728	0.3166963295638550	53	0.07085747382223	-0.0578937621414660
22	1.49507622031612	0.3312996917963020	54	0.09850625382494	-0.0654368133395909
23	1.41739437811052	0.3441007344722740	55	0.13018260812202	-0.0711348311230539
24	1.33858494606893	0.3549253688752650	56	0.16572275806463	-0.0750486757010220
25	1.25898613982278	0.3636218123137940	57	0.20495351554964	-0.0772502331435680
26	1.17894912017703	0.3700626588761810	58	0.24769467206222	-0.0778228876590728
27	1.09883618981441	0.3741473861336690	59	0.29376127668807	-0.0768619393780826
28	1.01901857813913	0.3758041715919970	60	0.34296564521346	-0.0744748268686233
29	0.93987381087638	0.3749918544590460	61	0.39511903829901	-0.0707811543829739
30	0.86178268931070	0.3717013524770710	62	0.45003288961558	-0.0659123966842887
31	0.78512592639821	0.3659565338194360	63	0.50751954334712	-0.0600112451240419
32	0.71028054538690	0.3578146530389780	64	0.56739249863161	-0.0532306131348012
65	0.62946615066251	-0.0457321649044751	68	0.82703102404377	-0.0206356343477964
66	0.69355506379298	-0.0376844376195221	100	0.8117128446632370	0.0021985508375801
67	0.75947289724550	-0.0292605731710792	99	0.8132269352181940	0.0014008253775537

Key points	X -Coordinate	Y -Coordinate	Key points	X -Coordinate	Y -Coordinate
69	0.89603699416566	-0.0119836485609412	101	0.8086880197904890	0.0037833420066163
70	0.96629296659884	-0.0034743995368481	102	0.8041592338861260	0.0061340584522113
71	1.03759419609278	0.0047299004790839	103	0.7981367960110430	0.0092194288708269
72	1.10972774231504	0.0124779322743416	104	0.7906347185821540	0.0129985663387924
73	1.18247144919049	0.0196324717327952	105	0.7816709250606070	0.0174216274246573
74	1.25559329080969	0.0260733364596961	106	0.7712674850332850	0.0224305950980633
75	1.32885112180161	0.0316999381799250	107	0.7594508618151510	0.0279601683989167
76	1.40199284765756	0.0364333452619611	108	0.7462521636092220	0.0339387240372598
77	1.47475700220865	0.0402177676670252	109	0.7317073816366880	0.0402893415950238
78	1.54687369792636	0.0430213879756628	110	0.7158576095939140	0.0469308408424258
79	1.61806590321060	0.0448365044333039	111	0.6987492351143000	0.0537788493409752
80	1.68805097519512	0.0456790291555224	112	0.6804340999030710	0.0607468231022358
81	1.75654239994794	0.0455872983522713	113	0.6609696288603330	0.0677470702752470
82	1.82325166562292	0.0446203557811676	114	0.6404189243334470	0.0746917294040322
83	1.88789022535731	0.0428556912653148	115	0.6188508333711550	0.0814937083125113
84	1.95017151099846	0.0403865932151675	116	0.5963399813097130	0.0880675563588735
85	2.00981297026215	0.0373192468471825	117	0.5729667794529200	0.0943303548619150
86	2.06653809734379	0.0337696008048951	118	0.5488173994997730	0.1002025469541550

87	2.12007847264225	0.0298602065332234	119	0.5239837083345320	0.1056087432056660
88	2.17017578434137	0.0257170599233357	120	0.4985631530422490	0.1104785272479060
Key points	X -Coordinate	Y -Coordinate	Key points	X -Coordinate	Y -Coordinate
89	2.21658384859394	0.0214665632974356	121	0.4726585846611370	0.1147472916841510
90	2.25907061029153	0.0172326520094648	122	0.4463779988326640	0.1183569831401110
91	2.29742011936466	0.0131341674020514	123	0.4198341803428720	0.1212569866329430
92	2.33143446708820	0.0092824772549793	124	0.3931442308055460	0.1234048161059620
93	2.36093564939270	0.0057793845953420	125	0.3664289673171120	0.1247669503390780
94	2.38576733572353	0.0027153348030988	126	0.3398121837682990	0.1253194386810060
95	2.40579648969722	0.0001679016944981	127	0.3134197736843720	0.1250485552400340
96	2.42091481121078	-0.0017994357977295	128	0.2873787228915490	0.1239512713551510
97	2.43103995249570	-0.0031382538247853	129	0.2618159877611740	0.1220355463474990
98	2.43611646765016	-0.0038158861841075	130	0.2368572942574050	0.1193204728960990
Lower Camber			131	0.2126258767619140	0.1158361801207060
132	0.1892412155869790	0.1116235670596360	167	0.2988015078985550	-0.0039961879737675
133	0.1668178047055200	0.1067336363643400	168	0.3222297710602370	-0.0011586082130671
134	0.1454639941163030	0.1012267431914800	169	0.3460065961539920	0.0015772801843705
135	0.1252809599490200	0.0951714806556697	170	0.3700609739549340	0.0041610167920589
136	0.1063618185044050	0.0886433956772089	171	0.3943188220639330	0.0065468414761126
137	0.0887909269866030	0.0817234504222868	172	0.4187027667876440	0.0086946770064532

138	0.0726433851324115	0.0744963625967503	173	0.4431320598952860	0.0105709802052006
139	0.0579847365985439	0.0670487821921706	174	0.4675226354165700	0.0121494297366589
140	0.0448708714461825	0.0594673834294080	175	0.4917873022131390	0.0134114212933927
Key points	X -Coordinate	Y -Coordinate	Key points	X -Coordinate	Y -Coordinate
141	0.0333481181865624	0.0518369324728846	176	0.5158360608753600	0.0143463447187095
142	0.0234534875128530	0.0442383914887905	177	0.5395765296596470	0.0149516317080706
143	0.0152150487205771	0.0367470348179340	178	0.5629144556331550	0.0152325884755700
144	0.0086523876802180	0.0294307468682527	179	0.5857542949785380	0.0152019989993423
145	0.0037771184612157	0.0223484517540782	180	0.6079998376338950	0.0148795526046305
146	0.0005933971909874	0.0155487670563161	181	0.6295548618603330	0.0142910898271948
147	0.0009016013506797	0.0090689066899940	182	0.6503238057595350	0.0134677195586264
148	0.0045097241283759	-0.0079168691569939	183	0.6702124466050580	0.0124448513891548
149	0.0094159819051661	-0.0123654822986573	184	0.6891285779903620	0.0112611507195979
150	0.0158025540825832	-0.0161584032028913	185	0.7069826900156490	0.0099574847873300
151	0.0236288458644279	-0.0193058361858129	186	0.7236886434247470	0.0085758694494143
152	0.0328488861196382	-0.0218212179020047	187	0.7391643432759950	0.0071584560954943
153	0.0434120018060709	-0.0237213362194597	188	0.7533324061390530	0.0057465734551661
154	0.0552635776482951	-0.0250264861956238	189	0.7661208191318570	0.0043798515577801
155	0.0683458605996118	-0.0257606396824121	190	0.7774635856204690	0.0030954282232560
156	0.0825987565162375	-0.0259516028165817	191	0.7873013465776300	0.0019272517128848

157	0.0979605898061521	-0.0256311553381383	192	0.7955819704443110	0.0009054828527151
158	0.1143687734038320	-0.0248351247925311	193	0.8022610935700740	0.0000559901877059
159	0.1317603683909320	-0.0236033956166357	194	0.8073026011133580	-0.0006000579587999
160	0.1500724935428500	-0.0219798107072710	195	0.8106790325590660	-0.0010465136831626

Key points	X -Coordinate	Y -Coordinate	Key points	X -Coordinate	Y -Coordinate
161	0.1692425712638260	-0.0200119533576071	196	0.8123718983591390	-0.0012724837849382
162	0.1892084091006970	-0.0177508156187832			
163	0.2099081134079670	-0.0152503076568246			
164	0.2312798469498320	-0.0125666315769776			
165	0.2532614706565170	-0.0097575250156224			
166	0.2757900830794020	-0.0068813661709428			

Appendix B

Laminated Composite Shell-99 element Defined dialog box

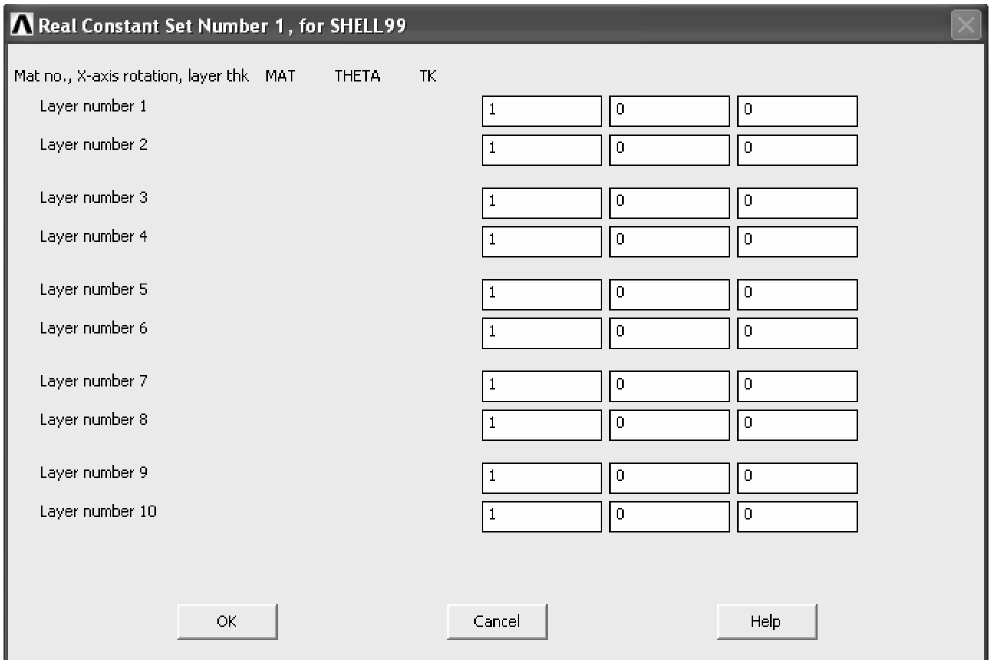

Figure B.1 Real constant Set number

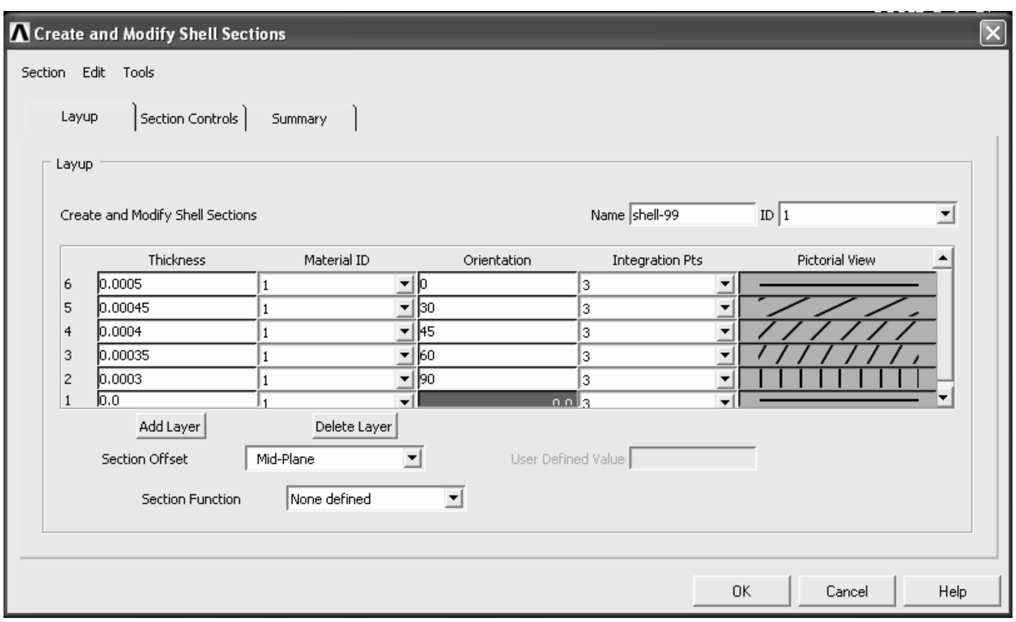

Figure B.2 Shell section control lay up page

Appendix C

C. Mathematical formulation for twist angle parameter

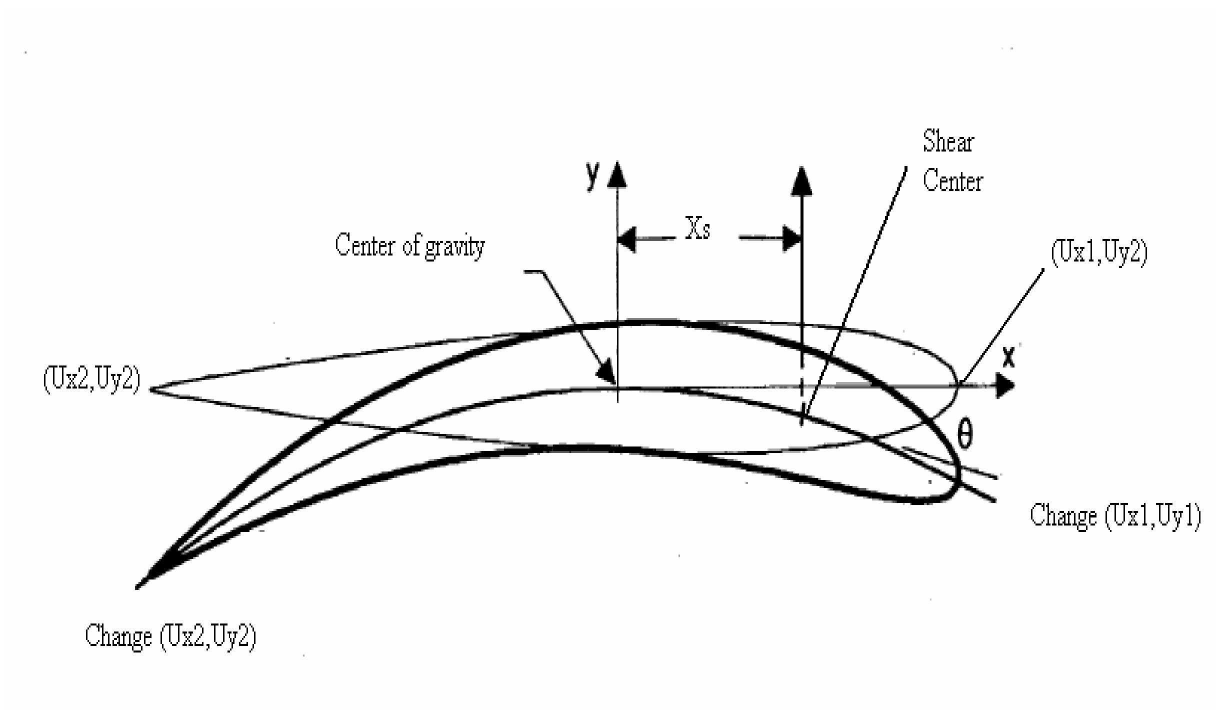

Figure-C Deformed and Undeformed Airfoil Cross section (*source from literature review*)

Step-1:-determin the slope of chords of airfoil (θ_1)

$$\tan^{-1}\left(\frac{Uy_1 - Uy_2}{Ux_1 - Ux_2}\right) = \theta_1$$

Where:-

$Uy_1 = \text{y} - \text{coordinates of leading edge location before deformation}$

$\text{Ux}_1 = \text{x} - \text{coordinates of leading edge location before deformation}$

$Uy_2 = \text{y} - \text{coordinates of trailing edge location before deformation}$

$\text{Ux}_2 = \text{x} - \text{coordinates of trailing edge location before deformation}$

Step-2:-Total displacement of the model

$$Y_1^{'} = Uy_1 + \Delta Uy_1 \quad , X_1^{'} = Ux_1 + \Delta Ux_1$$

$$Y_2^{'} = Uy_2 + \Delta Uy_2 \quad , X_2^{'} = Ux_2 + \Delta Ux_2$$

Where: $Y_1^{'}$ = total displacing along the y-axis at leading edge

$Y_2^{'}$ = total displacing along the y-axis at trailing edge

$X_1^{'}$ = total displacing along the x-axis at leading edge

$X_2^{'}$ = total displacing along the x-axis at trailing edge

ΔUx_1 = location of leading edge after deformation

ΔUy_1 = location of leading edge after deformation

ΔUx_2 = location of leading edge after deformation

ΔUy_2 = location of leading edge after deformation

Step-3 Determine total angle twist with respect to global axis (θ_2)

$$\tan^{-1}\left(\frac{Y_1^{'} - Y_2^{'}}{X_1^{'} - X_2^{'}}\right) = \tan^{-1}\left(\frac{(Uy_1 + \Delta Uy_1) - (Uy_2 + \Delta Uy_2)}{(Ux_1 + \Delta Ux_1) - (Ux_2 + \Delta Ux_2)}\right) = \theta_2$$

Step-4 Twisted angle (θ)

$$\theta = \theta_2 - \theta_1$$

Appendix D

Results of twist angle parameter for different thickness variation

(Subsonic aircraft wing)

Table D.1. Results of twist angle parameter for a thickness variation-1 (subsonic aircraft wing)

Modes	Twist angle Parameter				
	Cross Ply	Upper camber cross ply and lower camber angle ply	Angle ply (Antisymmetric)	Angle ply (Symmetric)	Upper amber angle ply and lower Camber cross ply
1	0.0948	0.0927	0.0819	0.0816	0.0017
2	1.1439	0.9654	1.0615	1.0649	0.1554
3	1.1851	1.2701	1.0434	1.0430	0.4375
4	1.9660	1.7982	1.9743	1.9732	1.4274
5	0.8071	0.6241	0.7293	0.7201	0.1471
6	2.3608	2.3526	2.3617	2.3638	1.3461
7	0.2016	0.0225	0.2001	0.2016	1.0002
8	0.3795	0.3238	0.4123	0.4155	0.3121
9	2.6674	2.6219	2.6256	2.6242	1.2438
10	1.1432	0.8769	1.1254	1.121	0.1462

Table D.2. Results of Twist Angle Parameter for a thickness variation-2(subsonic wing)

Modes	Twist angle Parameter				
	Cross Ply	Upper camber cross ply and lower camber angle ply	Angle ply (Antisymmetric)	Angle ply (Symmetric)	Upper amber angle ply and lower Camber cross ply
1	0.1284	0.1227	0.1122	0.1120	0.0048
2	1.0078	0.0127	0.9151	0.9190	0.0801
3	1.9068	1.9503	1.8280	1.8294	0.8577
4	0.7706	0.6265	0.8165	0.8128	1.1275
5	0.3374	0.0918	0.2637	0.2571	0.1453
6	2.6763	2.5733	2.6104	2.6101	1.2417
7	0.3627	0.1267	0.3589	0.3609	0.8948
8	0.4790	0.3523	0.5223	0.5233	0.3674
9	2.7794	2.7171	0.7458	2.7229	1.7663
10	1.1894	0.8341	1.1663	1.1602	0.2610

Table D.3. Results of Twist Angle Parameter for a thickness variation-3(subsonic wing)

	Twist angle Parameter				
Modes	Cross Ply	Upper camber cross ply and lower camber angle ply	Angle ply (Antisymmetric)	Angle ply (Symmetric)	Upper amber angle ply and lower Camber cross ply
1	0.1043	0.0988	0.0896	0.0894	0.0054
2	0.9754	0.6647	0.8827	0.8864	0.0963
3	2.0278	2.0555	1.9614	1.9617	1.2329
4	0.4635	0.3328	0.4802	0.4791	0.6654
5	0.4081	0.1532	0.3427	0.3373	0.0657
6	2.7400	2.6233	2.6648	2.6647	1.3353
7	0.2559	0.0112	0.2753	0.2773	0.7996
8	0.2138	0.1943	0.2403	0.2436	0.2825
9	3.0931	3.0298	3.0363	3.0341	1.3054
10	0.7711	0.4670	0.7738	0.7700	1.3968

Table D.4. Results of Twist Angle Parameter for a thickness variation-4(subsonic wing)

	Twist angle Parameter				
Modes	Cross Ply	Upper camber cross ply and lower camber angle ply	Angle ply (Antisymmetric)	Angle ply (Symmetric)	Upper amber angle ply and lower Camber cross ply
1	0.0573	0.0562	0.0474	0.0472	0.0115
2	1.1505	1.0584	1.0615	1.0649	0.2169
3	1.2953	1.4171	1.1317	1.1312	0.4917
4	2.0857	1.8686	2.1181	2.1167	1.5122
5	0.9069	0.8218	0.8628	0.8557	0.4361
6	2.2484	2.2649	2.2564	2.2587	1.5999
7	0.2222	0.0218	0.2362	0.2364	0.7759
8	0.0624	0.1244	0.0887	0.0936	0.1616
9	2.7867	2.7892	2.7503	2.7499	2.0739
10	0.7532	0.5809	0.7593	0.7548	0.2720

Table D.5. Results of Twist Angle Parameter for a thickness variation-5(subsonic wing)

Modes	Twist angle Parameter				
	Cross Ply	Upper camber cross ply and lower camber angle ply	Angle ply (Antisymmetric)	Angle ply (Symmetric)	Upper amber angle ply and lower Camber cross ply
1	0.0669	0.0639	0.0556	0.0554	0.0144
2	1.1092	0.9257	1.0154	1.0189	0.1710
3	1.9488	2.0270	1.8260	1.8256	0.8719
4	1.1780	0.8840	1.2469	1.2461	1.1832
5	0.9476	0.6831	0.8736	0.8668	0.2916
6	2.5770	2.5783	2.5619	2.5633	1.5364
7	0.2263	0.0652	0.2474	0.2486	0.8392
8	0.1214	0.2219	0.1349	0.1397	0.2412
9	3.0463	3.0713	3.0119	3.0107	2.0069
10	0.6541	0.5273	0.6635	0.6602	0.8188

Table D.6. Results of Twist Angle Parameter for a thickness variation-6(subsonic wing)

Modes	Twist angle Parameter				
	Cross Ply	Upper camber cross ply and lower camber angle ply	Angle ply (Antisymmetric)	Angle ply (Symmetric)	Upper amber angle ply and lower Camber cross ply
1	0.0810	0.0763	0.0679	0.0678	0.0162
2	0.8109	0.4808	0.7333	0.7365	0.0821
3	2.1193	2.1299	2.0455	2.0457	1.3574
4	0.1583	0.0122	0.1637	0.1651	0.2387
5	0.4090	0.0938	0.3551	0.3512	0.0032
6	2.8752	2.7173	2.7817	2.7815	1.3757
7	0.2140	0.1029	0.2471	0.2496	0.7508
8	0.0540	0.2252	0.0552	0.0597	0.2568
9	3.5092	3.5166	3.4512	3.4485	0.0236
10	0.4668	0.2892	0.4673	0.4642	2.1213

Appendix E

Results of twist angle parameter for different thickness variation

(Supersonic aircraft wing)

Table E.1 Results of twist angle parameter for a thickness variation-1 (supersonic aircraft wing)

	Twist angle Parameter				
Modes	Cross Ply	Upper camber cross ply and lower camber angle ply	Angle ply (Antisymmetric)	Angleply (Symmetric)	Upper amber angle ply and lower Camber cross ply
1	0.0548	0.0362	0.0338	0.0343	0.0480
2	0.0889	0.0311	0.0961	0.1003	0.1728
3	0.5828	0.4494	0.0409	0.0149	0.8688
4	3.8348	3.5950	3.3515	3.3711	3.6172
5	0.0555	0.2573	0.0347	0.0090	0.3748
6	0.2864	0.4574	0.1264	0.1443	0.3558
7	2.8399	2.9291	2.9267	2.9128	2.7682
8	0.1062	0.0351	0.0172	0.1020	0.0469
9	2.5146	2.5284	2.6004	2.6149	2.6003
10	2.1884	1.1626	0.4173	0.9280	1.8219

Table E.2 Results of twist angle parameter for a thickness variation-2 (supersonic aircraft wing)

	Twist angle Parameter				
Modes	Cross Ply	Upper camber cross ply and lower camber angle ply	Angle ply (Antisymmetric)	Angle ply (Symmetric)	Upper amber angle ply and lower Camber cross ply
1	0.0392	0.0537	0.0532	0.0528	0.0679
2	0.0430	0.0689	0.1277	0.1240	0.2316
3	0.1565	0.2031	0.0158	0.0106	0.3443
4	3.3755	2.8946	2.2985	2.3231	3.1623
5	0.1806	2.0026	1.9822	1.9308	1.5977
6	1.1745	2.0116	2.4883	2.4990	2.1703
7	2.8342	1.8098	0.0276	0.0287	1.4905
8	0.0685	0.1755	0.4335	0.6489	0.1113
9	2.8232	2.8443	2.9467	2.9305	2.9394
10	0.7424	0.4265	0.2652	0.3703	0.3961

Table E.3 Results of twist angle parameter for a thickness variation-3 (supersonic aircraft wing)

Modes	Twist angle Parameter				
	Cross Ply	Upper camber cross ply and lower camber angle ply	Angle ply (Antisymmetric)	Angle ply (Symmetric)	Upper amber angle ply and lower Camber cross ply
1	0.0180	0.0018	0.0046	0.0051	0.0094
2	0.1907	0.2251	0.1674	0.1698	0.1076
3	0.2334	0.2601	0.0045	0.0039	0.4968
4	3.4707	2.9430	2.2360	2.2452	3.1478
5	1.3700	1.6542	2.0639	2.0573	1.5568
6	0.0220	1.9248	0.0031	0.0738	0.9877
7	3.0177	1.9871	2.6234	2.6477	2.1644
8	0.6103	1.2651	0.1728	0.0483	1.5256
9	1.4966	1.6934	2.0387	2.0224	1.7509
10	0.3263	1.0852	0.7170	1.2480	1.9631

Table E.4 Results of twist angle parameter for a thickness variation-4 (supersonic aircraft wing)

Modes	Twist angle Parameter				
	Cross Ply	Upper camber cross ply and lower camber angle ply	Angle ply (Antisymmetric)	Angle ply (Symmetric)	Upper amber angle ply and lower Camber cross ply
1	0.0638	0.0456	0.0515	0.0009	0.0742
2	0.4553	0.3330	0.2649	0.0046	0.4269
3	3.4245	3.2370	3.0576	0.5828	3.2749
4	0.0192	0.1748	0.0175	0.0011	0.2883
5	0.8538	1.1834	1.4460	0.3748	1.0546
6	0.1971	0.3850	0.0111	0.0000	0.5019
7	0.2585	1.0855	0.2032	0.0002	1.3267
8	3.0104	2.6657	2.5757	0.0458	2.3321
9	1.2086	1.2553	1.4377	0.2893	1.5024
10	0.0008	0.3021	0.1408	0.0021	0.5534

Table E.5 Results of twist angle parameter for a thickness variation-5 (supersonic aircraft wing)

Modes	Twist angle Parameter				
	Cross Ply	Upper camber cross ply and lower camber angle ply	Angle ply (Antisymmetric)	Angle ply (Symmetric)	Upper amber angle ply and lower Camber cross ply
1	0.0718	0.0507	0.0572	0.0575	0.0835
2	0.5282	0.4035	0.3389	0.3396	0.4982
3	3.2361	2.0495	0.1074	0.0768	2.1021
4	1.0453	2.2764	2.4604	2.4587	2.3227
5	1.3445	1.7118	2.2145	2.2228	1.6106
6	0.1191	0.1807	0.0266	0.0075	0.2938
7	0.0314	0.5035	0.1078	0.0047	0.6625
8	3.0472	2.9524	2.5112	2.8131	2.5088
9	1.2785	1.1373	1.6963	1.1670	1.7766
10	0.0024	1.9544	0.0952	0.0784	0.2667

Table E.6 Results of twist angle parameter for a thickness variation-6 (supersonic aircraft wing)

Modes	Twist angle Parameter				
	Cross Ply	Upper camber cross ply and lower camber angle ply	Angle ply (Antisymmetric)	Angle ply (Symmetric)	Upper amber angle ply and lower Camber cross ply
1	0.0828	0.0574	0.0011	0.0654	0.0965
2	0.6283	0.4988	0.0076	0.4345	0.5902
3	0.1988	0.3898	0.3442	0.0041	0.2830
4	2.7195	1.9681	0.0176	1.0073	1.8998
5	2.2636	2.5566	0.3748	2.6273	2.6620
6	0.0305	0.2912	0.0016	0.0219	0.4193
7	0.2335	1.8119	0.0305	1.8094	1.8010
8	2.3155	0.9942	0.0011	0.0273	0.4594
9	2.4255	2.4593	0.5538	2.4447	2.5424
10	0.0417	0.0471	0.0016	0.0158	0.1204

Table E.7 Results of twist angle parameter for a thickness variation-7 (supersonic aircraft wing)

Modes	Twist angle Parameter				
	Cross Ply	Upper camber cross ply and lower camber angle ply	Angle ply (Antisymmetric)	Angle ply (Symmetric)	Upper amber angle ply and lower Camber cross ply
1	0.0272	0.0545	0.0958	0.0980	0.0308
2	0.1522	0.0336	0.1401	0.1410	0.0503
3	0.0101	0.0016	0.0005	0.0027	0.0020
4	0.1097	0.1116	0.0155	0.0176	0.1207
5	0.0078	0.0104	0.0048	0.0016	0.0194
6	0.0385	0.1167	0.1315	0.1339	0.1434
7	0.1202	0.1021	0.0817	0.0875	0.0425
8	0.0124	0.0383	0.0082	0.0028	0.0217
9	0.0348	0.1294	0.1947	0.1902	0.1338
10	0.0225	0.0361	0.0216	0.0287	0.0467

Appendix F
Mode shape character for subsonic aircraft wing

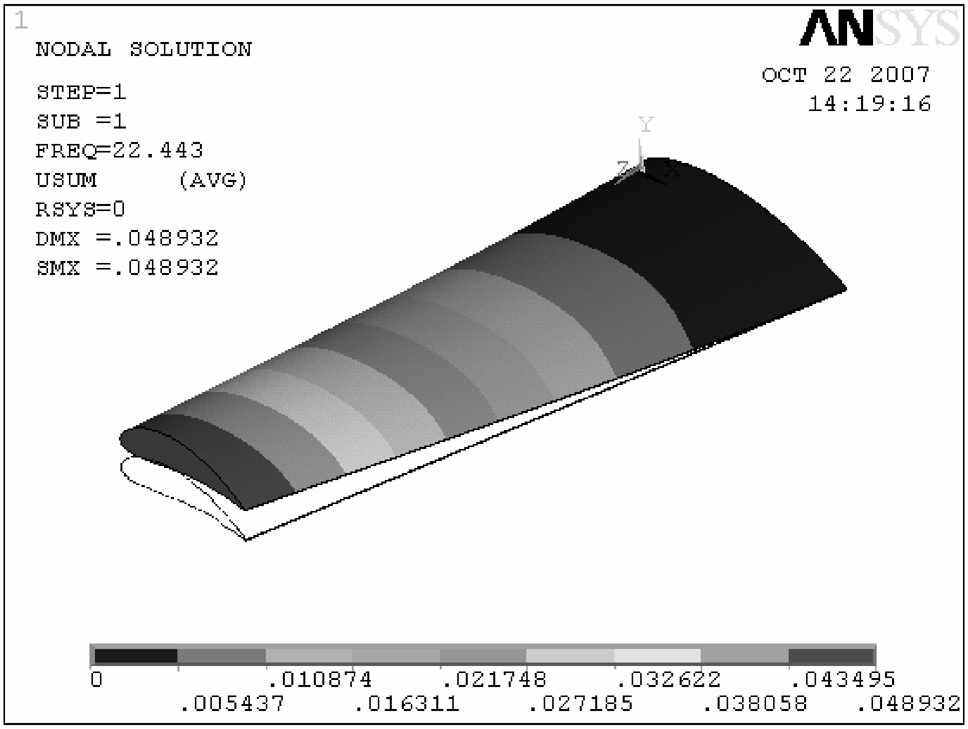

Figure F.1 First mode shape for a thickness varation-1

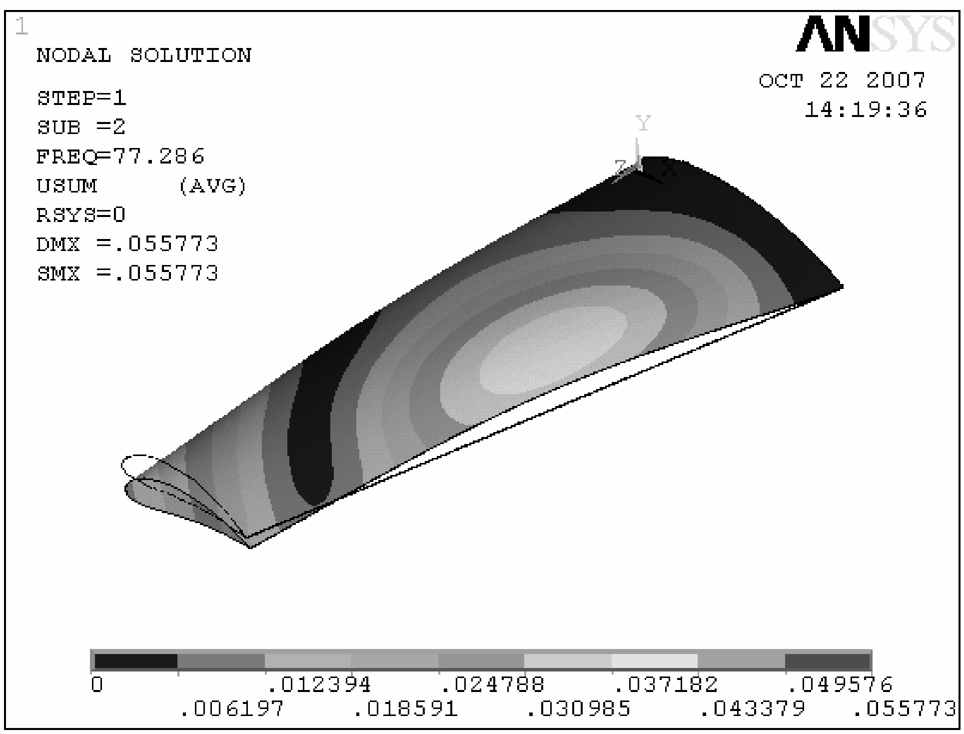

Figure F.2 second mode shape for a thickness varation-1

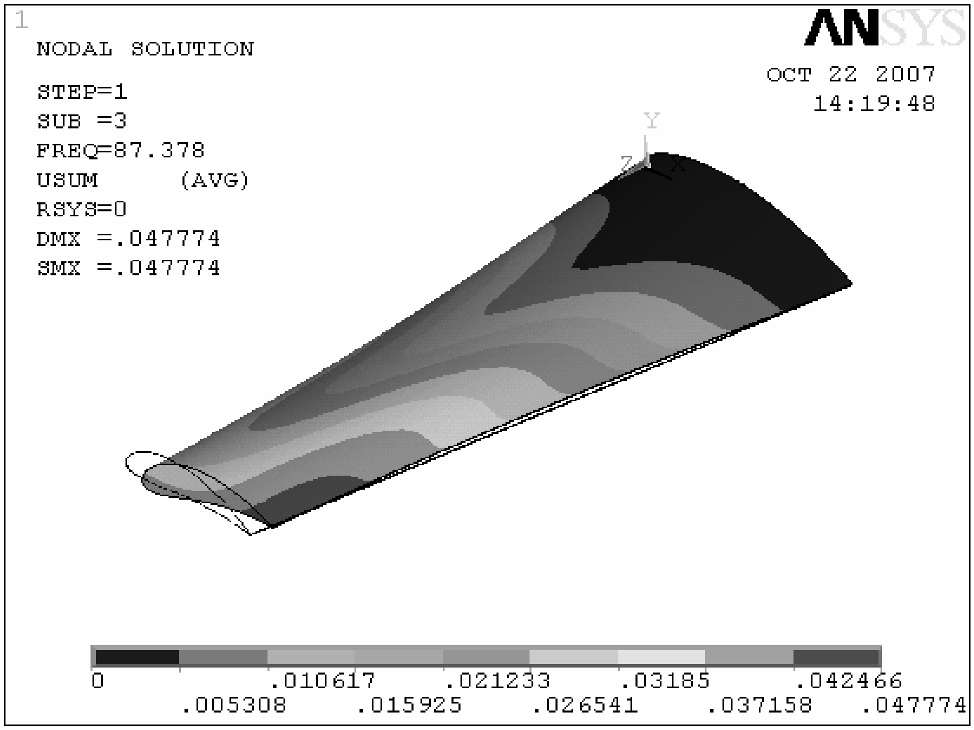

Figure F.3 Third mode shape for a thickness varation-1

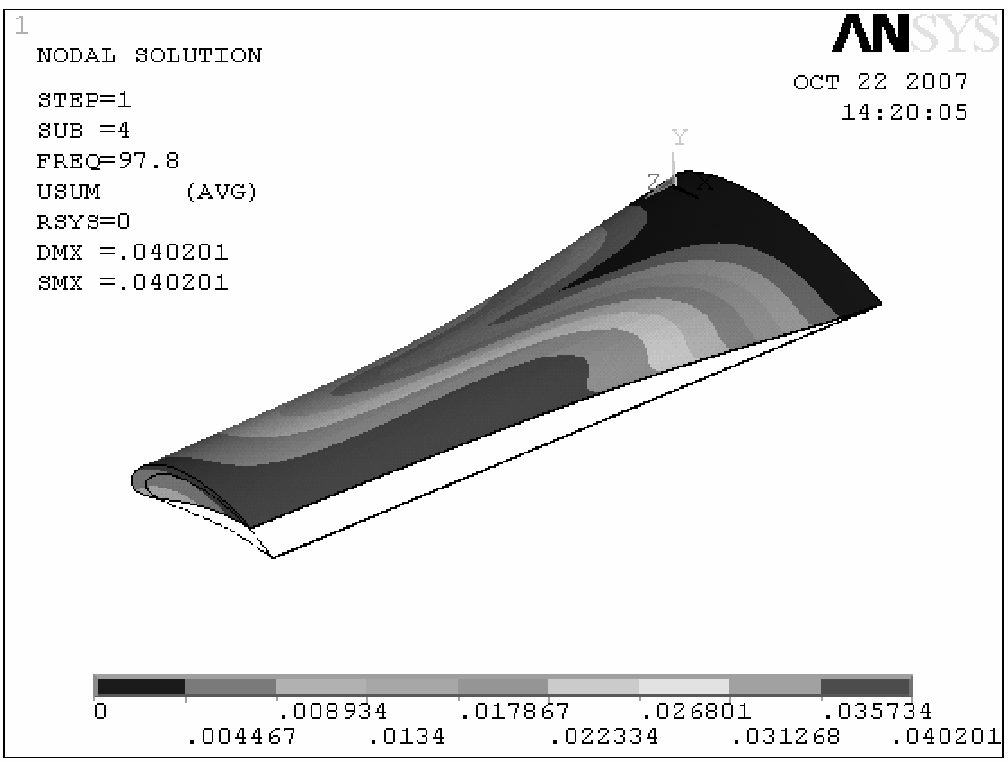

Figure F.4 Fourth mode shape for a thickness varation-1

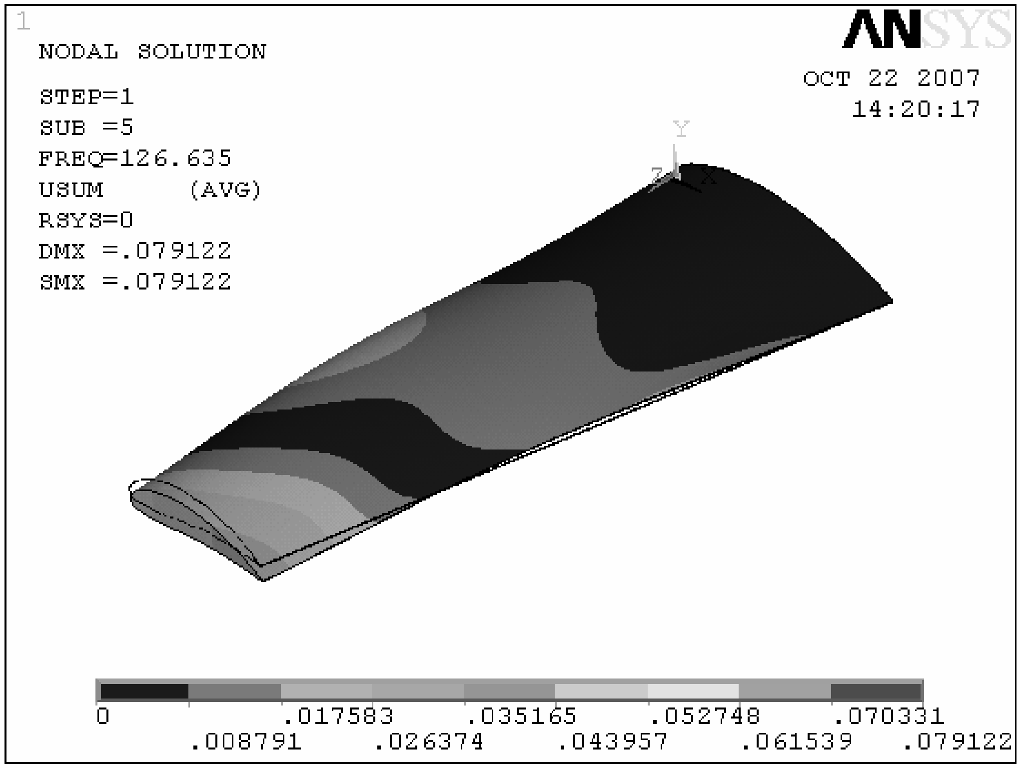

Figure F.5 Fifth mode shape for a thickness varation-1

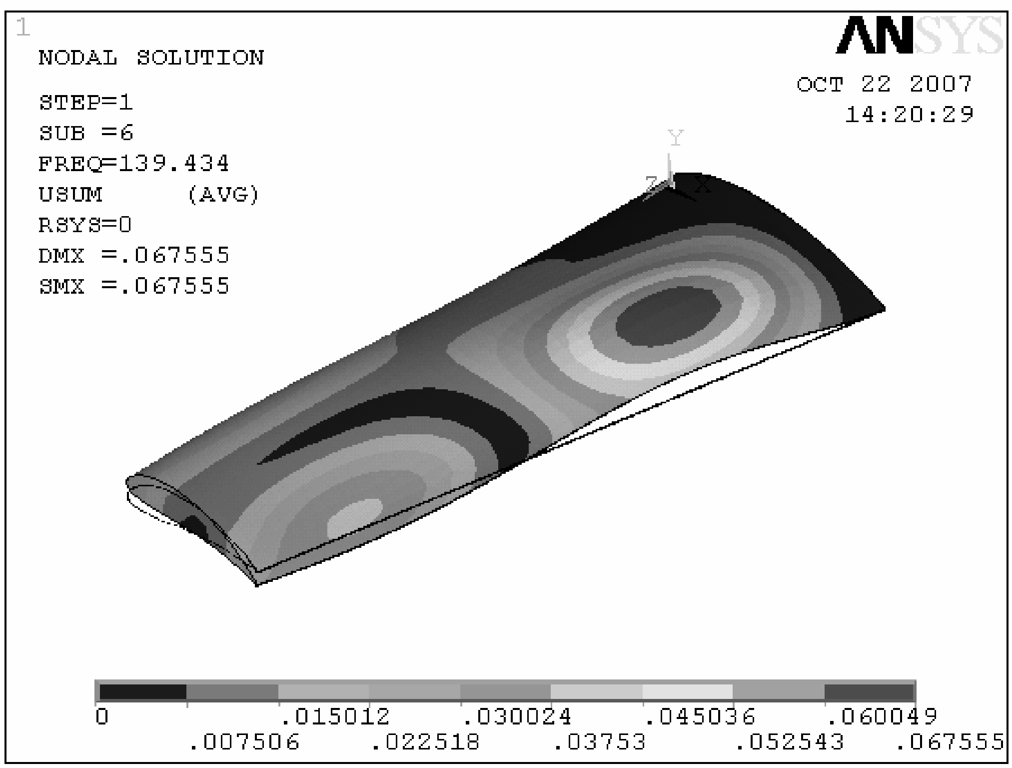

Figure F.6 Sixth mode shape for a thickness varation-1

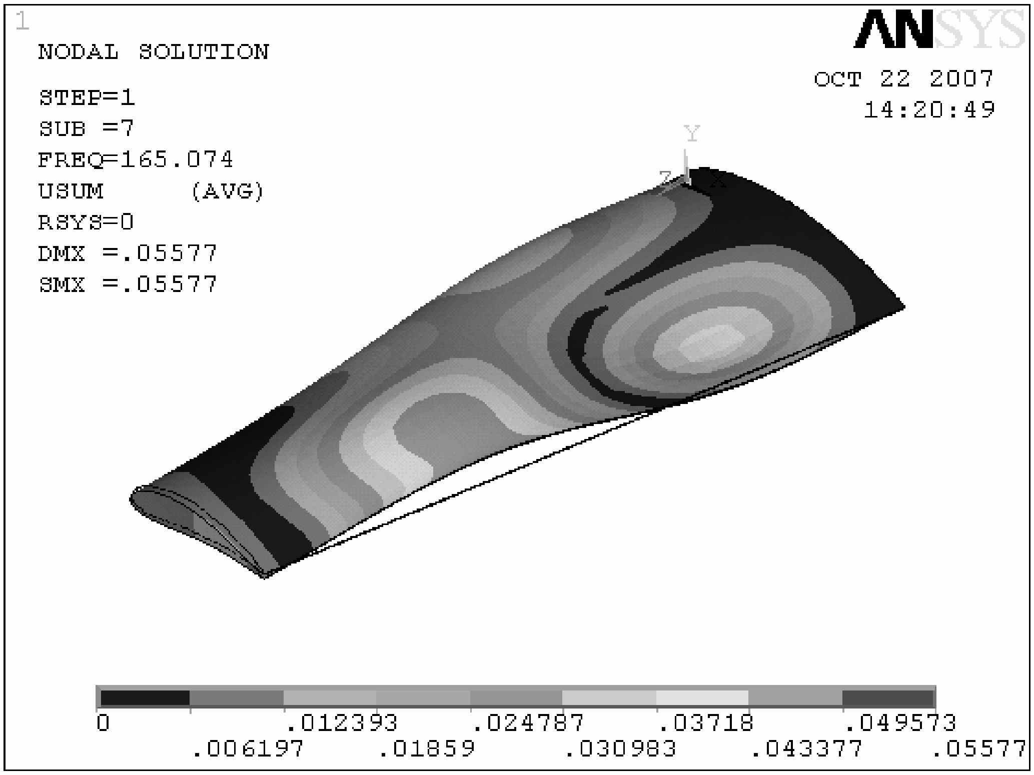

Figure F.7 Seventh mode shape for a thickness varation-1

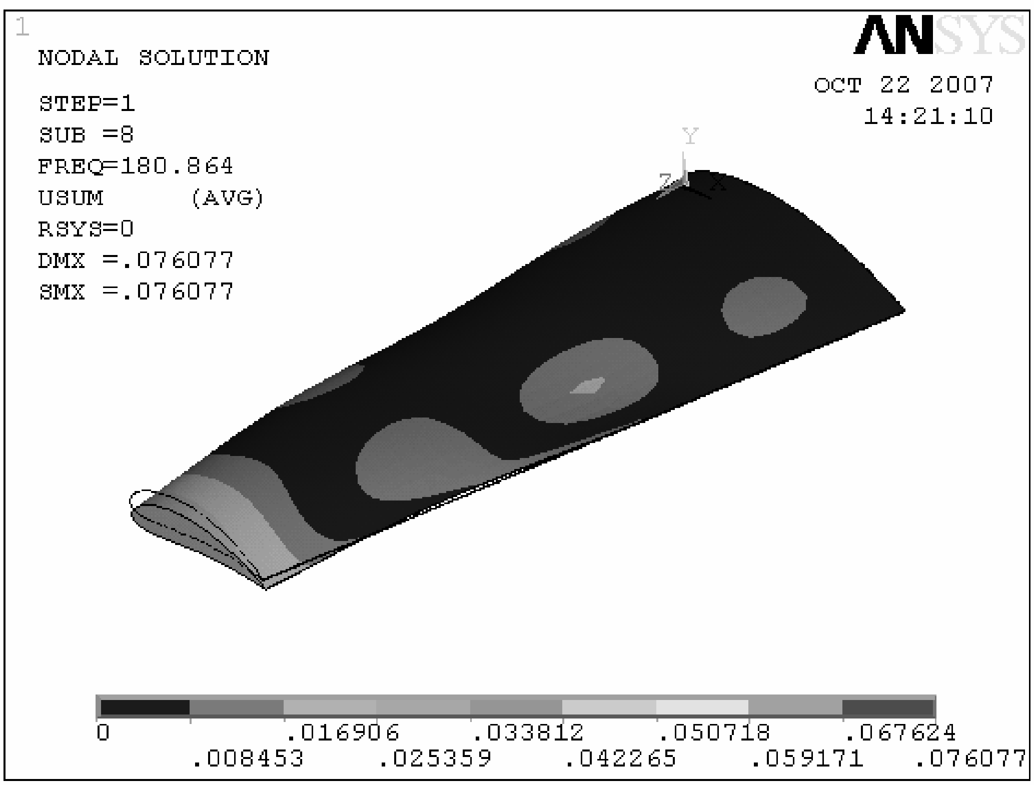

Figure F.8 Eighth mode shape for a thickness varation-1

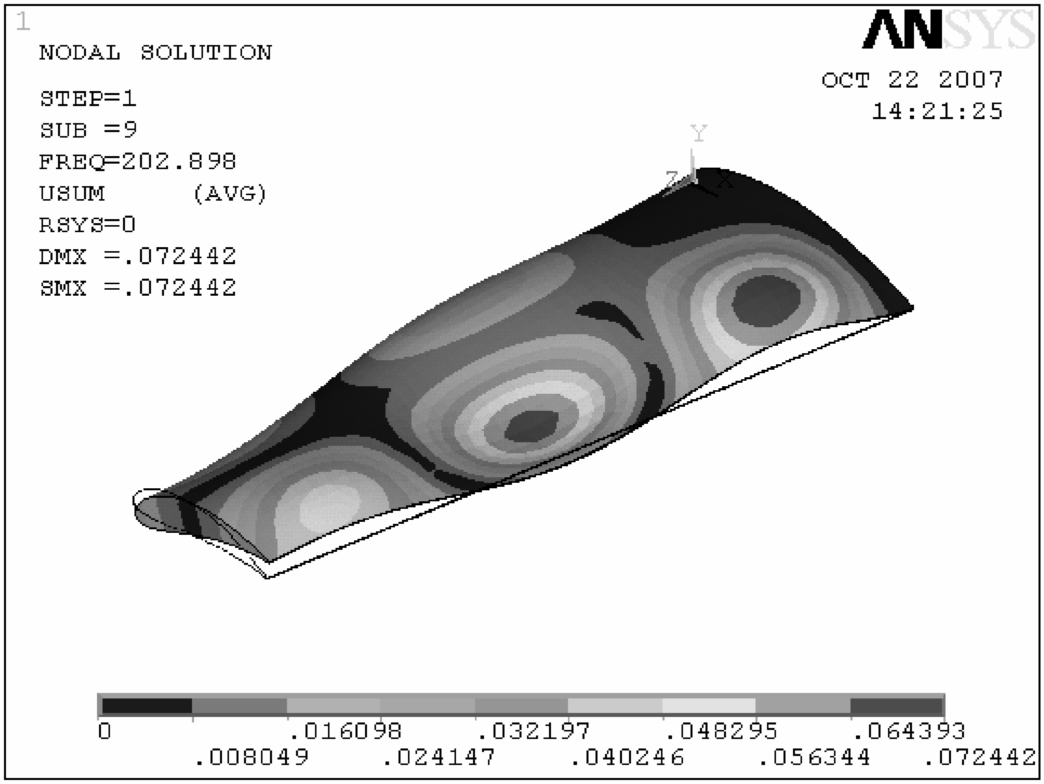

Figure F.9 Ninth mode shape for a thickness varation-1

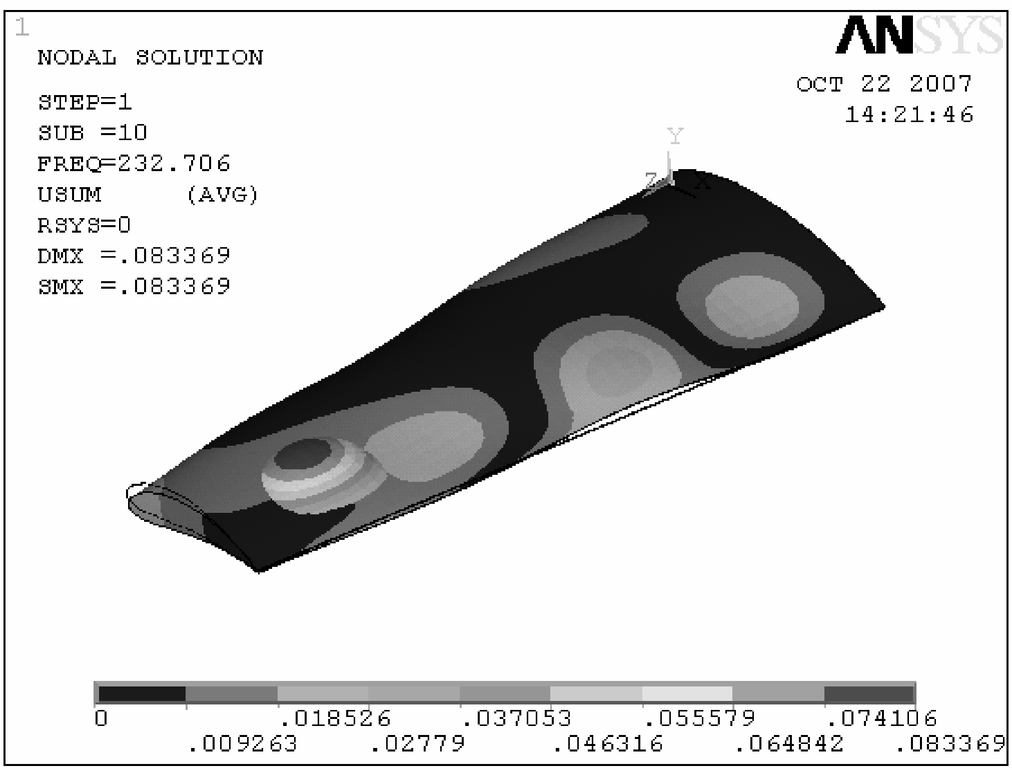

Figure F.10 Tenth mode shape for a thickness varation-1

Appendix G
Mode shape character for supersonic aircraft wing

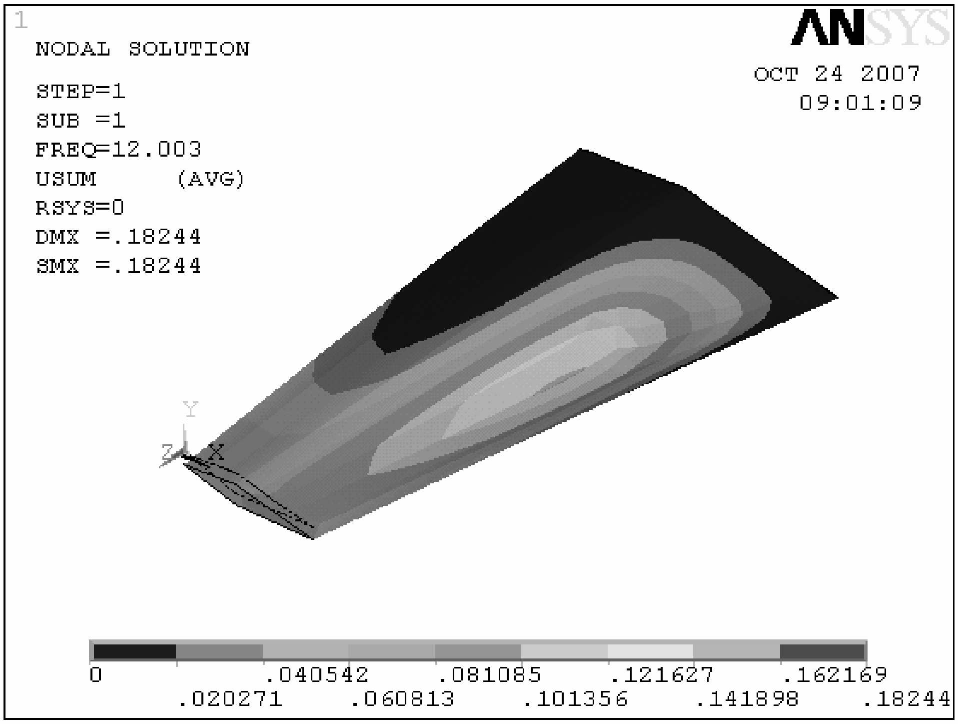

Figure G.1 First mode shape for a thickness varation-7

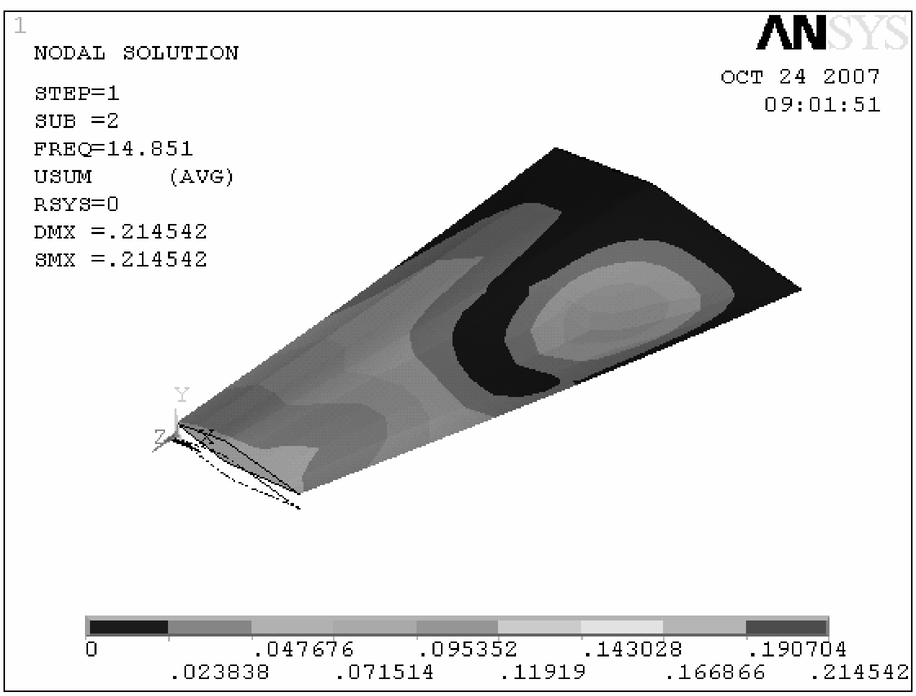

Figure G.2 Second mode shape for a thickness varation-7

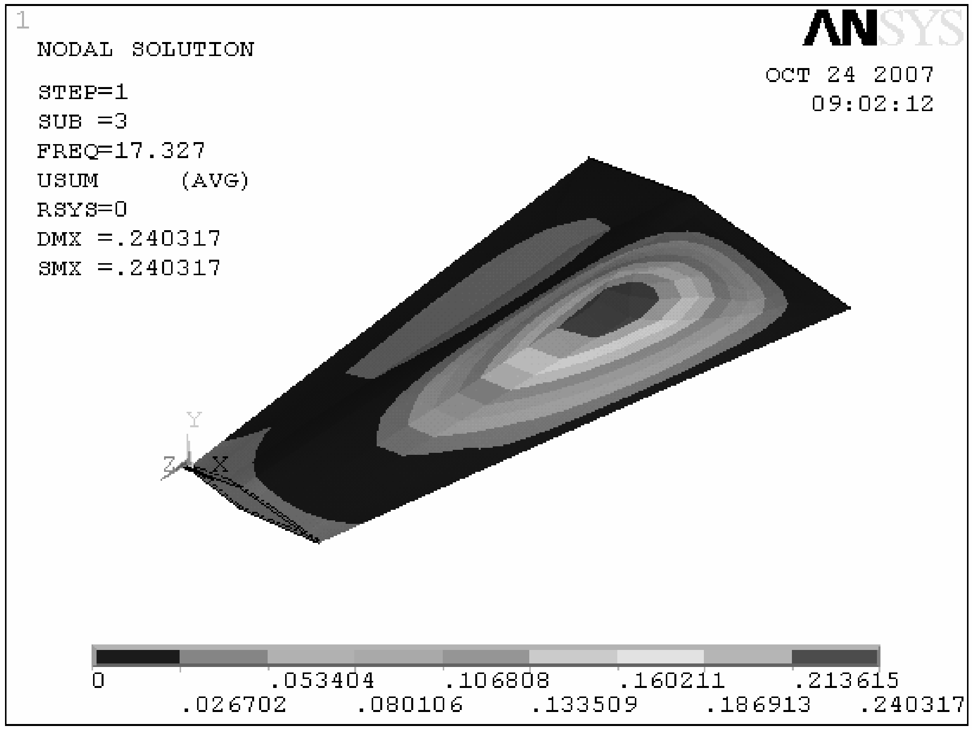

Figure G.3 Third mode shape for a thickness varation-7

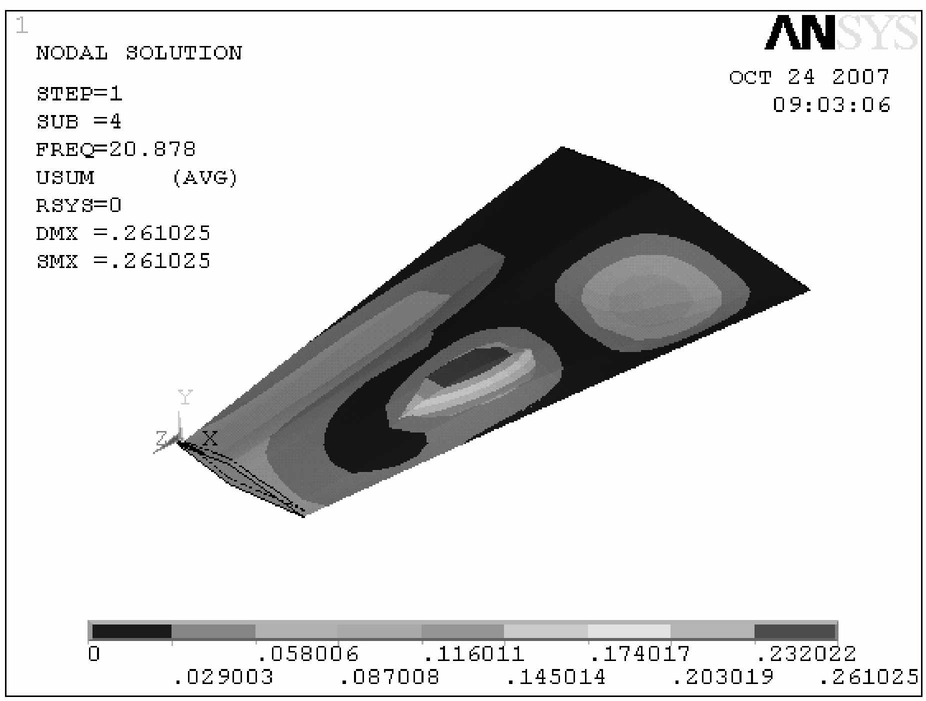

Figure G.4 Fourth mode shape for a thickness varation-7

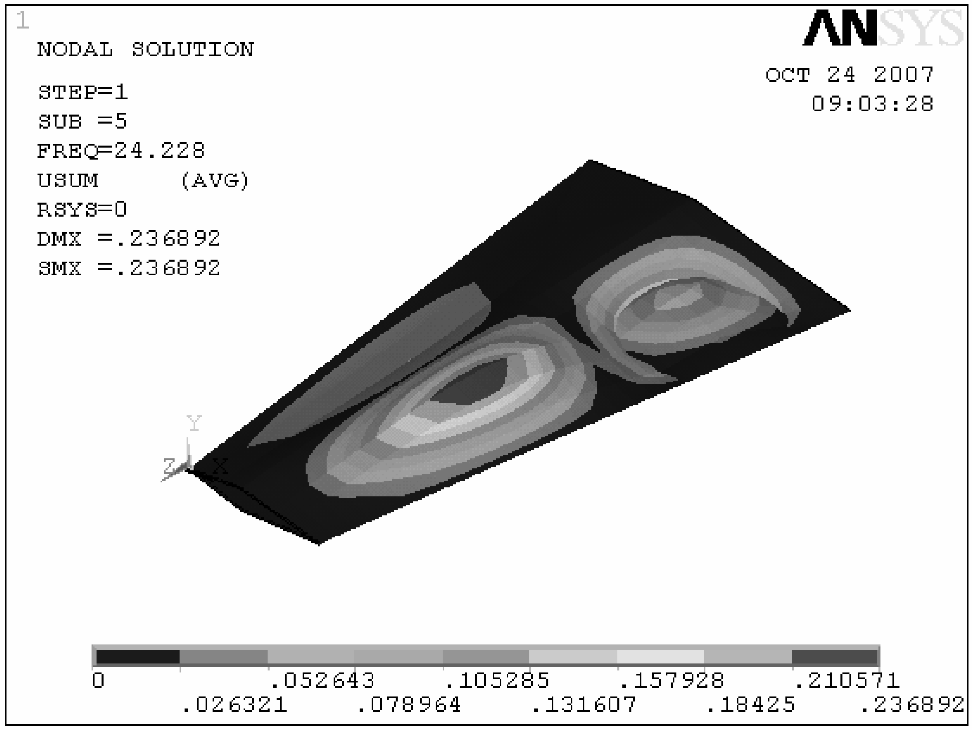

Figure G.5 Fifth mode shape for a thickness varation-7

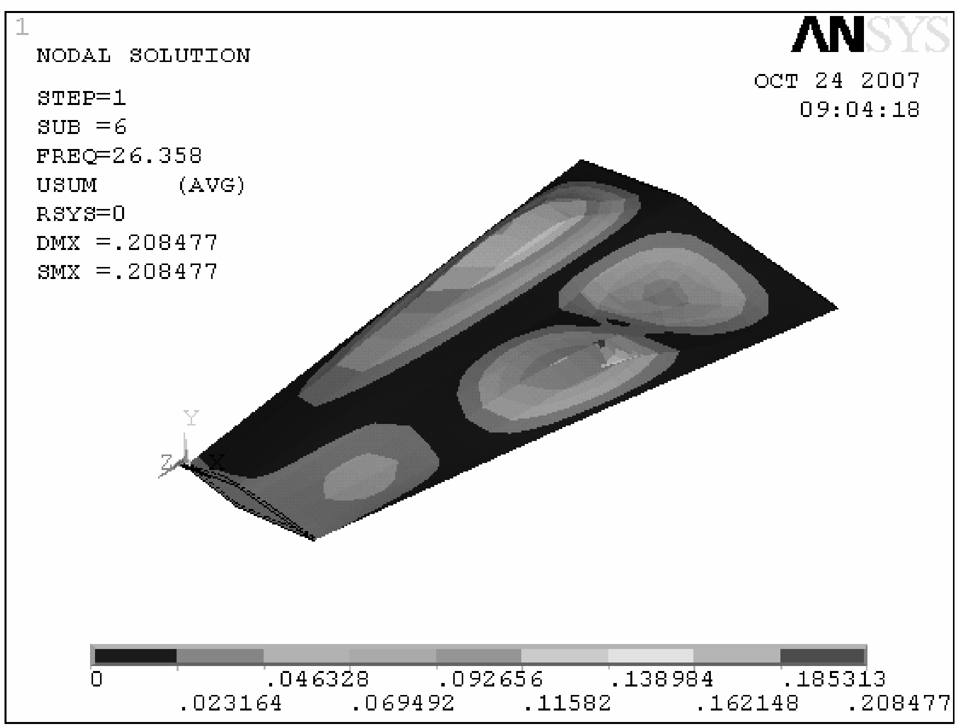

Figure G.6 Sixth mode shape for a thickness varation-7

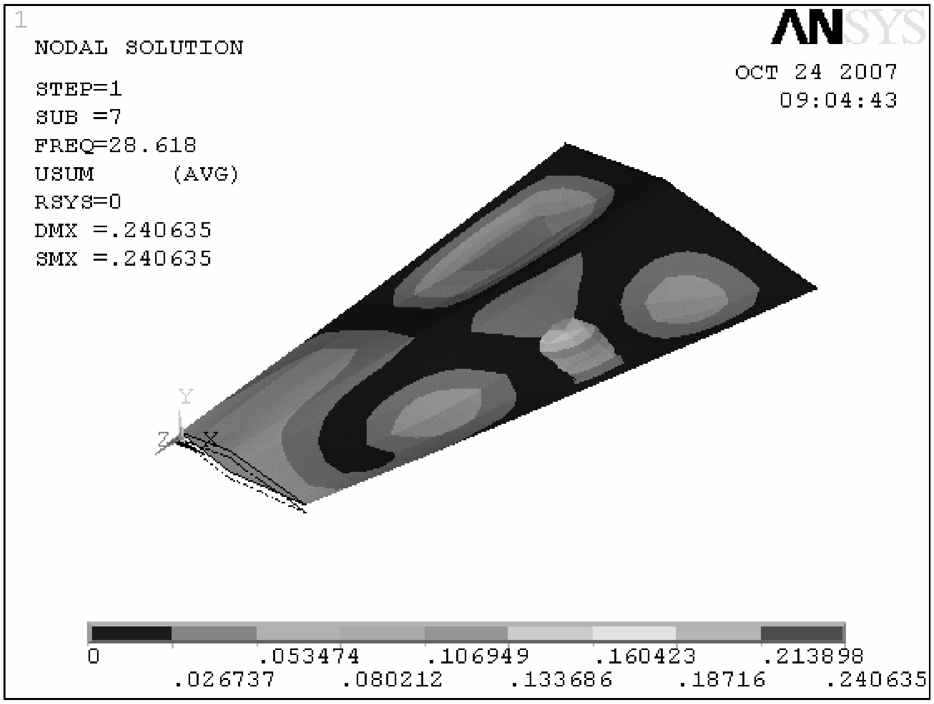

Figure G.7 Seventh mode shape for a thickness varation-7

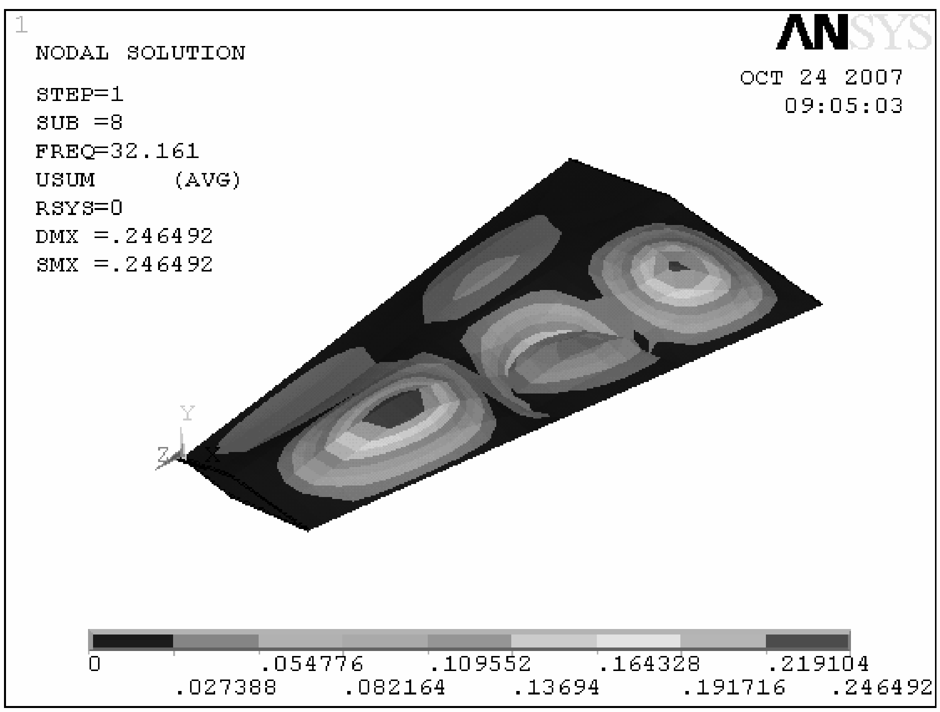

Figure G.8 Eighth mode shape for a thickness varation-7

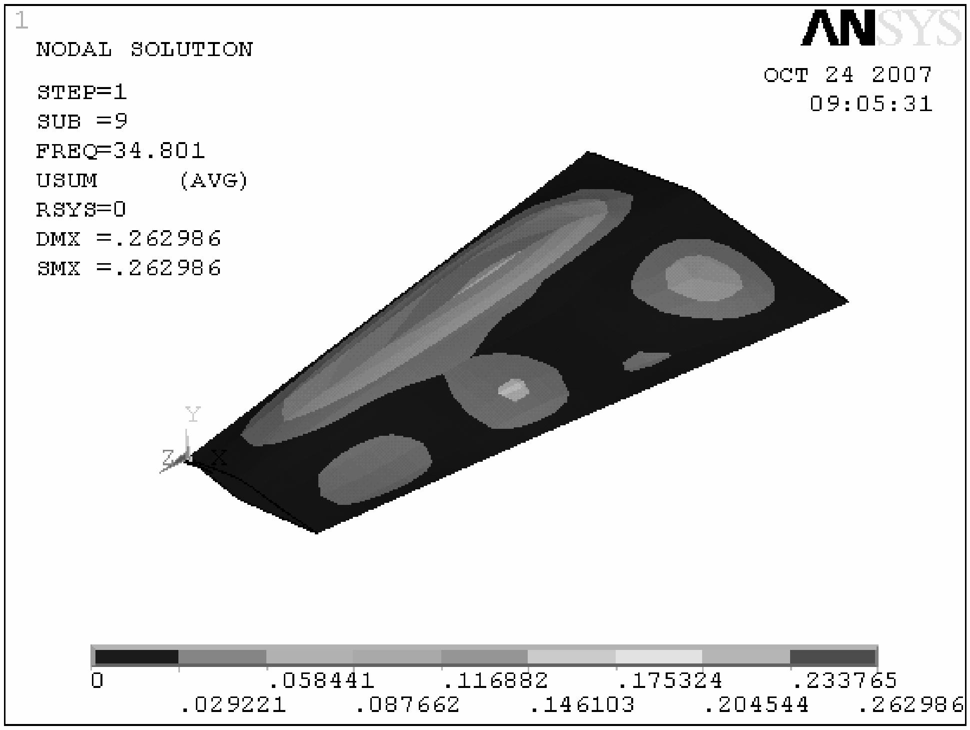

Figure G.9 Ninth mode shape for a thickness varation-7

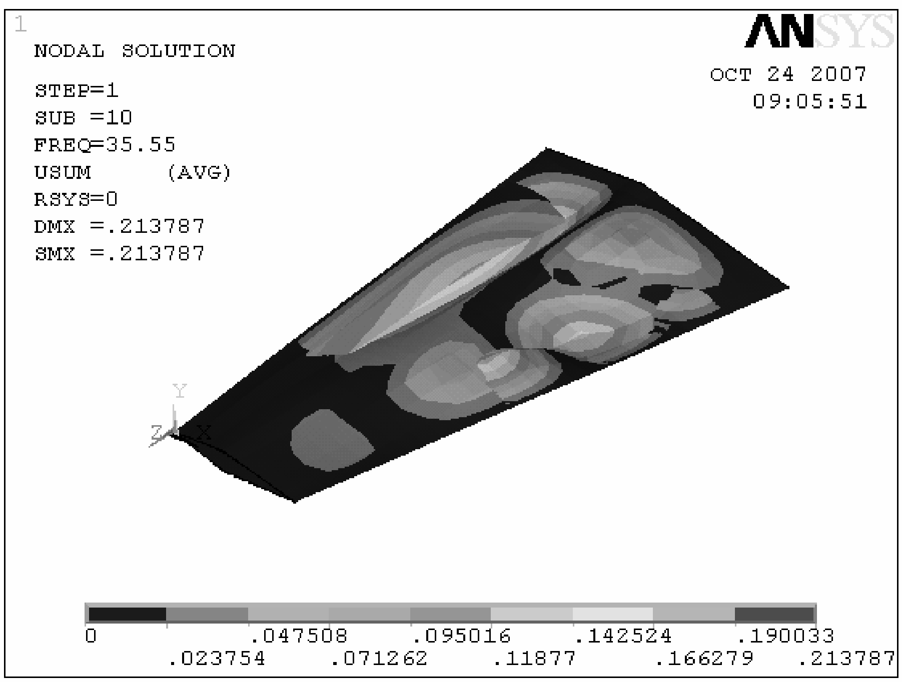

Figure G.10 Tenth mode shape for a thickness varation-7